Modeling 2011 in Massachusetts Bay using the unstructured grid Bays Eutrophication Model

Massachusetts Water Resources Authority
Environmental Quality Department
Report 2012-13

Citation:

Zhao LZ ,Tian Chen C, Leo WS, Mickelson MJ. 2012. **Modeling 2011 in Massachusetts Bay using the unstructured-grid Bays Eutrophication Model**. Boston: Massachusetts Water Resources Authority. Report 2012-13. 138p.

Modeling 2011 in Massachusetts Bay using the unstructured-grid Bays Eutrophication Model

Submitted to

Massachusetts Water Resources Authority
Environmental Quality Department
100 First Avenue
Charlestown Navy Yard
Boston, MA 02129
(617) 242-6000

Prepared by

Liuzhi Zhao and Changsheng Chen
School for Marine Science and Technology
University of Massachusetts-Dartmouth
New Bedford, MA 02744

And

Wendy S. Leo and Michael J. Mickelson
Environmental Quality Department
Massachusetts Water Resources Authority
Boston, MA 02129

December 2012

Key word acronyms and definitions

ECOM-si	Estuarine and Coastal Ocean Model-semi-implicit. A structured-grid hydrodynamic model
FVCOM	Finite-Volume Coastal Ocean Model: An unstructured-grid hydrodynamic model
GoM/GB FVCOM	FVCOM applied to the Gulf of Maine/Georges Bank[1]
MB FVCOM	FVCOM applied to Massachusetts Bay[2]
RCA	Row Column Advanced (RCA) ecological systems operating program: a water quality model
UG-RCA	Unstructured-grid version of RCA
MB	Massachusetts Bay
BEM	Massachusetts Bays Eutrophication Model: a coupled water quality and hydrodynamics model system.
BH	Boston Harbor
WRF	Weather Research and Forecast Model[3]

[1] http://fvcom.smast.umassd.edu/research_projects/GB/index.html
[2] http://fvcom.smast.umassd.edu/research_projects/MassBay/index.html
[3] http://fvcom.smast.umassd.edu/research_projects/GB/WRF/index.html

EXECUTIVE SUMMARY

The Massachusetts Water Resources Authority (MWRA) contracted the Marine Ecosystem Dynamics Modeling laboratory of University of Massachusetts at Dartmouth (UMASSD) to simulate currents, temperature, salinity, dissolved oxygen, and other water quality parameters in Massachusetts Bay for calendar year 2011. This report presents the simulation, validation, and interpretation of the model results. Projection of the impact of the MWRA effluent on water quality parameters such as algal development and dissolved oxygen level is presented as well.

The water quality model is driven by a hydrodynamic model, which simulates currents, temperature, and salinity within Massachusetts Bay, based on known or assumed tides, offshore currents, weather from a weather model, and river inputs. The hydrodynamic model successfully reproduced field observations of temperature and salinity for 2011.

The water quality simulation reproduced most of the observed magnitudes and seasonal cycles of water quality variables, including nitrogen, chlorophyll, and oxygen. The 2011 chlorophyll simulation correctly showed absence of the dominant spring phytoplankton bloom typical of most other years; the model results were fairly consistent with field observations which showed a modest and somewhat late-starting spring bloom. Instead of an intense bloom, multiple peaks of chlorophyll concentration were simulated from spring through fall, with limited amplitudes and durations, particularly at the nearfield stations. The open boundary with the Gulf of Maine is the major source of nutrients to Massachusetts Bay; boundary nutrient levels were lower than usual in 2011 and this could have resulted in the lack of a strong bloom.

Predicted and measured dissolved oxygen (DO) both showed high values during the spring as a result of photosynthetic production, and low levels in fall. In the 2011 simulation, the model underpredicted DO concentrations and percent oxygen saturation. Many factors affect dissolved oxygen; it appears that the model may have overestimated the amount of oxidation by organic matter in the water.

Based on our projection analysis removing the MWRA outfall from the simulation, the outfall plume was mostly restricted to a local area about 20 km wide. However, consistent with past studies, long-distance effluent nutrient dispersal as far as Cape Cod Bay was predicted under

certain circumstances in January and December 2011. Except very close to the outfall, the nutrients from the effluent discharge are a small percentage of the natural background levels. The plume was trapped near the bottom during the stratified season in summer and early fall. In winter and late fall when the vertical mixing was strong, the outfall effluent plume can reach to the surface layer, as predicted by earlier model studies and as observed in the field monitoring. However, no substantial bay-wide influence on chlorophyll or DO levels was seen. Although effluent nutrients can be dispersed farther from the outfall in surface waters in winter, darkness slows phytoplankton growth such that effluent nutrients are dispersed more quickly than they are taken up and translated into phytoplankton biomass. These model results support the conclusions of MWRA's long-term monitoring program that shows that although nitrogen levels are higher near the Massachusetts Bay outfall, no effect of this increase is seen in biomass or dissolved oxygen.

Table of Contents

List of Figures

List of Tables

1. Introduction

1.1 *Project overview*

The Massachusetts Water Resources Authority (MWRA) has established a long-term monitoring program to evaluate the impact of MWRA sewage treatment plant effluent on the ecosystem function and water quality in the Massachusetts Bay system (MBS) including Boston Harbor (BH), Massachusetts Bay (MB) and Cape Cod Bay (CCB). The monitoring program primarily consists of an array of field observations, but is complemented by water quality modeling as required by the MWRA permit for effluent discharge into MB. Up to 2007, the water quality model RCA (Row-Column Advanced Ecological Systems Operating Program) developed by HydroQual was applied to MBS by HydroQual (1994-1999), University of Massachusetts Boston (2000-2005) and University of Massachusetts Dartmouth (2006-2007) (HydroQual, 2000; HydroQual, 2003; Jiang and Zhou, 2004b, 2006b, 2008; Tian *et al.* 2009). RCA was driven by the structured-grid hydrodynamic model ECOM-si (HydroQual and Signell, 2001, Jiang and Zhou, 2004a, 2006a). For the 2008 water quality simulation, we upgraded RCA to the unstructured-grid UG-RCA driven by the Finite-Volume Coastal Ocean Model FVCOM (Chen *et al.*, 2010). Two major updates were included in this upgrade. First, the newly developed RCA version 3 was adapted to MBS whereas an older version was used prior to the 2008 simulations. RCA-v3 is a modular system which has more options and greater flexibility than the previously used version. Secondly, the unstructured-grid finite-volume algorithms, well-suited to resolve the complex coastline and bottom topography in MBS, were adapted from FVCOM. We tested the newly developed system for the case of 2006 and applied it for the 2008 simulation, which showed that UG-RCA can be successfully applied to MBS. We used this system for the 2009, 2010 and 2011 simulations. This report presents the details of data treatment, model setup, model-data comparison and interpretation of the simulated results for the year 2011. Following the 2009 simulation report (Tian *et al.*, 2010), the figures in this report make use of new color scales suggested by MWRA.

1.2 *Physical background*

The MBS comprises Boston Harbor in the west, Cape Cod Bay in the south and Massachusetts Bay in the central region (**Figure 1.1**). It is a semi-enclosed coastal embayment with a length of approximately 100 km and a width of 50 km. The water depth averages about 35

m, with the maximum depth of 90 m in Stellwagen Basin, shoaling to 20 m on Stellwagen Bank. Stellwagen Bank, located on the east side of MB, limits deep-water exchange between MB and the Gulf of Maine (GoM). Deep water exchange occurs mainly through the North Passage off Cape Ann and the South Passage off Race Point.

The hydrodynamic circulation in the MBS is subject to both local forcing such as wind and remote forcing by tides and intrusion of the Western Maine Coastal Current (WMCC) (Bigelow, 1927; Butman *et al.*, 2002). The general circulation pattern within MBS is counterclockwise with inflow through the North Passage and outflow through the South Passage. The inflow is primarily determined by (a) the WMCC which bifurcates near Cape Ann with one branch flowing into MBS (Bigelow, 1927; Lynch *et al.*, 1996) and (b) Gulf of Maine coastal freshwater discharges, particularly from the Merrimack River located north of the bay (Butman, 1976). Driven by buoyancy and the Coriolis force, a considerable portion of the Merrimack River freshwater discharge often enters into Massachusetts Bay. Manohar-Maharaj (1973) estimated that in May, up to 90% of the freshwater found in Massachusetts Bay originated from the Merrimack River. However, the amount of fresh water intrusion into Mass Bay varies depending on the path of the WMCC and on the wind forcing. Local wind forcing can significantly alter the current pattern and velocity (Geyer *et al.*, 1992; Butman *et al.*, 2002; Jiang and Zhou, 2004a). Wind-induced upwelling and downwelling were observed and simulated in previous studies (e.g., Geyer *et al.*, 1992; HydroQual and Signell, 2001; Jiang and Zhou, 2004a; Tian *et al.*, 2009). However, the water column stratification is primarily controlled by seasonal variations in net surface heat flux and freshwater discharge. Water stratification starts in spring due to increased insolation and freshwater discharge, intensifies in summer due to surface heating, and erodes in fall due to surface cooling and increased wind stress, following which the water column becomes well mixed again in winter.

1.3 *Biological background*

Phytoplankton abundance in the MBS generally shows seasonal cycles typical of temperate regions due to the seasonality in solar radiation, water column stratification and nutrient availability (Libby *et al.* , 2000, 2001). During winter when the water column is well-mixed and solar radiation is weak, phytoplankton growth is restricted due to limited light exposure in most of the MBS. Phytoplankton usually bloom in spring following the establishment of water column

stratification and increases in solar radiation. However, spatial differences and interannual variations in the timing of the phytoplankton spring bloom can occur due to local forcing and the physical environment. For example, the spring phytoplankton bloom often develops earlier in CCB than in Stellwagen Basin due to CCB's shallow water depth. During the post-bloom season in summer, phytoplankton biomass is low in most of the MBS due to nutrient limitation, but local phytoplankton growth can still occur due to, for example, wind-driven upwelling activity and river discharge. The fall bloom in the MBS usually occurs in late September and early October when increased wind stress and cooling at the sea surface erode the stratification, increasing vertical mixing and replenishing nutrients from the deeper layer to the euphotic zone. With further increases in vertical mixing and decreases in solar radiation, phytoplankton growth is limited again, but now by light, leading to high nutrient concentrations and low phytoplankton abundance in winter.

The seasonal cycle of phytoplankton production is accompanied by succession in phytoplankton species. Centric diatoms dominate the spring phytoplankton bloom under nutrient-replete conditions, particularly with high silicate concentrations, although especially in recent years the haptophyte *Phaeocystis pouchettii* has become dominant in spring (Libby *et al.,* 2009, 2010). Phytoflagellate species prevail during the summer stratified season under nutrient-depleted conditions. With the replenishment of surface nutrients in fall, pennate diatoms and small dinoflagellates develop. Phytoplankton seasonal succession results in variations in biological parameter values and carbon:chlorophyll ratio. The seasonality in phytoplankton production and biomass is reflected in the secondary production level as variations in zooplankton abundance and species through bottom-up control (Turner, 1994; Libby *et al.*, 2000).

Benthic biological and biogeochemical dynamics directly affect nutrient supply and oxygen demand and thus the water quality of the MBS. BH, CCB and Stellwagen Basin are characterized by a soft sea floor with fine sediment and high organic matter content, whereas the coastal regions are mostly covered by coarse sediment and rocks (Kropp *et al.*, 2001; Kropp *et al.*, 2002; Maciolek *et al.*, 2003). In regions of soft floor with fine sediments, sediment oxygen demand (SOD) is higher than that in the hard-floor regions. In BH, for example, high values of SOD and nutrient flux have been observed. Outside of the harbor in MB and CCB, physical

processes significantly affect benthic biogeochemical processes in these relatively well-oxygenated sediments (Maciolek *et al.*, 2003; Tucker *et al.*, 2002; Jiang and Zhou, 2008). Most of these biological and biogeochemical processes are parameterized in the BEM.

1.4 *Modeling updates*

The modeling project has played a valuable role in both scientific investigation and decision making for the MWRA outfall design and monitoring program. Before the relocation of the outfall from Boston Harbor to its new offshore position in September 2000, Signell *et al.* (2000) conducted a series of simulations to analyze the impact of the relocation. They found that the effluent concentration decreased by ten-fold in the harbor, while only slightly elevated effluent concentration was predicted, and only within several kilometers around the offshore outfall, due to dilution and dispersal in the larger water body. During the summer stratified season, the effluent was more highly concentrated around the outfall as compared to the winter season when dispersal and dilution dominated. Previous modeling work also showed that the outfall effluent discharge did not have considerable bay-wide effect on the function of the bay ecosystem (Jiang and Zhou, 2006b, 2008; Tian *et al.*, 2009).

The reliability of model predictions depends on the correctness of the parameterization and the robustness of the simulation. Over the years, efforts have been continuously made to improve the modeling system. For example, HydroQual and Signell (2001) found that the parameterization of short-wave radiation in the water column is of primary importance to the simulation of temperature variation and distribution. Shortwave radiation energy was initially introduced to the first sigma layer in the physical ECOM-si model, which led to an overheating in surface waters. An exponential decay function with depth was then implemented in the model which considerably improved temperature predictions. Chen *et al.* (2009) and Tian *et al.* (2009) found that wind forcing plays a key role in both physical and biological simulations. A spatially resolved wind field improved model-data comparison and increased DO level in the bottom layer by 9–18% for the case of 2007 as compared with runs driven by spatially uniform wind forcing. The improvement is particularly notable during storm events and passage of fronts. HydroQual (2001a) conducted a sensitivity analysis on the impact of boundary conditions on the simulation of water quality variables. They found that certain variables such as DO in the interior of the bay are correlated with values at the open boundary, particularly at the north-northeast region of MB.

Certain variations in bottom DO were directly caused by the boundary conditions. To improve the open boundary condition, Jiang and Zhou (2004a) introduced the objective analysis (OA) method of interpolating boundary conditions based on field observations, which has been used up to the present (Jiang and Zhou, 2008; Tian *et al.*, 2009; Chen *et al.*, 2010 and Zhao *et al.*, 2011). HydroQual (2001b) found that the Bays Eutrophication Model with two phytoplankton groups failed to reproduce observed fall chlorophyll levels in 1993. The addition of a third group notably improved the model prediction. The major characteristic of the third "fall" phytoplankton group is the lower carbon-to-chlorophyll ratio than that in the previous two groups, winter/spring and summer phytoplankton groups. As shown by HydroQual (2002), the chlorophyll simulation could be improved on an annual basis by altering parameter values, but seasonal deviation such as that observed in the fall of 1993 was better resolved by adding the additional fall phytoplankton group, compared to sensitivity runs using the two original phytoplankton groups.

Massachusetts Bay (MB) is a complex embayment. First, its varying coastline and bottom topography can induce complex hydrodynamic features such as mesoscale eddies, filaments and coastal jets (Jiang and Zhou, 2006a, b). Second, the Western Maine Coastal Current bifurcates at Cape Ann, with one branch intruding into MB, which strongly affects both physical and biochemical dynamics. Third, wind forcing, combined with the coastline and bottom topography, can generate upwelling and downwelling. Fourth, river discharges further complicate hydrodynamics and nutrient loadings. All of these features are a challenge for the modeling community to get right in the modeling dynamics and setup. Improvements have been made over the years as described above; one major step was the introduction of the Finite-Volume Coastal Ocean Model (FVCOM) and the development of the unstructured-grid water quality model driven by FVCOM (Chen *et al.*, 2009, 2010). FVCOM is one of the models most suitable for resolving a complex coastline and bottom topography. The nesting setup of FVCOM can ensure mass conservation and continuity in physical forcing at the common boundary (Chen *et al.*, 2010).

Prior to 2008 the water quality model used was RCA-v2 (HydroQual, 2003, Chen *et al.*, 2010). With the use of FVCOM for the hydrodynamic model, we upgraded the water quality model to an unstructured-grid water quality model and named it "UG-RCA". We based UG-

RCA on the latest version of RCA, RCA-v3 (HydroQual, 2004). As described in more detail in Chen *et al.* (2010), Tian *et al.* (2010), and Zhao *et al.* (2011), UG-RCA has the same basic model structure and biological dynamics of RCA-v2, but has more model parameters, uses photosynthetically active radiation (PAR) to drive phytoplankton growth rather than total solar radiation, and eliminates the need for RCA to recalculate salinity as a check on transport – salinity and transport are derived directly from FVCOM.

2. Methods

This section consists of six subsections. The first briefly describes the Finite-Volume Coastal Ocean Model used to simulate the physical fields to drive the water quality model. Next we describe the structure and functionality of the unstructured-grid water quality model used for the 2011 simulation. The third section describes the unstructured triangular grids including the nesting domain and the vertical coordinate. The section on forcing describes both the meteorological forcing for FVCOM and surface forcing for UG-RCA. The fifth section, "Nutrient loadings," describes most of the nutrient and organic matter sources including the MWRA outfall. The final section describes how the open boundary condition of the UG-RCA state variables was determined, and describes the data set used for open boundary conditions.

2.1 *FVCOM*

The unstructured-grid, finite volume, 3D, free surface primitive equation Coastal Ocean Model (FVCOM) was developed originally by Chen *et al.* (2003). FVCOM is a message-passaging interface parallelized model updated by a team of scientists at UMASSD and Woods Hole Oceanographic Institution (Chen *et al.*, 2006a, b). In the horizontal, FVCOM uses a non-overlapping unstructured triangular grid, which is particularly suitable for resolving the complex coastal geometry of Massachusetts Bay. In the vertical, FVCOM is discretized by layers using the generalized terrain-following hybrid coordinate (Pietrzak *et al.*, 2002). This vertical coordinate system allows for vertical layers of uniform thickness near the surface and bottom over the offshore deep slope with a smooth transition to topography-following layers in the inner shelf and estuaries, which is critical to resolving the wind-driven surface mixed layer and sloping bottom boundary layer. FVCOM is solved numerically by the flux calculation in an integral form of the governing equations with options of either mode-split (like the Princeton Ocean Model, or the Regional Ocean Modeling System developed at Rutgers) or semi-implicit (like ECOM-si) schemes. The mode-split option was used for the present study. The flux calculation ensures the conservation of mass and momentum over individual control volumes and thus the whole computational domain. The finite-volume numerical approach combines the advantage of finite-element methods for geometric flexibility and finite-difference methods for simple discrete code structure and computational efficiency.

FVCOM uses the modified MY-2.5 and Smagorinsky turbulent closure schemes for vertical and horizontal mixing, respectively (Mellor and Yamada, 1982; Smagorinsky, 1963). FVCOM provides optional vertical turbulence closure schemes using the General Ocean Turbulence Model (GOTM) developed by Burchard *et al.*, 2002. The present version of FVCOM contains several new modules: non-hydrostatic dynamics (Lai *et al.*, submitted); advanced data Kalman Filter data assimilation packages (Chen *et al.*, 2009); an unstructured-grid surface wave model (FVCOM-SWAVE) (Qi *et al.*, 2009), an unstructured-grid sea ice model (UG-CICE, Gao *et al.*, submitted), a sediment model (FVCOM-SED) and generalized biological model (FVCOM-GEM). An automatic nesting grid system is also implemented in FVCOM, which allows two different FVCOM models to run through the nested boundary without the need of interpolation from one to another.

2.2 *UG-RCA*

UG-RCA adapts the biological dynamics and model structure of RCA, but integrates transport and eddy diffusivity using the finite volume algorithms employed in FVCOM. Briefly, it consists of 26 water quality state variables and 23 sediment variables, including various forms of organic carbon, nitrogen and phosphorus, inorganic nutrients, phytoplankton and dissolved oxygen (Figure 2.1). Dissolved oxygen (DO) is a primary state variable of environmental concern in the simulation system. In the model, DO is computed by the reaeration flux at the sea surface, sediment oxygen demand (SOD) at the bottom and internal biological and biogeochemical dynamics in the water column such as phytoplankton photosynthetic production, respiration consumption, biogeochemical oxygen demand through the mineralization of particulate and dissolved organic matter, and nitrification. Phytoplankton growth is sustained by solar radiation and dissolved inorganic nutrients including ammonium NH_4^+, nitrate NO_3^- and nitrite NO_2^-, phosphate PO_4^{3-} and dissolved silica SiO_3^{2-}. Nutrients are formed through the mineralization of organic substances in the water column and at the sediment-water interface. In the model, organic matter is divided into dissolved and particulate forms with each being further divided into refractory and labile categories. Zooplankton grazing is not explicitly modeled with trophodynamics, but represented by a first order, temperature-dependent rate of transformation of phytoplankton into particulate and dissolved organic matter. Phosphorus, nitrogen, and silicon were parameterized in a similar way as the organic carbon pools. The total number of state

variables is 26: salinity, three phytoplankton groups (spring, summer and fall groups), four nutrients (ammonia, nitrate+nitrite, phosphate and dissolved silica), four organic phosphorus forms, four organic nitrogen pools, seven organic carbon pools (four labile and refractory dissolved and particulate forms plus two reactive and one exudate components), biogenic silica, dissolved and aqueous oxygen.

UG-RCA has 180 parameters in total. In the present model setup, however, 30 of the total 180 parameters are not used, so that there are effectively 150 parameters, listed in Table 2.2. Parameters 1–4 are the "option" parameters that control the model setup. Parameter #1 "AGMOPT" stands for "Algal Growth Model Option", by which users can select different phytoplankton growth functions: "0" to select the standard phytoplankton growth function, "1" to select the Laws-Chalup function. Parameter #2 "ACTALG" defines the number of "Active Algal Groups" effectively simulated in the model. It is assigned a value of 3 for winter-spring, summer and fall phytoplankton groups in Massachusetts Bay. Parameter #3 "KAOPT" defines the choice of reaeration parameterization: 0 for constant, 1 for spatially variable, 2 for current velocity shear dependent, and 3 for wind stress dependent. Parameter "KEOPT" defines the choice of light attenuation function: 0 for constant, 1 for spatially variable, 2 for temporally variable, 3 for 2D spatially and temporally variable, and 4 for 3D spatially and temporally variable. As PAR is used in UG-RCA whereas GoM-WRF predicts total solar radiation, parameter #5 "PAR" defines the PAR fraction or conversion factor from total solar radiation to PAR. Other parameters are defined in Table 2.2 which essentially control biological and biogeochemical rates in the model.

The sediment module in UG-RCA is essentially the same as the model developed by DiToro (2001). It is designed to capture the sinking flux of organic matter from the water column to sediments, sedimentary diagenesis transforming organic matter into inorganic nutrients, nutrient feedback from sediment to the water column, sediment oxygen demand during sedimentary diagenesis, and denitrification which converts nitrate into gaseous nitrogen (N_2) and thus leads to nitrogen loss from the system through outgassing to the atmosphere. For brevity, sediment module parameters are not listed in Table 2.2.

2.3 *Model grid*

FVCOM used for Massachusetts Bay is a sub-grid domain model (hereafter referred to as MB-FVCOM) nested within the Gulf of Maine regional domain model (hereafter referred to as GoM-FVCOM). The computational domain of MB-FVCOM is configured with 9739 cells and 5472 nodes. The horizontal resolution of this sub-grid domain varies from 290 m near the coast to 5–10 km near the nested boundary (Figure 2.2, upper panel). GoM-FVCOM consists of 27421 cells and 14777 nodes, with the horizontal resolution varying from 10–25 km in the open ocean to 1.0 km near the coast (Figure 2.2, lower panel). GoM-FVCOM uses hybrid terrain-following coordinates with a total number of 30 layers in the vertical. In shallow regions with depth < 60 m, the vertical layers are defined using the σ-coordinate, while in regions with depth ≥ 60 m, the s-coordinate is used. These two coordinates merge on the 60-m isobath at which the water column is divided by uniform layers with a thickness of 2 m. In the σ-coordinate, the layer thickness varies with water depth, with a maximum of 2 m. In the s-coordinate, five uniform layers with a thickness of 2 m are specified in the upper and lower layers adjacent to the surface and bottom, respectively. The remaining mid-depth is divided into 20 layers with thickness varying with water depth. The same vertical coordinate system was used for MB-FVCOM. The GoM regional and Massachusetts Bay sub-domain grids share common triangular cells along the nesting boundary. The model output from GoM-FVCOM at the nested boundary can directly drive MB-FVCOM with no need for any spatial interpolation. This one-way nesting approach ensures volume and mass conservation between the two computational domains.

Both GoM-FVCOM and MB-FVCOM are solved using the mode-split integration scheme. The time step is 12 seconds for the external mode and 120 seconds for the internal mode for GoM-FVCOM, and 5 seconds for the external mode and 50 seconds for the internal mode for MB-FVCOM.

UG-RCA is configured on the same grid as MB-FVCOM, but with a smaller offshore extent (Figure 2.2). It is driven by the hourly MB-FVCOM fields of water temperature, salinity, velocity and turbulence mixing diffusivities. UG-RCA is coded with the flexibility to allow users to select a different time step from the hydrodynamic model. For the Massachusetts Bay

modeling project, the time step used to drive UG-RCA is 50 seconds, with 72 time steps per hour.

2.4 *Forcing*

2.4.1 Hydrodynamic models

Both GoM-FVCOM and MB-FVCOM are driven by surface forcing (wind stress, precipitation, evaporation, surface net heat flux, and short-wave irradiance), river discharges and tidal forcing. Tidal forcing for MB-FVCOM consists of the GoM-FVCOM prediction of surface elevation at the common boundary. Available hydrographic and satellite sea-surface temperature data were assimilated for both simulations.

The surface forcing data were provided by the data-assimilated fields of the WRF (Weather Research and Forecast) model. WRF is the latest-generation mesoscale numerical weather prediction system developed principally by National Center for Atmospheric Research (NCAR) through collaboration with other government agencies (http://wrf-model.org/index.php). WRF uses the hydrostatic North American Mesoscale weather model fields as initial and boundary conditions with two-way nesting capability, and can provide continuous hindcasts and 3-day forecasts. WRF replaced the older MM5 in our GoM weather forecast model system (Chen *et al.*, 2005). GoM-WRF is configured with a "regional" domain (covering the Scotian Shelf, Gulf of Maine, Georges Bank, and the New England Shelf) and a "local" domain (covering Massachusetts coastal waters west to Long Island Sound) with horizontal grid spacing of 9 and 3 km respectively, and 31 sigma air pressure levels in the vertical with finer resolution in the Planetary Boundary Layer. All available data from the National Data Buoy Center's Coastal-Marine Automated Network (C-MAN) and meteorological buoys are assimilated. The surface wind stress, air-sea heat flux components, and evaporative flux are computed using GoM-WRF output, with a horizontal resolution of 9 km, the COARE 2.6 bulk algorithm (Fairall *et al.*, 1996, 2003), and satellite sea surface temperature. The surface radiative fluxes are computed using International Satellite Cloud Climatology Project (ISCCP) data. The resulting hindcast data-assimilated surface forcing fields are used to drive both the regional GoM-FVCOM and MB-FVCOM.

GoM-FVCOM includes 33 rivers emptying into the GoM region. Of those, 13 are inside the Massachusetts Bay sub-domain. Those, plus the MWRA outfall discharge, are included in MB-FVCOM. The freshwater discharge data from the rivers were directly downloaded from the US Geological Survey (USGS) http://waterdata.usgs.gov/ma/nwis. The Charles River discharge applying in FVCOM model is corrected by times factor of 1.13 to account for the watershed area downstream of the gage (following Menzie-Cura, 1991.) No accurate discharge data are available for the Mystic River, and its discharge was assumed to be 0.195 times the corrected Charles River discharge. The daily freshwater flow from the MWRA outfall was provided by MWRA.

Tidal forcing used to drive GoM-FVCOM was specified at the open boundary with the real o'clock time. The tidal elevation at the open boundary is calculated based on amplitudes and phases of five major tidal constituents: three semi-diurnal tides (M_2, S_2 and N_2,) and two diurnal tides (K_1 and O_1). In addition to the surface forcing and river discharge, MB-FVCOM is driven by the lateral boundary conditions specified through one-way nesting with the GoM-FVCOM model output. The surface elevation at the nesting node at the boundary is directly given by the GoM-FVCOM.

Wind, heat flux, and Merrimack River discharges in 2011 are plotted in Figure 2.3 and compared with those of 17-year (1995–2011) average. Northwest wind prevailed in January, February and March in both 2011 and the 17-year average, though the wind direction was slightly different between them, with wind slightly more northerly in 2011 than in the 17-year average in January. In terms of the monthly average, April was quiet both in 2011 and in the 17-year average, with wind speed < 1 m/s on average. The winds were mostly southerly from May through September. From October through December, north-northwesterly wind prevailed and in December, the average wind speed reached the level observed in January. Surface heat flux was mostly comparable between 2011 and the 17-year average, with high values in summer and low values in winter and late fall. Nevertheless, surface heat flux was visibly higher in June and July in 2011 than in the average. River discharge was higher in mid-February and March 2011 compared with the 17-year average. Due in part to Hurricane Irene, the summer was very wet; after the middle of July, The river discharge was particularly high in 2011 with river flow

more than triple that of the 17-year average during the same period of time. In general, in comparison to the 17-year average, 2011 was warmer in the summer and colder in the winter. The wind speed and river discharge in 2011 were both larger than the 17-year average.

2.4.2. UG-RCA surface forcing

UG-RCA is directly driven by the hourly model output field of MB-FVCOM. In addition to the initial and open boundary conditions, UG-RCA requires the surface wind speed and solar radiation as the surface forcing. The wind speed (w) is used to determine the reaeration rate for oxygen exchange at the air-sea interface, which is formulated as:

$$F_{O2} = k\left(DO_{sat} - DO\right) \tag{2.1}$$

$$k = 0.728\sqrt{w} - 0.317w + 0.0372w^2 \tag{2.2}$$

$$DO_{sat} = 14.6244 - 0.36713T + 0.0044972T^2 + 0.0966S + 0.00205S\cdot T + 0.0002739S^2 \tag{2.3}$$

where F_{O2} is the oxygen reaeration flux, DO_{sat} is the dissolved oxygen saturation concentration determined with an empirical function of temperature (T) and salinity (S) (Hyer *et al.*, 1971; HydroQual and Normandeau, 1993), and k is the piston coefficient (also called the piston velocity) of the oxygen air-sea exchange, determined by an empirical function depending on the wind speed (Banks and Herrera, 1977).

The solar radiation is used to compute the phytoplankton growth rate based on the Laws-Chalup function:

$$\mu_{\max} = \frac{G_{pre}\left(1-k_{RG}\right)\left(1-f_{SC}\right)I}{G_{pre}\Big/G_{pr0} + I\left[1+G_{pre}\Big/\left(I_S G_{pr0}\right)\right]}, \tag{2.4}$$

where I is the photosynthetically active radiation PAR (einsteins m^{-2} d^{-1}) and I_s is the half-saturation radiation (Laws and Chalup, 1990). These and other parameters are listed in Table 2.2.

Calibrated with satellite-derived shortwave irradiance and available measurement data at the coast, GoM-WRF provides the light intensity at surface required for UG-RCA. The GoM-WRF-predicted total short-wave radiation was then converted into PAR using a conversion

factor of 0.437 determined based on decadal SeaWIFs PAR data and GoM-WRF-predicted total solar radiation (Chen *et al.*, 2010).

2.5 *Nutrient loadings*

Nutrient and carbon loadings include the MWRA effluent outfall from the Deer Island Treatment Plant (DITP), non-MWRA point sources, non-point sources, river discharge and atmospheric sources. Each source was specified based on recent observed data when available, combined with historical observations and estimates.

MWRA conducts daily measurements of treated sewage flow in millions of gallons per day and daily or weekly concentration of various pollutants in mg l^{-1}. The data for NO_3^-, NO_2^-, NH_4^+ and PO_4^{3-} were directly used to drive UG-RCA, while the bulk-parameter data of Carbonaceous Biochemical Oxygen Demand (CBOD), Total Kjeldahl Nitrogen (TKN) and Total Phosphorus (TP) were first converted and partitioned into model variables (Tables 2.3). For example, CBOD was converted into total organic carbon using the function TOC = 0.7CBOD+18 (HydroQual and Normandeau, 1993) and then partitioned to each organic matter pool using the functions listed in Table 2.3. TKN and TP were converted into total organic nitrogen and phosphorus and then partitioned into their respective organic pools. Silicate was not analyzed on a regular basis in the MWRA effluent. To help determine the silicate loading, MWRA collected four samples over the period of May 19–22, 2009. MWRA's Department of Laboratory Services reported an average value for these samples of 90 μM Si. This value was less than one quarter of the value (12.5 mg/L = 446.4 μM Si) suggested by HydroQual and Normandeau (1993; p.3-6) for all RCA simulations. We replaced the previous value used in RCA with the value estimated from the 2009 measurements.

Values for non-MWRA treatment plants are primarily based on historical estimates (Menzie-Cura, 1991) rather than recently-measured wastewater flows and concentrations, and may therefore tend to be overestimated.

Non-point source loadings comprise the storm drain system-derived runoff, including combined sewer overflow (CSO), and groundwater discharge which are fully based on historical

estimates (Menzie-Cura, 1991; Alber and Chan, 1994). For runoff from combined sewer systems, updates were conducted using the total estimated CSO volume at the Mystic/Chelsea confluences, the upper Inner Harbor, the lower Inner Harbor, Fort Point Channel, North Dorchester Bay, South Dorchester Bay and the Neponset River estuary. Estimated annual outflow at these sites were provided by MWRA. These data were divided into monthly values following the same monthly variation in freshwater discharge as the Charles River. The Charles River discharge is correlated with the precipitation in the region (Appendix A of Libby *et al.* 2009). The pollutant concentrations in combined sewage reported by Alber and Chan (1994, their table 2.4) were used to estimate the contaminant loadings for all BEM simulations to date. The groundwater discharges and those from other non-MWRA treatment plants were specified using the same value estimated by Menzie-Cura (1991).

The river discharges included in the UG-RCA simulation were the Charles River, Neponset River and Mystic River. The Merrimack River was included in MB-FVCOM, but not in UG-RCA since it was located outside the UG-RCA sub-domain. The nutrient concentrations near the mouth of these three rivers were measured by MWRA as part of its CSO receiving-water monitoring program; the nutrient loading from these rivers were estimated using the monthly averaged values. Measurements were made of inorganic nutrients, organic phosphorus, particulate organic nitrogen (PON) and dissolved organic nitrogen (DON). The river loadings were estimated by multiplying the river discharge rate by the nutrient concentration. The measured inorganic nutrients can be directly used, whereas the total organic phosphorus must be converted into model variables using the functions listed in Table 2.3. PON and DON measured in rivers were split equally into refractory and labile pools of RPON, LPON, RDON and LDON, respectively. Because standard aquatic measurements of nutrients and carbon do not determine how much is refractory, labile, or very labile (reactive), the coefficients in Table 2.4 are used to partition the measured amounts into the model state variables (HydroQual and Normandeau, 1993.)

The atmospheric loadings were determined using the values estimated by Menzie-Cura (1991). These values were used in the previous BEM simulations (HydroQual and Normandeau, 1995; HydroQual, 2000; HydroQual, 2003; Jiang and Zhou, 2004b; Tian *et al.*, 2009, 2010). The

loadings included both dry-fall and wet-fall inorganic and organic nitrogen, phosphorus, and carbon.

For organic carbon loading, non-MWRA sewage treatment plants contributed the largest value in 2011 (31%), followed by the MWRA outfall (24%), atmospheric (17%), non-point sources (15%) and rivers (13%) (Figure 2.4). The load of carbon from the MWRA outfall was similar to most recent years; 2005 was relatively high and 2007 slightly lower than other years from 2005-2011 (Figure 2.5). The 2011 nitrogen loading from the MWRA outfall represented the same percentage as in 2010 and was similar to other recent years; the MWRA outfall represented the largest input (48%), followed by the atmospheric flux (28%), non-MWRA point sources (13%), non-point sources (7%) and river discharge (4%). For phosphorus loading, the MWRA outfall again contributed the largest portion (49%), followed by non-MWRA point sources (28%), non-point sources (15%), river discharge (5%) and atmospheric flux (3%). In contrast to nitrogen, the phosphorus discharge from the MWRA outfall was 12% lower than the average load from 2005 to 2010.

2.6 *Open boundary conditions for UG-RCA*

The UG-RCA simulation requires the open boundary conditions of water quality state variables. Following the previous BEM simulation approach, bi-weekly open boundary conditions were specified by using the objective analysis (OA) procedure to interpolate the MWRA field data (Libby *et al.* 2012) onto the boundary nodes. The field measurements were made approximately monthly from February through October, at five stations near the MWRA outfall (called "nearfield" stations indicated by "N") and six farfield stations indicated by "F" (Figure 2.6). Three additional cruises were conducted for the *Alexandrium* red tide monitoring program on May 25, June 1, and 8; these included a subset of the nearfield and farfield stations plus additional ("AF") stations (Figure 2.6). The stations in red in Figure 2.6 denote those stations sampled in past years but not in 2011.

The 2011 data included 12 variables: Chlorophyll, DO, NH_4^+, NO_3^-, PO_4^{3-}, SiO_3^{2-}, DON, DOP, PON, POC, POP, and salinity. DOC and Biogenic silica were measured in past years but not in 2011; these two variables were replaced by the climatology data provided by MWRA. DON was

estimated by the difference between the total dissolved nitrogen (TDN) and total dissolved inorganic nitrogen (NO_3^-, NO_2^-, NH_4^+). DOP was estimated by the difference between total dissolved phosphorus (TDP) and dissolved phosphate (PO_4^{3+}). Particulate phosphorus (PARTP) was used as POP. DON and PON were split equally into labile and refractory pools. The partition coefficients for organic carbon and phosphorus are listed in Table 2.4.

The OA-mapped chlorophyll field at the open boundary was partitioned to the three phytoplankton groups using the partition coefficients listed in Table 2.5. The fraction of the phytoplankton community represented by each group changes over time along the open boundary, and over time and space in the interior. The coefficients in Table 2.5 are the partitions imposed at the open boundary during each season of the year. From January to April, the chlorophyll along the boundary was considered as entirely comprised of the winter-spring phytoplankton group with a zero partition coefficient for the other two phytoplankton groups. May was considered as a transition period with boundary chlorophyll being equally split into winter-spring and summer phytoplankton groups. In June and July, the boundary chlorophyll belonged to the summer phytoplankton group. August was another transitional period with boundary chlorophyll being split into the summer and fall phytoplankton groups. Chlorophyll on the boundary consisted of only fall phytoplankton in September and October and was split into winter-spring and fall phytoplankton groups in December. The carbon to chlorophyll ratios of phytoplankton were 40, 65 and 15 for winter-spring, summer and fall phytoplankton, respectively (HydroQual, 2000; HydroQual, 2003; Jiang and Zhou, 2004b; Tian *et al.*, 2009).

The OA analysis was done using the OA software called OAX. This software was developed by Bedford Institute of Oceanography (Hendry and He, 1996). We used this method in the 2006–2010 BEM simulations (Tian *et al.*, 2009, Chen *et al.*, 2010, Tian *et al.*, 2010 and Zhao *et al.*, 2011). In the OAX, the covariance function (R) between data and estimation site is based on their pseudo-distance (r) determined as:

$$R(r) = (1 + r + \frac{r^3}{3})e^{-r} \tag{2.5}$$

$$r = \sqrt{\left(\frac{x_d - x_m}{a}\right)^2 + \left(\frac{y_d - y_m}{b}\right)^2 + \left(\frac{z_d - z_m}{c}\right)^2 + \left(\frac{t_d - t_m}{T}\right)^2} \tag{2.6}$$

where x, y, z, and t are the four spatial and temporal coordinates; the subscripts d and m indicate data and model positions, respectively; and parameters a, b, c, and T are the de-correlation scales for their corresponding coordinate. Given the fact that the measurement sites were away from the open boundary and measurements were made on a monthly basis, the OA analysis was done with relatively large de-correlation scales: 30 km in the horizontal, 15 m in the vertical and 45 days in time.

Examples of the OA-mapping results on the open boundary for April 15 and August 15 are presented in Figure 2.7. Given the low frequency of field observations and the large distance between the open boundary and the observation sites, particularly for the South Passage, the OA-mapped results should be interpreted with caution. Briefly, chlorophyll concentration was higher in April than in August and a slight subsurface chlorophyll maximum was observed on the April transect. Nutrients showed high concentrations in the deeper channel and low values in the surface layer with a strong stratification both in April and August. Ammonium showed higher values in deeper areas on the April transect but was low in August with slightly higher values at mid-depth. Similar to chlorophyll, DO concentration was higher in April than in August. In general, particulate organic substances were more abundant in surface layers than in deeper layers and slightly higher in the North Passage than in the South Passage. Dissolved organic substances displayed higher values at mid-depth in April; in August the higher values were found from the mid-depth to the bottom.

Interannual variability in nitrate concentration at the open boundary determined through OA mapping is illustrated in Figure 2.8 for the years 2011, 2010 and 2009. The observed nutrient concentrations in 2011 were quite uniform in the winter season along the open boundary, compared with the previous years such as 2010 and 2009. On the boundary transect of Jan 30, nitrate concentration in 2011 was mostly around 9 μM, compared to 4-9 μM increasing from South to North in 2010 and about 4–11 μM increasing from South to North in 2009. Similar patterns were observed on the March 1 transect, with nitrate concentration around 8 μM in 2011, compared to 2–8 μM in 2010 and 4–12 μM in 2009, in both cases increasing from South to North. As the North Passage is the major pathway for Gulf of Maine water flowing into MB, a low nutrient concentration at the open boundary, as was seen in 2011, can affect nutrient supply

to MB in winter and thus have the potential to influence phytoplankton development during the spring bloom season through nutrient limitation.

3. Results

3.1 *Physical Fields*

3.1.1 Model-data comparisons

The BEM is designed to assess the water quality of Massachusetts Bay (MB). Since this system is highly controlled by the physical environment, available data were assimilated into the hydrodynamic model MB-FVCOM to provide the best known physical fields for the water quality model. These data included the satellite-derived sea-surface temperature (SST) and all available hydrographic data. The model-data comparisons described here demonstrate how well MB-FVCOM, with these assimilated data, provides realistic physical fields.

Figures 3.1 and 3.2 show the comparison between model-predicted and observed temperature and salinity at selected MWRA monitoring stations N01, N07, F10, F06, F13, and F22. Stations N01 and N07 are located in western MB. Station F10, F06, and F13 are located in the middle of the study area close to the coast. Station F22 is in the northern part of the study area (see Figure 2.6). Assimilation of SST and hydrographic data made the model-predicted temperature and salinity match the observations well, but in several cases, data assimilation caused rapid adjustments in the simulated results.

The water column was stratified from spring to late fall, with large temperature and salinity differences between the surface and bottom. The largest temperature differences occur at the end of July and may reach about 13 °C as shown in Figure 3.1 with Stations N07 and F22. High-frequency (weekly) fluctuations in temperature were observed at the selected stations.

Salinity displayed larger fluctuations near the surface than near the bottom. The variation was particularly high at Stations N07 in MB and F22 in the northern part of the study area, signaling the impact of the freshwater discharge from the Merrimack River just north of MB.

Figures 3.3–3.7 compare the near-surface distributions of temperature and salinity. Note that the plots of observed data gathered all the observations for the month. For most months there is only one survey, generally completed on one day; only in May and June 2011 were there

multiple one-day surveys because of the red tide bloom. The model plots gathered model results for the same time as each observed data point. After the observed data and modeled results were gathered for the month, they were contoured. The assimilation worked well to reproduce observed fields of temperature and salinity. In February, there was a mostly homogeneous distribution of both temperature and salinity (Figure 3.3). Only a slight inshore-offshore gradient was observed in the model results for temperature, within a range of 0.8 °C. In April, both temperature and salinity showed a slight inshore-offshore gradient and good agreement between model and observations (Figure 3.4). In June, the temperature showed an offshore-inshore gradient with low temperature in the offshore region and high temperature in the inshore region (Figure 3.5). In contrast, salinity displayed an opposite gradient, with high values in the offshore region and low values in the inshore region and Boston Harbor (Figure 3.5). Temperature was considerably higher in June (ranging from 15 to 16 °C) than in April (6–7 °C). In August, the surface temperature reached 18–19 °C, but with little spatial variation (Figure 3.6). Although the surface temperature was slightly higher in the southern end of the domain than in the northern part of the bay, the difference remained < 0.5 °C. The difference between the model prediction and observation was also smaller than 1 °C with the model being slightly warmer. Salinity, on the other hand, displayed a notable inshore-offshore gradient, with particularly low values in the northwestern part of the simulation domain and high values in the offshore region. In October, the surface temperature decreased to below 13 °C, but no notable spatial distribution pattern is discernable with the color scales used for mapping (Figure 3.7).

3.1.2 Monthly surface sub-tidal currents, temperature and salinity

The surface monthly sub-tidal current field from January through April was characterized by four major features (Figure 3.8):

(1) Offshore coastal current flowing south-southeastward from the Western Gulf of Maine Coast toward the offshore side of Cape Cod. This current was strong in January and weakened gradually through April;

(2) Current bifurcation at the North Passage entrance, with one branch flowing south-southeastward and the other entering MB. The bifurcation was the most evident in March among the four months depicted in Figure 3.8 and weakest in April;

(3) General counter-clockwise circulation in MB with inflow through North Passage and outflow in South Passage. This counterclockwise circulation was also the strongest in March and weakest in April, similar to the offshore coastal current;

(4) Mesoscale eddies that change in space and time.

Eddies were barely discernible in January and February, but well-developed in March and April at the north passage. The surface current pattern in May persisted more weakly into June, with a combination of a baywide counterclockwise circulation pattern and smaller-scale eddies. In July and August, however, the current pattern was essentially dominated by eddies rather than a baywide circulation pattern (Figure 3.9). In July, two eddies were developed and could be identified at the North Passage and in Cape Cod Bay. Three eddies were identified in August: one in the North Passage, another in the northwestern corner of the simulation domain and the other one in Cape Cod Bay at the southern end of the simulation domain. From September through December, the eddies became weaker and the currents gradually returned to the winter-spring pattern; the offshore coastal current and the counterclockwise circulation within the bay intensified, and mesoscale eddies diminished (Figure 3.10).

To examine the seasonal variability of water properties, we present in Figures 3.11–3.16 the model-predicted temperature and salinity field near the surface at the end of each month. In section 3.1.1, we showed that the water is seasonally well-stratified in Massachusetts Bay except in the shallow area of Boston Harbor. The monthly fields show that surface water temperature was not spatially uniform in the Bay. The surface temperature was the coldest in January and February, with temperature ranging from 2 °C within the bay, particularly in Cape Cod Bay, to 4 °C in the offshore region (Figure 3.11). Surface temperature started to rise in March, ranging from 3 to 5 °C. In April, surface temperature rose to 7–9 °C. The surface water temperature distribution in May and June was characterized by high temperature in Cape Cod Bay and much of MB; temperature reached 16 °C in May and 20 °C in June (Figure 3.12). In July, the surface layer in the whole simulation domain was occupied by warm water with temperature reaching 20 °C everywhere except along the coast north of Cape Ann. The northern part of the study area cooled during August. Surface temperature decreased to below 15 °C in September and 13 °C in October, without notable spatial variation within the simulation domain (Figure 3.13). This cooling trend continued through the remainder of the year; the temperature dropped below 11 °C in November and below 9 °C in December.

Salinity in January through March showed little influence of freshwater inputs (Figure 3.14). Low salinity surface waters were perceptible only near the mouth of the Merrimack River and in Boston Harbor. In April, the lower salinity water extended to a great part of the Bay while forming an inshore-offshore gradient and in May, fresher waters extended further offshore. Surface salinity decreased in May and started to increase again in June in the offshore region. During July–September, high-salinity waters were found throughout most of MB (Figure 3.15). Surface salinity increased again in the offshore region in October and November and the high-salinity water extended into the Bay in December, forming a spatial distribution at the end of the year similar to that observed in January (Figure 3.16).

3.1.3 Comparison with previous years' simulations

As a comparison with the previous year, the monthly surface current, temperature and salinity are shown for April and September 2011 and 2010 (Figures 3.17–3.19). As mentioned earlier, the coastal current in the offshore region from MB was well developed in April 2011 and much stronger than that in 2010 (Figure 3.17). The basin-wide clockwise circulation in MB was visible in 2011, but was mostly absent in 2010. For the case of September, the major difference in the surface current field was the eddies that developed in 2011 near the North Passage and the South Passage, which were mostly absent or weak in the 2010 simulation.

As for the temperature comparison, surface waters were considerably cooler in 2011 than in 2010 (Figure 3.18). In April 2011, the surface water temperature was 1.5-3 °C lower than in 2010. The surface water temperature was also slightly cooler in September 2011 than in 2010, but with a much smaller difference between the two years. The temperature difference was mostly around 1 °C in MB in September while it had reached above 3 °C in April. On the other hand, surface waters were considerably saltier in April 2011 than during the same period in 2010 (Figure 3.19) by more than 2 psu through much of the simulation domain. It should be pointed out that this difference coincides with the relatively high river discharge observed in early spring 2010. In September, in contrast, surface salinity was lower in 2011 than in 2010 (Figure 3.19). The difference was particularly high in Boston Harbor and at the Merrimack River mouth, where the surface salinity was about 1 psu lower in 2011 than in 2010. The river discharge was

particular high in September 2011 due to Hurricane Irene in late August, as we previously noted (Figure 2.3), while summer 2010 was quite dry (Zhao *et al.*, 2011).

3.2 *Water quality fields*

3.2.1 Model-data comparisons

Data-model correlation analyses of key variables are presented in Figure 3.20, including surface chlorophyll, NO_3^-, SiO_3^{2-}, NH_4^+, and bottom DO and DO saturation. Good correlations were found between the modeled and observed results for NO_3^- near the surface and DO near the bottom, although for NO_3^- especially, the model tends to underestimate the values. The correlation coefficient was 0.91 for surface nitrate and 0.92 for bottom DO. For the near-surface silicate, the correlation was not as good as that for nitrate and DO. Basically the model tended to underestimate silicate at the high end of the concentration range. The correlations for surface chlorophyll and ammonium data were poorer than other variables. Unlike the dissolved oxygen concentration, for which the model prediction was well-correlated to and just slightly lower than the observation, the model tended to underestimate the saturation of dissolved oxygen. The saturation of dissolved oxygen was not directly modeled, rather it is calculated based on temperature, salinity and DO concentration. Biases in the simulation of these different parameters could all influence the accuracy of DO saturation estimates.

Annual cycles of key variables were plotted with the observational data for visual comparison (Figures 3.21–3.23). Chlorophyll concentration showed less variation over the year in the simulation compared to the observation; both high and low values observed at certain stations were not reproduced by the model (Figures 3.21–3.23). The absence of dominating bloom events was a common feature in the 2011 simulation at most of the nearfield stations (Figure 3.21). The higher chlorophyll concentration can be observed in summer and fall, but the low amplitudes and short duration do not constitute dominant blooms. Instead, the predicted highest values of chlorophyll concentration in the near field stations occurred at the very beginning of the year, rapidly decreasing to the yearly low at the end of January with values falling from about 4μg/l to 1 μg/l (Figures 3.21–3.22). In the report on model results for 2010 (Zhao *et al.*, 2011), the chlorophyll concentration at the same stations were observed to rise particularly high (higher than 4 μg/l) in the winter of 2010. It may be that a winter bloom

occurred in late 2010 and the early January of 2011, as we have no shipboard observations during that time. However, data from continuous monitoring buoys off Cape Ann and the New Hampshire coast show low surface chlorophyll during winter 2010-2011. The 2011 spring bloom was slightly better developed at some farfield stations (e.g., F29 and F01), but essentially absent at others (e.g., stations F10 and F15) (Figure 3.22). The data did not show a typical fall bloom at these stations either. At the harbor stations, neither the model nor the data revealed dominating bloom events (Figure 3.23). Basically, chlorophyll concentration stayed at the relatively high level during a long period of time from spring through fall. As mentioned in Tian *et al.* (2009), the shallow depth and multiple anthropogenic and natural nutrient sources contribute to the sustained high primary production in the harbor during the summer. Taylor *et al.* (2010) did a comparison of multi-year averaged seasonal cycles of major water quality variables. They found that even though chlorophyll levels remain relatively high during the summer season in Boston Harbor, chlorophyll decreased after the diversion of the MWRA outfall from the harbor to the offshore location.

The vertical distribution of modeled chlorophyll along a west-east transect (see Figure 2.6) across the outfall to the end of the model boundary is shown in Figures 3.24–3.25. As expected, chlorophyll concentrations were generally higher in the upper layer. In January, vertical mixing and subsequent light limitation kept chlorophyll levels low except in the harbor, with its shallower depths. Higher chlorophyll values were seen throughout most of the bay out to Stellwagen Bank in February. The higher concentration occurred in the at mid-depths in March, as density stratification began developing. A surface or subsurface chlorophyll maximum persisted across the bay through October, after which the vertical variation in chlorophyll was less pronounced.

Model-estimated and observed dissolved inorganic nitrogen (DIN) showed similar seasonal variation at most of the monitoring stations, for the surface as well as near the bottom (Figures 3.26 and 3.27). Typically, DIN was replenished during the winter mixing season. DIN depletion in surface waters was observed in March and April when DIN concentration decreased to a very low level due to the consumption by phytoplankton. DIN remained at a low level through summer and early fall and was replenished again in late fall and winter by vertical mixing. In contrast to surface waters, DIN in the bottom layer stayed at a relatively high level all through

the summer and fall seasons, indicating a stratification in DIN concentration at most of the monitoring stations. At some farfield stations—Station F06 and F13 for example—the model tended to underestimate nutrient concentration in the bottom layer (Figure 3.27). Surface and bottom layers were observed to have had low concentrations of DIN in the spring, and this predicted by the model. However, during the summer high DIN concentrations—up to 7 μM—were observed in bottom waters at these stations. These stations are located in of the northern part of Cape Cod Bay with a depth about 32 m and 28 m. These bottom depths would be expected to be within the euphotic zone and nutrients should be taken up within a reasonable period of time. As such, there might be local nutrient sources that are not captured by the model. One possible nutrient input is through groundwater (Becker, 1992, Jiang *et al.* 2007). Although groundwater sources were considered in the UG-RCA setup, the configuration was based on historical estimates without spatial structure. Another possible source is through horizontal advection. As we will show later in the report, the dispersion of the MWRA outfall effluent is mostly restricted to the local domain during the summer stratified season. Only during the well-mixed season in winter was dispersion found down to Cape Cod Bay, as for the 2009 and 2010 model projection (Tian *et al.*, 2010; Zhao *et al.*, 2011). At most of the harbor stations including the farfield station F23 off the harbor mouth, similar magnitudes and seasonal cycles were observed and simulated. Nutrient depletion affects the whole water column—there is no stratification in nutrient concentration (Figure 3.28). Only at stations 024 and 124 were higher DIN concentrations found in the bottom layer than in the surface layer. Station 024 is located in the Charles River mouth and Station 124 is located in the southeastern corner of Boston Harbor, within Hingham Bay, where freshwater discharge and local events can modify nutrient concentration on a local scale.

Along the west-east transect across the outfall to the end of the model boundary, the DIN plume located at the outfall could reach at the sea surface in January and February (See Figure 3.29). From March to October, the DIN plume at the outfall is only visible up to mid-depth, gradually spreading along the bottom layer. In November and December, the higher DIN concentrations begin to reach the surface and as the water column becomes vertically well mixed as shown in Figure 3.30).

Model-simulated primary production was depicted at three monitoring stations where field observations had been made in past years (Figure 3.31). Modeled primary production did not show typical peaks for spring and fall blooms, but rather remained at a relatively high level throughout the summer season. Primary production at the nearfield station N18 close to the MWRA outfall was not particularly higher than that at other stations. At all three stations, modeled primary production increased gradually in spring and dropped somewhat more abruptly in late fall.

Most of the DON and PON data were reproduced by the model (Figures 3.32–3.33; 3.36–3.37) except for particularly high observed DON values (e.g., DON at Stations F15 and N18 in Figure 3.32) and some of the lower PON values (e.g., PON in the bottom layer at Stations F10, F13, and F06). DON showed very little seasonal variation, in contrast to PON which manifested relatively high values from spring through late summer and low values during the winter mixing season. Approximately following the chlorophyll distribution, predicted PON did not display dominant bloom events, rather short-term fluctuations with limited amplitudes. No anomalous signal was found near the outfall in either DON or PON, showing that the organic nitrogen pools are essentially controlled by internal dynamics within the water column and the outfall effluent did not noticeably alter their distribution. As shown in Figures 3.34–3.35, DON is well mixed vertically from along the whole transect from east to west in winter and fall seasons. In the spring and summer, the higher concentrations occupied the upper layer of the water. The higher concentration of PON appeared near shore first and then spread across the upper layer of the bay (See Figures 3.38–3.39).

Predicted POC displayed high frequency variations without dominant seasonal events (Figures 3.40 and 3.41). POC was relatively low in winter and high during all other seasons. At most of the nearfield stations and at Station F22 as well (Figure 3.40), the model tended to overestimate the concentration of POC, particularly in the bottom layer. Model-data comparison of surface (but not bottom) POC appeared to be better at certain farfield stations in terms of magnitude, but both the data and simulation are characterized by high frequency variations with relatively little seasonal pattern. The POC along the west-east transect is relatively low and well mixed vertically. Higher POC water appears at the outer boundary in April and then spreads

down to the bottom in June (See Figure 3.42). The concentration of POC decreases after July as shown in Figure 3.43.

Relatively good comparison of DO has been obtained between simulation and observation (Figures 3.44 and 3.45). The annual variation is well-reproduced by the model, but in 2011 the predicted values were low compared to the observations. Comparing the bottom DO model *vs*. observation correlation, the correlation coefficient is 0.95 in 2010 (Figure 3.21 in the 2010 report) and 0.91 in 2011 (Figure 3.20). To find out what factor caused the model results to be less accurate than 2010, we did some dynamic analysis for DO. As shown in Figure 3.46, the Oxidation (consumed DO) was larger in 2011 than 2010. The difference is shown in the lower panel of Figure 3.46. That may cause the simulated value of DO to be lower in 2011. A remaining question is whether the oxidation is accurately represented, or if the low value is caused by not having observations of DOC along the boundary. Future work may include a test such as adjusting the DOC climatology data to see how it affects the value of oxidation.

DO displayed high values during the spring, but stayed at a low level during the summer and fall season. The model tended to underestimate the DO level during the spring peak DO concentration period, but the difference remained minimal compared to the total concentration. As pointed out by Tian *et al.* (2009), the high DO values in spring reflected photosynthesis production through phytoplankton growth, whereas remineralization of organic substances occurred in summer and fall so that DO stayed low during that period of time. Water mass inflow through the open boundary and horizontal advection can also alter bottom DO concentration in the region (Libby *et al.*, 2008). As shown in Figures 3.47–3.48, DO concentration on the east-west transect was vertically well-mixed along the whole transect in winter, and concentrations were high. From spring onward, the DO concentration decreases and becomes stratified; the stratification persists through October.

Most selected stations shown for DO saturation had the same pattern (Figures 3.49–3.51). In the winter season, mixing throughout the water column ensures the DO saturation was the same surface and bottom. Beginning in the spring, the surface DO saturation increased and reached a maximum in early summer then decreased. In contrast, the bottom DO saturation decreased continuously from the spring to late fall and then increased back to typical high winter levels.

Note that observed percent saturation in Figures 3.49–3.51 was calculated from observed oxygen concentration, temperature, and salinity using equation 2.3. In comparison to these calculated data, the model underestimates the value at most stations shown in Figure 3.49–3.51.

For some stations within Boston Harbor such as 139, 140 and 142, the DO saturation was quite uniform year round. Along the west-east transect across the outfall to the eastern model boundary, the predicted DO saturation was well mixed vertically in winter, and then the stratification increased as shown in Figures 3.52–3.53.

Sediment nutrient fluxes and oxygen demand (SOD) at three stations in BH (BH02, BH03 and BH08A) and three stations in Massachusetts Bay (MB01, MB03 and MB05) at which these fluxes were measured in earlier years (Figure 2.6). Figures 3.54–3.55 only show the 2011 model results. The predicted ammonium fluxes were higher during summer and early fall at the harbor stations as compared with the bay stations (Figures 3.54), indicating that remineralization contributed a substantial share to the increased nutrient supplies in summer in BH. A similar pattern was observed for SOD (Figure 3.55), with low flux at the bay stations and high flux in the harbor during summer and fall.

In summary, the UG-RCA 2011 simulation reproduced most of the observed magnitudes and seasonal variations of an array of parameters. For some specific cases, however, model-data deviation was observed, such as the underestimation of chlorophyll concentration in the Boston Harbor station 024 and 124 during the summer, overprediction of bottom PON in Massachusetts Bay, and underprediction of dissolved oxygen percent saturation.

3.2.2 Comparison with previous years simulations

In this section we compare the UG-RCA simulations of 2009, 2010 and 2011. Indicated by the chlorophyll concentration (Figure 3.56), 2009 was characterized by a large spring phytoplankton bloom. The bloom started around early April, reached its peak at the end of April and early May, and terminated around mid-June. In 2010, however, there was only a small short bloom that started in early April and terminated near the end of the same month. The timing of the bloom was earlier than 2009, with peak concentration reached in early April, but an

amplitude considerably lower than that in the previous year. There was no significant spring bloom simulated in 2011. The peak concentration of chlorophyll appeared in the winter season, and two-week duration small blooms were predicted during September. In 2009, in contrast, the fall bloom was mostly absent from the simulation, without a typical peak of chlorophyll concentration. In 2010, an earlier, small bloom was predicted with a peak concentration around the end of September and early October. The DIN seasonal cycle was generally similar among the three years, with high values in winter, low values in summer and replenishment in late fall (Figure 3.57). Nonetheless, slight differences can be seen from year to year. DIN concentration was high in winter and early spring 2009, but relatively lower in 2010 and 2011.

For bottom DO, no substantial difference was observed between the three simulation years (Figure 3.58). DO displayed high values during the spring phytoplankton bloom season and low values in late summer and early fall over all three years. The DO level was quite similar at the end of the annual simulation in 2009 and 2011, but was relatively higher at the end of 2010.

4. Projection Experiments

We conducted a model run without MWRA effluent to assess the potential influence of the MWRA outfall on the water quality and ecosystem function in Massachusetts Bay. In this section, we refer the initial run with the MWRA outfall as the "control run" and the sensitivity-analysis run as the "non-sewage" run. We compared the chlorophyll concentration, dissolved inorganic nitrogen, and DO between the two simulations. The results are similar to those of "no sewage" projection runs conducted for other years in past model studies (HydroQual and Normandeau 1995; Jiang and Zhou 2006b; Tian *et al.* 2009; Chen *et al.* 2010; Tian *et al.* 2010, Tian *et al.* 2011). In field observations we can only compare "prediversion" with "postdiversion", and except in the immediate area of the outfall no changes have been observed, and those changes are no greater than predicted prior to outfall operation. In contrast, the Bays Eutrophication Model allows us to isolate effects of the discharge that may be seen some distance away, even though those effects are too small to have any ecological significance.

The intensities and seasonal variations of the chlorophyll concentration for these two runs were almost identical (Figure 4.1). Even though the two simulation lines were not fully superposed on each other, the difference between them remained negligible throughout the year. Thus the model predicts that nutrients from the outfall have no notable influence on chlorophyll concentrations.

The seasonal cycle of DIN near the surface was also similar between the two simulations (Figure 4.2). The results of the two model runs were almost the same in summer. A noticeable difference was found in winter, during which the "non-sewage" run predicted lower surface DIN concentration than the control run with the MWRA outfall. Near the bottom, the non-sewage run predicted a notably lower DIN concentration than the control run near the outfall, whereas the two predictions were more comparable at other stations (Figure 4.3). This result is consistent with field measurements that show elevated levels of DIN near the outfall (Libby *et al.* 2009, 2012). The DO results were practically identical between the two simulations, indicating that the MWRA outfall does not have a notable influence on the DO level in the simulation domain (Figures 4.4–4.5).

To investigate the extent of the difference between the two runs for ammonium—the most abundant form of nitrogen in the outfall sewage discharge—we plotted the spatial distribution of bottom-layer ammonium difference (Figures 4.6–4.8). This is consistent with field observations of dissolved inorganic nitrogen concentrations (Libby *et al*. 2009) and with nitrogen stable isotope studies (Tucker and Giblin 2002; Tucker *et al*. 1999.) In January, ammonium from the outfall was spread along the coast down to Cape Cod Bay (CCB), but limited to the coastal region (Figure 4.6). This was also the pattern predicted when the outfall was located in Boston Harbor (Fitzpatrick and Isleib 2003, Signell *et al.* 2000). Ammonium levels in Boston Harbor were also affected by effluent dispersion. However, since local sources to the harbor have decreased so much (Taylor 2006b), the ammonium levels in Boston Harbor have dropped significantly since the outfall was moved offshore (Taylor 2006a.) In February, the effluent signal retreated to the middle of MB, and in March and April, the effluent ammonium was mostly restricted to a local domain. Restricted effluent dispersion continued through the summer and early fall until November and December when effluent ammonium dispersal extended into the Boston Harbor (Figures 4.7 and 4.8). Effluent ammonium concentration at the MWRA outfall was the highest in April, July and lowest in August. This seasonal variation is consistent with results from nitrogen stable isotope studies (Montoya *et al.*, 2003) which show the effects of sewage derived nitrogen on the food web confined to areas relatively near the outfall in summer, but occurring in Cape Cod Bay in winter months.

Certainly, effluent dispersal is controlled by the current system which can vary over time subject to wind forcing and cold water intrusion from the Western Maine Coastal Current. If we consider ammonium as a semi-conservative tracer of effluent, the two long-distance dispersions in 2011 occurred in January and December, when the stratification was weak or absent. In summary, the effluent is in most cases restricted horizontally within a local domain of about 20 km wide around the outfall location. However, based on the model prediction, long-distance dispersion can occur under particular circumstances, with nutrients transported as far as CCB. This dispersion has been previously shown (Fitzpatrick and Isleib, 2003) to be insensitive to the location of the outfall in Boston Harbor *vs.* Massachusetts Bay.

We plotted model results along a west-east transect across the outfall for the end of each month (Figures 4.9 and 4.10). The height of the effluent plume, as inferred from the ammonium concentration, varied from month to month. In January and February, the outfall plume reached to the surface (Figure 4.9). From March through October, however, the plume was mostly restricted to the bottom 10 m or so. Only in April and August did the effluent ammonium plume reach the surface in the coastal region during the stratified season. This projection of effluent plume rise is in approximate agreement with the rise height of 5-15 m predicted by Blumberg *et al.* (1996) using nearfield and farfield models. The core of the plume remained contained within the bottom layers from November to December, but its influence was perceptible up to the surface (Figure 4.10). As the plume spreads along the slope of the topography toward the coast, the absolute depth of the plume changes from place to place. Surfacing of the plume occurred during months of weak stratification, indicating that the vertical mixing basically controls the upward spread of the effluent.

Libby *et al.* (2009) did a comparison between data collected before and after the September 6 2000 diversion of the MWRA outfall from Boston Harbor to MB. Higher ammonium concentration after the diversion was found at the nearfield stations. Although field measurements are consistent with the model projection shown here, they are not directly comparable. Field measurements before the diversion were conducted when the outfall was located in Boston Harbor, while the non-sewage run here was configured without any effluent discharge into the system. A comparison of data collected before and after the relocation of the outfall shows the actual changes that have occurred; the model projection, in contrast, allows us to separate out the direct influence of the outfall on effluent concentration and distribution. Also, the data comparison in Libby *et al.* (2009) was based on the ammonium averaged over depth, region, and season, whereas here we output the instantaneous difference in the bottom layer, which represents the maximum difference predicted by the model.

As shown at the beginning of this section, no anomaly was observed in either chlorophyll or DO level corresponding to the ammonium distribution around the outfall. In fact, during the stratified season when light is available, the effluent was basically trapped within the bottom layers around the outfall. During the well-mixed season when effluent could effectively reach the surface, both light and vertical mixing were unfavorable to phytoplankton growth. As a result,

the nutrient discharge from the outfall is not projected to result in differences in biomass and DO.

5. Summary

The UMass/Dartmouth Marine Ecosystem Dynamic Modeling laboratory simulated currents, temperature, salinity, dissolved oxygen, and other water quality parameters in Massachusetts Bay for the calendar year 2011 using the unstructured grid model system MB-FVCOM/UG-RCA. The surface forcing was based on meteorological data collected at Buoy 44013 and weather model predictions; nutrient loadings were based on the MWRA monitoring data and river discharges; and open boundary conditions were established from the data collected during the MWRA monitoring program.

We first conducted a hydrodynamic simulation using the Finite-Volume Coastal Ocean Model (FVCOM) which was then used to drive the UG-RCA water quality simulation. The hydrodynamic simulation was conducted in a nesting mode within a regional domain covering the entire Gulf of Maine and Georges Bank and a more detailed local domain for Massachusetts Bay (MB). Surface forcing including solar radiation, heat flux and wind was simulated using the Weather Research and Forecast model (WRF). For the regional model, 33 rivers were included of which 13 were located in the local domain. Five major tidal constituents were included at the open boundary of the regional domain; the local model was forced by the output of the regional model at their common boundary. Data assimilation was conducted with the data from the MWRA monitoring program and other available data in the region. The hydrodynamic model successfully reproduced field observations in terms of temperature and salinity.

The UG-RCA 2011 water quality simulation reproduced most of the magnitudes and seasonal variations of the observations of nitrogen, chlorophyll, and oxygen. For some specific cases, a deviation between simulation and data was observed. The main water quality feature distinguishing 2011 from other years' simulations is that there is a high chlorophyll concentration throughout the MBS at the beginning of the year which then rapidly drops from about 4 $\mu g\ l^{-1}$ to about 1 $\mu g\ l^{-1}$ over one month. If we look back to the 2010 simulation, the chlorophyll concentration showed an increase from late fall to the end of the year. The predicted chlorophyll at the end of 2010 was high, thus the initial chlorophyll concentration at the beginning of 2011 was also high. Since during late fall 2010-early winter 2011 there are no

shipboard observations for comparison, it is not clear whether the chlorophyll variation is real or a model simulation error.

Chlorophyll was underestimated at high-concentration ranges and overestimated at low concentrations. The seasonal variation of model-predicted water quality variables was dominated by multiple small phytoplankton blooms during relatively short periods of time, particularly at nearfield stations, as compared to the previous years. Nutrient concentration in winter 2011 was again low as it was in 2010, notably lower than in 2009, which might be the reason why no dominant spring bloom was predicted. Low nutrient concentrations were also observed near the end of the year as compared with other years, particularly in the deep layers; inflow from the open boundary constitutes the major nutrient source for MB. DO showed high values during the spring phytoplankton bloom as a result of photosynthetic production, but remained at a low levels in fall, kept low by high DO consumption and low DO solubility under high temperatures. Although the annual cycle of DO was well-reproduced, the model-predicted values of DO and oxygen saturation were underpredicted in the 2011 simulation. DO dynamics are controlled by multiple factors including high consumption by increased remineralization and low solubility under the high temperatures characteristic of late summer and early fall. Horizontal advection and characteristics of the open boundary inflow can also influence the local DO level.

In our projection analysis removing the MWRA outfall from the simulation, we determined the horizontal and vertical extent of the outfall effluent plume using ammonium as a proxy. In the horizontal scale, the plume was mostly restricted to a local area around the outfall within about 20 km. However, long-distance effluent dispersal as far as Cape Cod Bay was predicted under certain circumstances in January and December 2011, consistent with past studies. In the vertical, the height of the plume was essentially controlled by vertical dynamics and mixing in the water column. In winter and late fall when the stratification is weak, the outfall effluent plume can reach to the surface layer. During the stratified season in summer and early fall, the ammonium plume was basically constrained within the bottom 10 m. However, no substantial bay-wide influence was observed in chlorophyll or DO. We believe that the timing of the effluent spreading influences its effect on the ecosystem. As the upward mixing and long-distance dispersal occurred during winter and late fall when light intensity limits phytoplankton growth, effluent nutrients were not effectively taken up and translated into

phytoplankton biomass. As predicted prior to outfall construction, the trapping of effluent nutrients in the lower layer during the summer limits the magnitude and geographical extent of their effect on the ecosystem.

6. References

Alber M. and Chan A. 1994. Sources of contaminants to Boston Harbor: revised loading estimates. Boston: Massachusetts Water Resources Authority. Report 1994-01. 113p.

Banks R.B. and Herrera F.F. 1977. Effect of wind and rain on surface reaeration. *J. Envir. Engr. Div., ASCE*. **103**: 489-504.

Becker S. 1992. The seasonal distribution of nutrients in Massachusetts and Cape Cod Bays. Masters Thesis, University of New Hampshire, Durham. 127p.

Bigelow H.B. 1927. Physical oceanography of the Gulf of Maine (Part II). *Bulletin of the Bureau of Fisheries*, **40**: 511-1027.

Blumberg A., Ji Z. and Ziegler C.K., 1996, Modeling outfall plume behavior using a far field model, *J. Hydraulic Engineering*, **112**: 610-616.

Burchard H., Bolding K., Rippeth T.P., Stips A., Simpson J.H. and Sündermann J. 2002. Microstructure of turbulence in the Northern North Sea: a comparative study of observations and model simulations. *J. Sea Res.,* **47**: 223–238.

Butman B. 1976. Hydrography and low frequency currents associated with the spring runoff in Massachusetts Bay. *Memoires. Societe Royale des Sciences de Liege*, **6**: 247-275.

Butman B., Bothner M.H., Lightsom F.L., Gutierrez B.T., Alexander P.S., Martini M.A. and Strahle W.S. 2002. Long-term Oceanographic Observations in Western Massachusetts Bay offshore of Boston, Massachusetts: Data Report for 1989-2000, U.S. Geological Survey Digital Data Series 74.

Chen C., Liu H. and Beardsley R. 2003. An unstructured grid, finite-volume, three dimensional, primitive equations ocean model: Application to coastal ocean and estuaries. *Journal of Atmospheric and Ocean Technology*, **20 (1)**: 159–186.

Chen C., Beardsley R.C., Hu S., Xu Q. and Lin H. 2005. Using MM5 to hindcast the ocean surface forcing fields over the Gulf of Maine and Georges Bank region. *Journal of Atmospheric and Ocean Technology.* **22**: 131-145.

Chen C., Beardsley R.C. and Cowles G. 2006a. An unstructured grid, finite-volume coastal ocean model (FVCOM) system. Special Issue entitled "Advance in Computational Oceanography", *Oceanography*, **19(1)**: 78-89.

Chen C., Beardsley R.C. and Cowles G. 2006b. An unstructured grid, finite-volume coastal ocean model-FVCOM user manual, School for Marine Science and Technology, University of Massachusetts Dartmouth, New Bedford, Second Edition. SMAST/UMASSD Technical Report-06-0602, 318p.

Chen C., Malanotte-Rizzoli P., Wei J., Beardsley R.C., Lai Z., Xue P., Lyu S., Xu Q., Qi J. and Cowles G.W. 2009. Application and comparison of Kalman filters for coastal ocean problems: An experiment with FVCOM, *J. Geophys. Res.*, **114**, C05011, doi:10.1029/2007JC004548.

Chen C., Tian R., Beardsley R.C., Qi J. and Xu Q. 2010. Modeling 2008 in Massachusetts Bay using an upgraded unstructured-grid Bays Eutrophication Model. Boston: Massachusetts Water Resources Authority. Report 2010-15. 127p.

DiToro D.M. 2001. *Sediment Flux Modeling*. Wiley-Interscience, New York, 624p.

Fairall C.W., Bradley E.F., Rogers D.P., Edson J.B. and Young G.S. 1996. Bulk parameterization of air–sea fluxes in TOGA COARE. *J. Geophys. Res.*, **101**: 3747–3767.

Fairall C.W., Bradley E.F., Hare J.E.,Grachev A.A. and Edson J.B. 2003. Bulk Parameterization of Air-Sea Fluxes: Updates and Verification for the COARE Algorithm. *Journal of Climate* 2003; **16:** 571-591.

Fitzpatrick, J.J. and Isleib, R. 2003. A post-audit analysis of the impacts of wastewater treatment plant outfall relocation on Boston Harbor, Massachusetts Bay and Cape Cod Bay water quality. Proceedings of the Water Environment Federation, WEFTEC 2003: Session 61 through Session 70, p. 530-555(26).

Gao G., Chen C., Qi J. and Beardsley R.C. Submitted. Development of Unstructured-grid Version CICE: Validation and Applications, Submitted to *J. Geophys. Res.*

Geyer W.R., Gardner G.B., Brown W.S., Irish J., Butman B., Loder T. and Signell R.P. 1992. Physical oceanographic investigation of Massachusetts and Cape Cod Bays. Boston: Massachusetts Bays Program. MBP-92-03. 497p.

Hendry R. and He I. 1996. Technical report on objective analysis (OA) project, Bedford Institute of Oceanography, Dartmouth, Nova Scotia. 105p.

HydroQual, Inc. and Normandeau Associates, Inc. 1993, A water quality model for Massachusetts and Cape Cod Bays. Boston: Massachusetts Water Resources Authority. Report 1993-05. 222p.

HydroQual, Inc. and Normandeau Associates, Inc. 1995. A water quality model for Massachusetts and Cape Cod Bays: Calibration of the Bay Eutrophication Model (BEM). Boston: Massachusetts Water Resources Authority. Report 1995-08. 402p.

HydroQual, Inc. 2000. Bays Eutrophication Model (BEM): modeling analysis for the period 1992-1994. Boston: Massachusetts Water Resources Authority. Report 2000-02. 158p.

HydroQual, Inc. 2001a. Boundary sensitivity for the Bays Eutrophication Model (BEM). Boston: Massachusetts Water Resources Authority. Report 2001-14. 90p.

HydroQual. 2001b. Analysis of the addition of a third algal group to the Bays Eutrophication Model (BEM) kinetics. Boston: Massachusetts Water Resources Authority. Report 2001-15. 110p.

HydroQual, Inc. and Signell R.P. 2001. Calibration of the Massachusetts and Cape Cod Bays Hydrodynamic Model: 1998-1999. Boston: Massachusetts Water Resources Authority. Report 2001-12. 170p.

HydroQual. 2002. Sensitivity of the Bays Eutrophication Model (BEM) to changes in algal model coefficients. Boston: Massachusetts Water Resources Authority Report 2002-16. 236p.

HydroQual, Inc. 2003. Bays Eutrophication Model (BEM): modeling analysis for the period 1998-1999. Boston, Massachusetts Water Resources Authority. Report 2003-03. 318p.

HydroQual, 2004. “User’s Guide for RCA, Release 3.0”, Hydroqual, Inc, New Jersey.

Hyer P.V., Fang C.S., Ruzeck E.P. and Hargis W.J. 1971. Hydrography and hydrodynamics of Virginia estuaries, studies of the distribution of salinity and dissolved oxygen in the upper York system. Gloucester Point, VA:Virginia Institute of Marine Science.

Jiang M.S. and Zhou M. 2004a. Calibration of the Massachusetts and Cape Cod Bays hydrodynamic model: 2000-2001. Boston: Massachusetts Water Resources Authority. Report 2004-08. 71p.

Jiang M.S. and Zhou M. 2004b. Bays Eutrophication Model (BEM) model verification for the period: 2000-2001. Boston: Massachusetts Water Resources Authority. Report 2004-09. 90p.

Jiang M. and Zhou M. 2006a. The Massachusetts and Cape Cod Bays hydrodynamic model: 2002-2004 simulation. Boston: Massachusetts Water Resources Authority. Report 2006-12. 128p.

Jiang M. and Zhou M. 2006b. Massachusetts Bay Eutrophication Model: 2002-2004 Simulation. Boston: Massachusetts Water Resources Authority. Report 2006-13. 126p.

Jiang, M., G. T. Wallace, M. Zhou, S. Libby and C. D. Hunt. 2007. Summer formation of a high-nutrient low-oxygen pool in Cape Cod Bay, USA, *J. Geophys. Res*., **112**, C05006, doi:10.1029/2006JC003889.

Jiang M. and Zhou M. 2008. Massachusetts Bay Eutrophication Model: 2005 simulation. Boston: Massachusetts Water Resources Authority. Report 2008-13. 82 p. Report 2008-12., 118p.

Kropp R.K., Diaz R., Hecker B., Dahlen D., Boyle J.D., Abramson S.L. and Emsbo-Mattingly S. 2001. 2000 Outfall Benthic Monitoring Report. Boston: Massachusetts Water Resources Authority. Report 2001-14, 148p.

Kropp R.K., Diaz R., Dahlen D., Boyle J.D. and Hunt C.D. 2002. 2001 Harbor Benthic Monitoring Report. Boston: Massachusetts Water Resources Authority. Report 2002-19, 74p.

Lai Z., Chen C., Cowles G. and Beardsley R.C. Submitted. A Non-Hydrostatic Version of FVCOM, Part I: Validation Experiments (submitted to *J. Geophys. Res.-Oceans*, in revision).

Laws E.A. and Chalup M.S. 1990. A microalgal growth model. *Limnol. Oceanogr.* 35, 597-608.

Libby P.S., Hunt C.D, Geyer W.R., Keller A.A., Oviatt C.A. and Turner J.T. 2000. 1999 Annual Water Column Monitoring Report. Boston: Massachusetts Water Resources Authority. Report 2000-09. 180p.

Libby P.S., Hunt C.D, McLeod L.A., Geyer W.R., Keller A.A., Borkman D., Oviatt C.A. and Turner J.T. 2001. 2000 Annual Water Column Monitoring Report. Boston: Massachusetts Water Resources Authority. Report 2001-17. 196p.

Libby P.S., Borkman D.G., Geyer W.R., Keller A.A., Turner J.T., Mickelson M.J. and Oviatt C.A. 2008. Water Column Monitoring in Massachusetts Bay: 1992-2007. Boston: Massachusetts Water Resources Authority. Report 2008-16. 170p.

Libby P.S., Borkman D., Geyer W.R., Keller A.A., Turner J.T., Mickelson M.J. and Oviatt C.A. 2009. Water column monitoring in Massachusetts Bay 1992-2007: focus on 2007 results. Boston: Massachusetts Water Resources Authority. Report 2009-04. 162p. (incl. appendices).

Libby P.S., Borkman D.G., Geyer W.R., Turner J.T. 2010. 2009 Water Column Monitoring Results. Boston: Massachusetts Water Resources Authority. Report 2010-13. 36p + appendices.

Libby P.S., Borkman D.G., Geyer W.R., Turner J.T., Mickelson M.J. and Costa A.S. 2012. 2011 Water Column Monitoring Results. Boston: Massachusetts Water Resources Authority. Report 2012-09. 41p + appendices.

Lynch D.R., Naimie C.E. and Werner F.E. 1996. Comprehensive coastal circulation model with application to the Gulf of Maine. *Cont. Shelf Res.*, 12: 37-64.

Maciolek N.J., Diaz R. J., Dahlen D., Hecker B., Gallagher E.D., Blake J.A., Williams I.P., Emsbo-Mattingly S., Hunt C. and Keay K.E. 2003. 2002 Outfall Benthic Monitoring Report. Boston: Massachusetts Water Resources Authority. Report 2003-13. 166p.

Manohar-Maharaj V. 1973. Spring run off in to Massachusetts Bay. Masters Thesis, MIT, Cambridge, 97p.

Mellor G.L. and Yamada T. 1982. Development of a turbulence closure model for geophysical fluid problems. *Rev. Geophys. Space Phys.*, **20**: 851-875.

Menzie-Cura. 1991. Sources and loadings of pollutants to Massachusetts Bays. Boston: Massachusetts Bays Program. Report MBP-91-01. 266p.

Montoya, J.P., Rathbun, K.M., and Mayo, C.S. 2003. Recent nitrogen isotope data from Massachusetts and Cape Cod Bays. Information Briefing for the MWRA Outfall Monitoring Science Advisory Panel, 6 January 2003.

Pietrzak J., Jakobson J.B., Burchard H., Vested H.J. and Peterson O. 2002. A three-dimensional hydrostatic model for coastal and ocean modeling using a generalized topography following coordinate system. *Ocean Modelling* **4**:173–205.

Qi J., Chen C., Beardsley R.C., Perrie W. and Cowles G. 2009. An unstructured-grid finite-volume surface wave model (FVCOM-SWAVE): implementation, validations and applications. *Ocean Modelling*, **28**: 153-166. doi:10.1016/j.ocemod.2009.01.007.

Signell, R.P., Jenter, H.L. and Blumberg, A.F. 2000, Predicting the physical effects of relocating Boston's sewage outfall, *J. Estuarine, Coastal and Shelf Sci*., **50**: 59-72.

Smagorinsky J. 1963. General circulation experiments with the primitive equations, I. The basic experiment. *Monthly Weather Review*, **91**: 99–164.

Taylor D.I., Oviatt C.A. and Borkman D.G. 2010. Non-linear Responses of a Coastal Aquatic Ecosystem to Large Decreases in Nutrient and Organic Loadings. *Estuaries and Coasts*:1-13. DOI 10.1007/s12237-010-9312-3.

Taylor D.I. 2006a. 5 years after transfer of Deer Island flows offshore: an update of water-quality improvements in Boston Harbor. Boston: Massachusetts Water Resources Authority. Report 2006-16. 77p.

Taylor D.I. 2006b. Update of patterns of wastewater, river and non-point source loadings to Boston Harbor (1990 - 2005). Boston: Massachusetts Water Resources Authority. Report 2006-22. 77p.

Tian, R.C., Chen C.S., Xu Q.C., Xue P.F., Cowles G.W., Beardsley R. and Rothschild B. 2009. Massachusetts Bay Eutrophication Model: 2006-2007 Simulation. Boston: Massachusetts Water Resources Authority. Report 2009-11. 147p.

Tian, R.C., Chen, C., Zhao, L.Z., Xue, P., Leo, W.S., Mickelson M.J. 2010. Modeling 2009 in Massachusetts Bay using the unstructured-grid Bays Eutrophication Model. Boston: Massachusetts Water Resources Authority. Report 2010-22. 100p.

Tucker J., Kelsey J., Giblin A. and Hopkinson C.S. 2002. Benthic Metabolism and Nutrient Cycling in Boston Harbor and Massachusetts Bay: Summary of Baseline Data and Observations after One Year of Harbor-to-Bay Diversion of Sewage Effluent. Boston: Massachusetts Water Resources Authority. Report 2002-13. 83p.

Turner J.T. 1994. Planktonic Copepods of Boston Harbor, Massachusetts Bay and Cape Cod Bay, 1992. *Hydrobiologia*, **293**: 405-413.

Zhao, L.Z., Tian, R.C., Xue, P., Chen, C., Leo, W.S. and Mickelson M.J. 2011. Modeling 2010 in Massachusetts Bay using the unstructured-grid Bays Eutrophication Model. Boston: Massachusetts Water Resources Authority. Report 2011-09. 118 p.

Table 2. 1 State variable numbers and units in UG-RCA.

Number	Variable	Unit
1	Salinity	ppt
2	Winter/spring phytoplankton	mg C l^{-1}
3	Summer phytoplankton	mg C l^{-1}
4	Fall phytoplankton	mg P l^{-1}
5	Particulate organic phosphorus – refractory component	mg P l^{-1}
6	Particulate organic phosphorus – labile component	mg P l^{-1}
7	Dissolved organic phosphorus – refractory component	mg P l^{-1}
8	Dissolved organic phosphorus – labile component	mg P l^{-1}
9	Total dissolved inorganic phosphorus	mg N l^{-1}
10	Particulate organic nitrogen – refractory component	mg N l^{-1}
11	Particulate organic nitrogen – labile component	mg N l^{-1}
12	Dissolved organic nitrogen – refractory component	mg N l^{-1}
13	Dissolved organic nitrogen – labile component	mg N l^{-1}
14	Total ammonia (ammonia in water and phytoplankton cell)	mg N l^{-1}
15	Nitrite + nitrate	mg Si l^{-1}
16	Biogenic silica	mg Si l^{-1}
17	Total silica – (silica in water and phytoplankton cell)	mg C l^{-1}
18	Particulate organic carbon – refractory component	mg C l^{-1}
19	Particulate organic carbon – labile component	mg C l^{-1}
20	Dissolved organic carbon – refractory component	mg C l^{-1}
21	Dissolved organic carbon – labile component	mg C l^{-1}
22	Dissolved organic carbon – algal exudate	mg C l^{-1}
23	Dissolved organic carbon – reactive component	mg C l^{-1}
24	Particulate organic carbon – reactive component	mg C l^{-1}
25	O2* - aqueous oxygen	mg O_2 l^{-1}
26	Dissolved oxygen	mg O_2 l^{-1}

Table 2. 2 Parameter definition, symbols, values and units in RCA-v3 and UG-RCA, and in RCA-v2. Where values used in RCA differ from those used in UG-RCA, they are shown in parentheses.

Order	Parameter definition	Symbol	Value	Unit
1	MODEL OPTION	AGMOPT	1	
2	Phytoplankton categories	ACTALG	3	
3	REAERATION FORMULATION	KAOPT	3	
4	EXTINCTION COEFFICIENT	KEOPT	1	
5	PAR FRACTION	PAR	0.437	
9	GROWTH TEMPERATURE FOR DIATOMS	TOPT1	8.000	°C
10	TEMPERATURE CORRECTION EFFECT ON GROWTH RATE BELOW TOPT1	K1BETA1	0.004	$°C^{-2}$
11	TEMPERATURE CORRECTION EFFECT ON GROWTH RATE ABOVE TOPT1	K1BETA2	0.006	$°C^{-2}$
12	GROSS PHOTOSYNTHETIC RATE PER UNIT CELL (ASSOCIATED WITH PHOTOSYNTHETIC DARK REACTIONS)	GPRE1	2.5	d^{-1}
13	GROSS PHOTOSYNTHETIC RATE PER UNIT CELL PER UNIT LIGHT INTENSITY UNDER NUTRIENT-SATURATED CONDITIONS AND ZERO IRRADIANCE	GPR01	0.64 (0.28)	m^2 Ein^{-1}
14	SATURATING ALGAL LIGHT INTENSITY	IS1	0.000	Ein m^{-2} d^{-1}
15	HALF SATURATION CONSTANT FOR NITROGEN	KMN1	0.010	mg N l^{-1}
16	HALF SATURATION CONSTANT FOR PHOSPHOROUS	KMP1	0.001	mg P l^{-1}
17	HALF SATURATION CONSTANT FOR SILICA	KMS1	0.020	mg Si l^{-1}
18	BASAL OR RESTING RESPIRATION RATE	K1RB	0.030	d^{-1}
19	TEMPERATURE COEFFICIENT FOR BASAL/ENDOGENOUS RESPIRATION	K1RT	1.0	dimensionless
20	GROWTH-RATE-DEPENDENT RESPIRATION COEFFICIENT	K1RG	0.280	dimensionless
21	DEATH RATE DUE TO GRAZING	K1GRZC	0.100	d^{-1}
22	TEMPERATURE COEFFICIENT	K1GRZT	1.100	dimensionless
23	FRACTION OF C ALLOCATED TO STRUCTURAL PURPOSES	FSC1	0.10	dimensionless
24	CARBON TO CHLOROPHYLL RATIO	WCCHL1	40.0	mg C $(mg\ chl)^{-1}$
25	CARBON TO PHOSPHORUS RATIO - NON-P LIMITED	WCP1	40.0	mg C $(mg\ P)^{-1}$
26	CARBON TO NITROGEN RATIO - NON-N LIMITED	WCN1	5.0	mg C $(mg\ N)^{-1}$
27	CARBON TO SILICA RATIO - NON-SI LIMITED	WCS1	2.500	mg C $(mg\ Si)^{-1}$
28	QUOTIENT OF NUTRIENT-LIMITED NUTRIENT:C RATIOS AT RELATIVE GROWTH RATES OF 0 AND 1	QF1	0.85	
29	CHLOROPHYLL SELF-SHADING EXTINCTION COEFFICIENT FOR ALGAL GROUP 1	XKC1	0.017	m^2 $(mg\ chl)^{-1}$
30	BASE ALGAL SETTLING RATE - GROUP 1	VSBAS1	0.500	m d^{-1}
31	NUTRIENT STRESSED ALGAL SETTLING RATE - GROUP 1	VSNTR1	1.000	m d^{-1}

Order	Parameter definition	Symbol	Value	Unit
Algal Group 2				
41	OPTIMAL GROWTH TEMPERATURE FOR SUMMER GROUP 2	TOPT2	18.000	°C
42	TEMPERATURE CORRECTION EFFECT ON GROWTH RATE BELOW TOPT2	K2BETA1	0.004	$°C^{-2}$
43	TEMPERATURE CORRECTION EFFECT ON GROWTH RATE ABOVE TOPT2	K2BETA2	0.006	$°C^{-2}$
44	GROSS PHOTOSYNTHETIC RATE PER UNIT CELL (ASSOCIATED WITH PHOTOSYNTHETIC DARK REACTIONS)	GPRE2	3.0	d^{-1}
45	PHOTOSYNTHETIC RATE PER UNIT CELL PER UNIT LIGHT INTENSITY UNDER NUTRIENT-SATURATED CONDITIONS AND ZERO IRRADIANCE	GPR02	0.64 (0.28)	m^2 Ein^{-1}
46	SATURATING ALGAL LIGHT INTENSITY	IS2	000.0	Ein m^{-2} d^{-1}
47	HALF SATURATION CONSTANT FOR NITROGEN	KMN2	0.010	mg N l^{-1}
48	HALF SATURATION CONSTANT FOR PHOSPHOROUS	KMP2	0.001	mg P l^{-1}
49	HALF SATURATION CONSTANT FOR SILICA	KMS2	0.005	mg Si l^{-1}
50	BASAL OR RESTING RESPIRATION RATE	K2RB	0.036	d^{-1}
51	TEMPERATURE COEFFICIENT FOR BASAL/ENDOGENOUS RESPIRATION	K2RT	1.0	
52	GROWTH-RATE-DEPENDENT RESPIRATION COEFFICIENT	K2RG	0.280	
53	DEATH RATE DUE TO GRAZING	K2GRZC	0.100	d^{-1}
54	TEMPERATURE COEFFICIENT	K2GRZT	1.100	
55	FRACTION OF C ALLOCATED TO STRUCTURAL PURPOSES	FSC2	0.10	
56	CARBON TO CHLOROPHYLL RATIO	WCCHL2	65.0	mg C $(mg\ chl)^{-1}$
57	CARBON TO PHOSPHORUS RATIO - NON-P LIMITED	WCP2	40.000	mg C $(mg\ P)^{-1}$
58	CARBON TO NITROGEN RATIO - NON-N LIMITED	WCN2	5.670	mg C $(mg\ N)^{-1}$
59	CARBON TO SILICA RATIO - NON-SI LIMITED	WCS2	7.000	mg C $(mg\ Si)^{-1}$
60	QUOTIENT OF NUTRIENT-LIMITED NUTRIENT:C RATIOS AT RELATIVE GROWTH RATES OF 0 AND 1	QF2	0.85	
61	CHLOROPHYLL SELF-SHADING EXTINCTION COEFFICIENT FOR ALGAL GROUP 2	XKC2	0.017	m^2 $(mg\ chl)^{-1}$
62	BASE ALGAL SETTLING RATE - GROUP 2	VSBAS2	0.300	m d^{-1}
63	NUTRIENT STRESSED ALGAL SETTLING RATE - GROUP 2	VSNTR2	0.700	m d^{-1}

Order	Parameter definition	Symbol	Value	Unit
Algal Group 3				
73	OPTIMAL GROWTH TEMPERATURE FOR DIATOMS	TOPT3	14.0	°C
74	TEMPERATURE CORRECTION EFFECT ON GROWTH RATE BELOW TOPT3	K3BETA1	0.004	$°C^{-2}$
75	TEMPERATURE CORRECTION EFFECT ON GROWTH RATE ABOVE TOPT3	K3BETA2	0.006	$°C^{-2}$
76	GROSS PHOTOSYNTHETIC RATE PER UNIT CELL (ASSOCIATED WITH PHOTOSYNTHETIC DARK REACTIONS)	GPRE3	2.5	d^{-1}
77	GROSS PHOTOSYNTHETIC RATE PER UNIT CELL PER UNIT LIGHT INTENSITY UNDER NUTRIENT-SATURATED CONDITIONS AND ZERO IRRADIANCE	GPR03	0.64 (0.28)	m^2 Ein^{-1}
78	SATURATING ALGAL LIGHT INTENSITY	IS3	000.0	Ein m^{-2} d^{-1}
79	HALF SATURATION CONSTANT FOR NITROGEN	KMN3	0.005	mg N l^{-1}
80	HALF SATURATION CONSTANT FOR PHOSPHOROUS	KMP3	0.001	mg P l^{-1}
81	HALF SATURATION CONSTANT FOR SILICA	KMS3	0.040	mg Si l^{-1}
82	BASAL OR RESTING RESPIRATION RATE	K3RB	0.030	d^{-1}
83	TEMPERATURE COEFFICIENT FOR BASAL/ENDOGENOUS RESPIRATION	K3RT	1.0	dimensionless
84	GROWTH-RATE-DEPENDENT RESPIRATION COEFFICIENT	K3RG	0.280	dimensionless
85	DEATH RATE DUE TO GRAZING	K3GRZC	0.100	d^{-1}
86	TEMPERATURE COEFFICIENT	K3GRZT	1.100	dimensionless
87	FRACTION OF C ALLOCATED TO STRUCTURAL PURPOSES	FSC3	0.10	dimensionless
88	CARBON TO CHLOROPHYLL RATIO	WCCHL3	15.0	mg C $(mg\ chl)^{-1}$
89	CARBON TO PHOSPHORUS RATIO - NON-P LIMITED	WCP3	40.000	mg C $(mg\ P)^{-1}$
90	CARBON TO NITROGEN RATIO - NON-N LIMITED	WCN3	5.670	mg C $(mg\ N)^{-1}$
91	CARBON TO SILICA RATIO - NON-SI LIMITED	WCS3	2.500	mg C $(mg\ Si)^{-1}$
92	QUOTIENT OF NUTRIENT-LIMITED NUTRIENT:C RATIOS AT RELATIVE GROWTH RATES OF 0 AND 1	QF3	0.85	
93	CHLOROPHYLL SELF-SHADING EXTINCTION COEFFICIENT FOR ALGAL GROUP 3	XKC3	0.017	m^2 $(mg\ chl)^{-1}$
94	BASE ALGAL SETTLING RATE - GROUP 3	VSBAS3	0.300	m d^{-1}
95	NUTRIENT STRESSED ALGAL SETTLING RATE - GROUP 3	VSNTR3	1.000	m d^{-1}

Order	Parameter definition	Symbol	Value	Unit
Biogeochemical parameters				
105	HALF SATURATION CONSTANT FOR PHYTOPLANKTON RECYCLE FRACTIONS MG C/L	KMPHYT	0.050	mg C l^{-1}
106	REFRACTORY PARTICULATE ORGANIC PHOSPHOROUS	FRPOP	0.150	
107	LABILE PARTICULATE ORGANIC PHOSPHOROUS	FLPOP	0.300	
108	REFRACTORY DISSOLVED ORGANIC PHOSPHOROUS	FRDOP	0.100	
109	LABILE DISSOLVED ORGANIC PHOSPHOROUS	FLDOP	0.150	
110	DISSOLVED INORGANIC PHOSPHOROUS	FPO4	0.300	
111	REFRACTORY PARTICULATE ORGANIC NITROGEN	FRPON	0.150	
112	LABILE PARTICULATE ORGANIC NITROGEN	FLPON	0.325	
113	REFRACTORY DISSOLVED ORGANIC NITROGEN	FRDON	0.150	
114	LABILE DISSOLVED ORGANIC NITROGEN	FLDON	0.175	
115	AMMONIA	FNH4	0.200	
116	REFRACTORY PARTICULATE ORGANIC CARBON	FRPOC	0.150	
117	LABILE PARTICULATE ORGANIC CARBON	FLPOC	0.350	
118	REFRACTORY DISSOLVED ORGANIC CARBON	FRDOC	0.100	
119	LABILE DISSOLVED ORGANIC CARBON PHOSPHORUS	FLDOC	0.400	
120	HYDROLYSIS RATE OF RPOP TO RDOP	K57C	0.010	d^{-1}
121	TEMPERATURE COEFFICIENT	K57T	1.080	
122	HYDROLYSIS RATE OF LPOP TO LDOP	K68C	0.050	d^{-1}
123	TEMPERATURE COEFFICIENT	K68T	1.080	
124	MINERALIZATION RATE OF RDOP TO PO4	K79C	0.010	d^{-1}
125	TEMPERATURE COEFFICIENT	K79T	1.080	
126	MINERALIZATION RATE OF LDOP TO PO4	K89C	0.100	d^{-1}
127	TEMPERATURE COEFFICIENT NITROGEN	K89T	1.080	
128	HYDROLYSIS RATE OF RPON TO RDON	K1012C	0.008	d^{-1}
129	TEMPERATURE COEFFICIENT	K1012T	1.080	
130	HYDROLYSIS RATE OF LPON TO LDON	K1113C	0.050	d^{-1}
131	TEMPERATURE COEFFICIENT	K1113T	1.080	
132	MINERALIZATION RATE of RDON TO NH4	K1214C	0.008	d^{-1}
133	TEMPERATURE COEFFICIENT	K1214T	1.080	
134	MINERALIZATION RATE OF LDON TO NH4	K1314C	0.050	d^{-1}
135	TEMPERATURE COEFFICIENT NITRIFICATION/DENITRIFICATION RATES	K1314T	1.080	
136	NITRIFICATION RATE AT 20 DEG C	K1415C	0.100	d^{-1}
137	TEMPERATURE COEFFICIENT	K1415T	1.080	
138	HALF SATURATION CONSTANT FOR NITRIF- ICATION OXYGEN LIMITATION	KNIT	1.000	mg O_2 l^{-1}
139	DENITRIFICATION RATE AT 20 DEG C	K150C	0.050	d^{-1}
140	TEMPERATURE COEFFICIENT	K150T	1.045	
141	MICHAELIS CONSTANT FOR DENITRIFICATION OXYGEN LIMITATION SILICA MINERALIZATION RATES AT 20 DEG C	KNO3	0.100	mg O_2 l^{-1}
142	MINERALIZATION RATE OF BIOGENIC SI TO AVAIL SI	K1617C	0.080	d^{-1}
143	TEMPERATURE COEFFICIENT CARBON HYDROLYSIS/OXIDATION RATES AT 20 DEG C	K1617T	1.080	
144	HYDROLYSIS RATE OF RPOC TO RDOC	K1820C	0.010	d^{-1}
145	TEMPERATURE COEFFICIENT	K1820T	1.080	
146	HYDROLYSIS RATE OF LPOC TO LDOC	K1921C	0.070	d^{-1}

Order	Parameter definition	Symbol	Value	Unit
147	TEMPERATURE COEFFICIENT	K1921T	1.080	
148	OXIDATION RATE OF RDOC	K200C	0.008	d^{-1}
149	TEMPERATURE COEFFICIENT	K200T	1.080	
150	OXIDATION RATE OF LDOC	K210C	0.100	d^{-1}
151	TEMPERATURE COEFFICIENT	K210T	1.080	
152	MICHAELIS CONSTANT FOR LDOC	KMLDOC	0.100	mg C l^{-1}
153	HALF SATURATION CONSTANT FOR ORG CARBON	KDOC	0.200	mg O_2 l^{-1}
154	ALGAL EXUDATE DOC OXIDATION RATE	K220C	0.300	d^{-1}
155	TEMPERATURE COEFFICIENT	K220T	1.047	
156	FRACTION OF PRIMARY PRODUCTIVITY GOING TO LABILE ORGANIC CARBON VIA EXUDATION REPOC/REDOC ARE ASSOCIATED WITH SANITARY/CSO SOLIDS	FLOCEX	0.100	
157	HYDROLYSIS RATE OF REPOC TO REDOC	K2324C	0.01	d^{-1}
158	TEMPERATURE COEFFICIENT	K2324T	1.0	
159	REACTIVE DOC OXIDATION RATE	K240C	0.150	d^{-1}
160	TEMPERATURE COEFFICIENT	K240T	1.047	
161	CARBON TO PHOSPHORUS RATIO OF CSO SOLIDS	CTOPCSO	0.0	
162	CARBON TO NITROGEN RATIO OF CSO SOLIDS	CTONCSO	0.0	
163	OXIDATION RATE FOR AQUEOUS SOD	K250C	0.150	d^{-1}
164	TEMPERATURE COEFFICIENT	K250T	1.080	
165	HALF SATURATION CONSTANT FOR O2*	KO2EQ	0.100	mg O_2 l^{-1}
166	MINIMUM VALUE FOR KL	KLMIN	0.0	m d^{-1}
167	DIFFUSIVITY OF OXYGEN ACROSS THE AIR-WATER INTERFACE	DIFUS	0.0	m^2 d^{-1}
168	TEMPERATURE CORRECTION COEFFICIENT FOR ATMOSPHERIC REAERATION	KAT	1.024	
169	TEMPERATURE CORRECTION	VSBAST	1.027	
170	PARTICULATE ORGANIC MATTER SETTLING RATE	VSPOM	1.000	m d^{-1}
171	TEMPERATURE CORRECTION	VSPMT	1.027	
172	TEMPERATURE CORRECTION FOR DEPOSITION TO SEDIMENT	VSSEDT	1.027	
173	POWER COEFF. FOR CSO SOLID SETTLING RATE (>=1	BVCSO	1.0	dimensionless
174	CRITICAL REPOC CONC. FOR CSO SETTLING FUNCTION	CRCSO	1.0	mg C l^{-1}
175	MINIMUM SETTLING RATE FOR CSO SOLIDS Vcso = VMINCSO+(VMAXCSO-VMINCSO)*(REPOC/CRCSO) **BVCSO)	VMINCSO	0.0	m d^{-1}
176	MAXIMUM SETTLING RATE FOR CSO SOLIDS	VMAXCSO	0.0	m d^{-1}
177	PARTITION COEFFICIENT FOR SORBED PHOSPHORUS	KADPO4	6.0	l mg SS^{-1}
178	PARTITION COEFFICIENT FOR SORBED SILICA	KADSI	6.0	l mg SS^{-1}
179	SETTLING RATE FOR PHOSPHORUS/SILICA SORBED TO SUSPENDED SOLIDS	VSPIM	0.0	m d^{-1}
180	BASE (CHL-A CORRECTED) EXTINCTION COEFFICIENT (USED WHEN KEOPT=0,2)	KECONST	0.001	m^{-1}

Table 2. 3 Data-model conversion for the MWRA effluent, rivers, and other sources.

	Model		**Conversion**	**Data**	
Variable	Definition	Units	Function	Variable	Units
Flow	Sewage flow	L day^{-1}	3.785mflow	mflow	gallon d^{-1}
TOC	Total organic C	mg C d^{-1}	0.7CBOD+18	CBOD	mg O d^{-1}
RPOC	Refractory POC	mg C d^{-1}	9	CBOD	mg O d^{-1}
LPOC	Labile POC	mg C d^{-1}	0.198CBOD	CBOD	mg O d^{-1}
RDOC	Refractory DOC	mg C d^{-1}	9	CBOD	mg O d^{-1}
LDOC	Labile DOC	mg C d^{-1}	0.132CBOD	CBOD	mg O d^{-1}
REDOC	Reactive DOC	mg C d^{-1}	0.37CBOD	CBOD	mg O d^{-1}
TON	Total organic N	mg N d^{-1}	(TKN-NH4)/1000	TKN	μg N d^{-1}
RPON	Refractory PON	mg N d^{-1}	0.4(TKN-NH4)/1000	TKN	μg N d^{-1}
LPON	Labile PON	mg N d^{-1}	0.4(TKN-NH4)/1000	TKN	μg N d^{-1}
RDON	Refractory DON	mg N d^{-1}	0.1(TKN-NH4)/1000	TKN	μg N d^{-1}
LDON	Labile DON	mg N d^{-1}	0.1(TKN-NH4)/1000	TKN	μg N d^{-1}
TOP	Total organic P	mg P d^{-1}	(TP-PO4)/1000	TP	μg P d^{-1}
RPOP	Refractory POP	mg P d^{-1}	0.3(TP-PO4)/1000	TP	μg P d^{-1}
LPOP	Labile POP	mg P d^{-1}	0.55(TP-PO4)/1000	TP	μg P d^{-1}
RDOP	Refractory DOP	mg P d^{-1}	0.05(TP-PO4)/1000	TP	μg P d^{-1}
LDOP	Labile DOP	mg P d^{-1}	0.1(TP-PO4)/1000	TP	μg P d^{-1}

Table 2. 4 Partition coefficients for organic substances in seawater and river water.

		Labile	Refractory	Reactive	Exudate
Nitrogen	PON	0.5	0.5		
	DON	0.5	0.5		
Phosphorus	POP	0.647	0.353		
	DOP	0.66	0.33		
Carbon	POC	0.4	0.6	-	-
	DOC	0.2	0.7	0.05	0.05

Table 2. 5 Partition coefficients of chlorophyll to phytoplankton groups at the open boundary.

	Winter-spring group	Summer group	Fall group
January-April	1.0	0	0
May	0.5	0.5	0
June-July	0	1.0	0
August	0	0.5	0.5
September-November	0	0	1.0
December	0.5	0	0.5

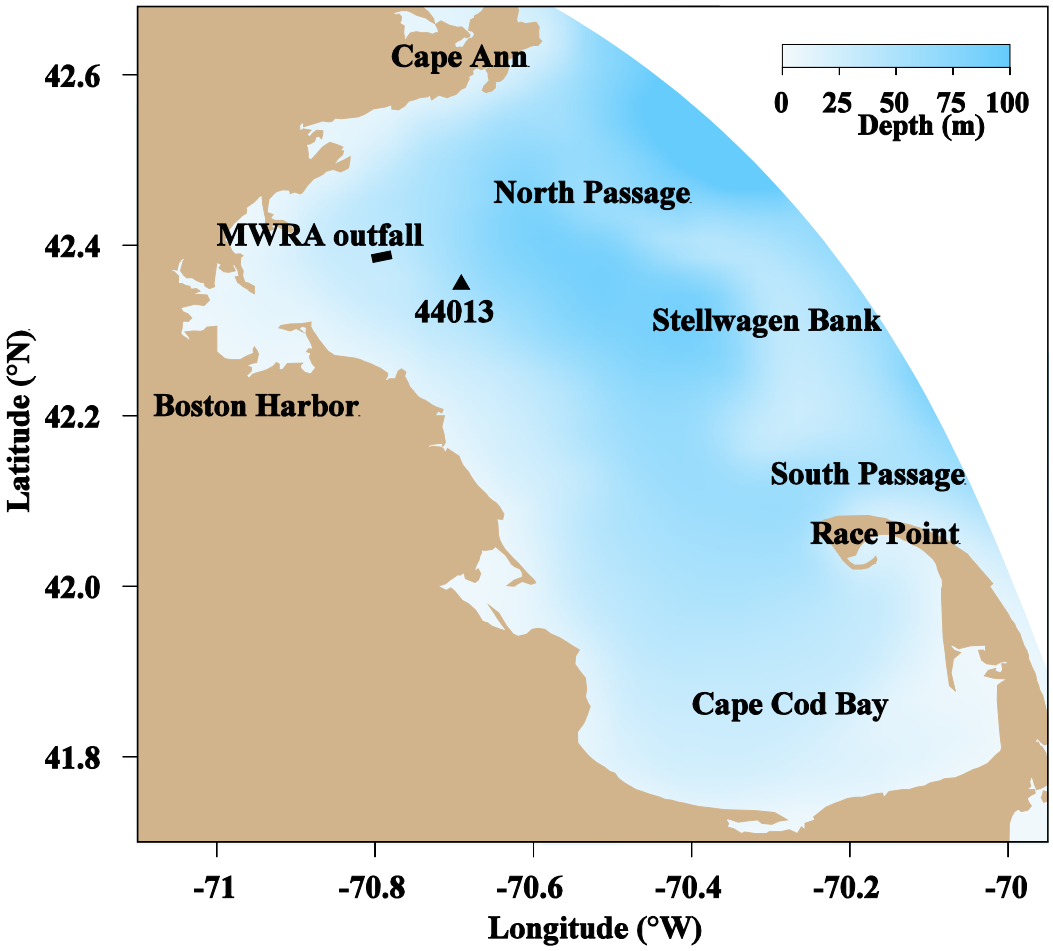

Figure 1. 1 The Massachusetts Bay system (MBS) and location of the MWRA outfall.

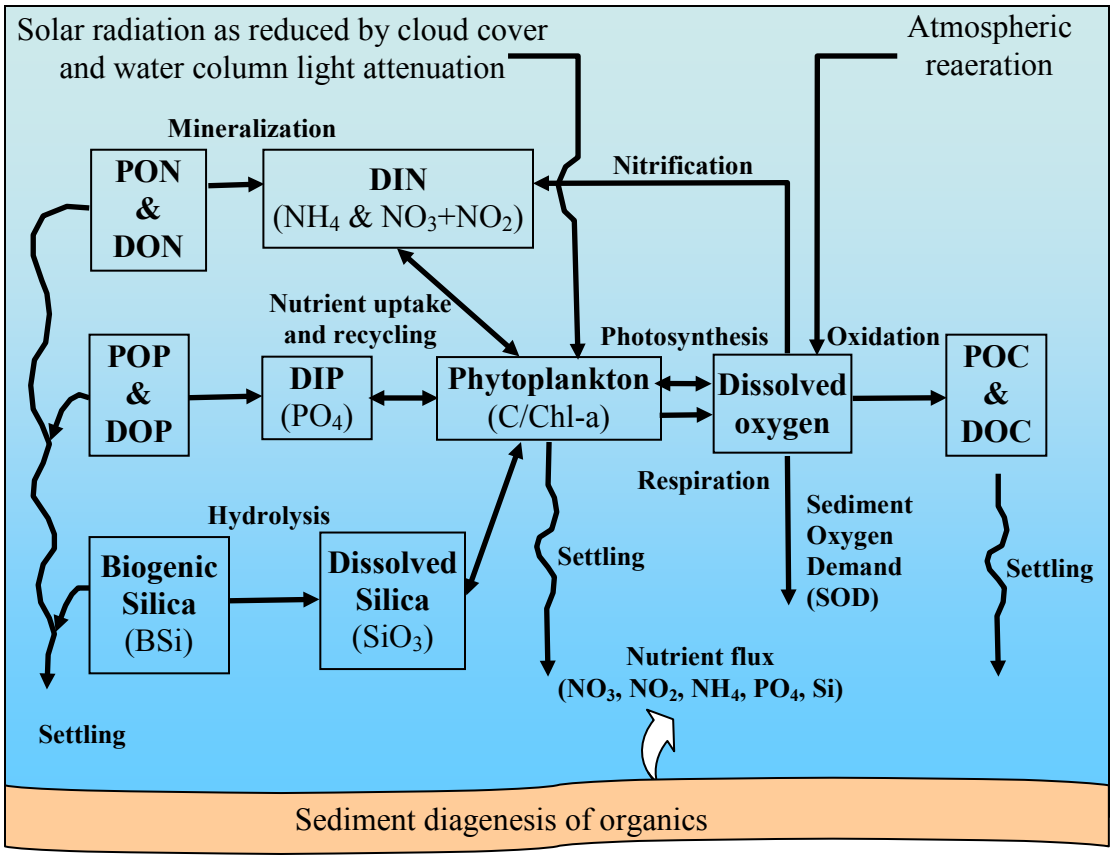

Figure 2. 1 The UG-RCA water quality model (reproduced from HydroQual, 2004).

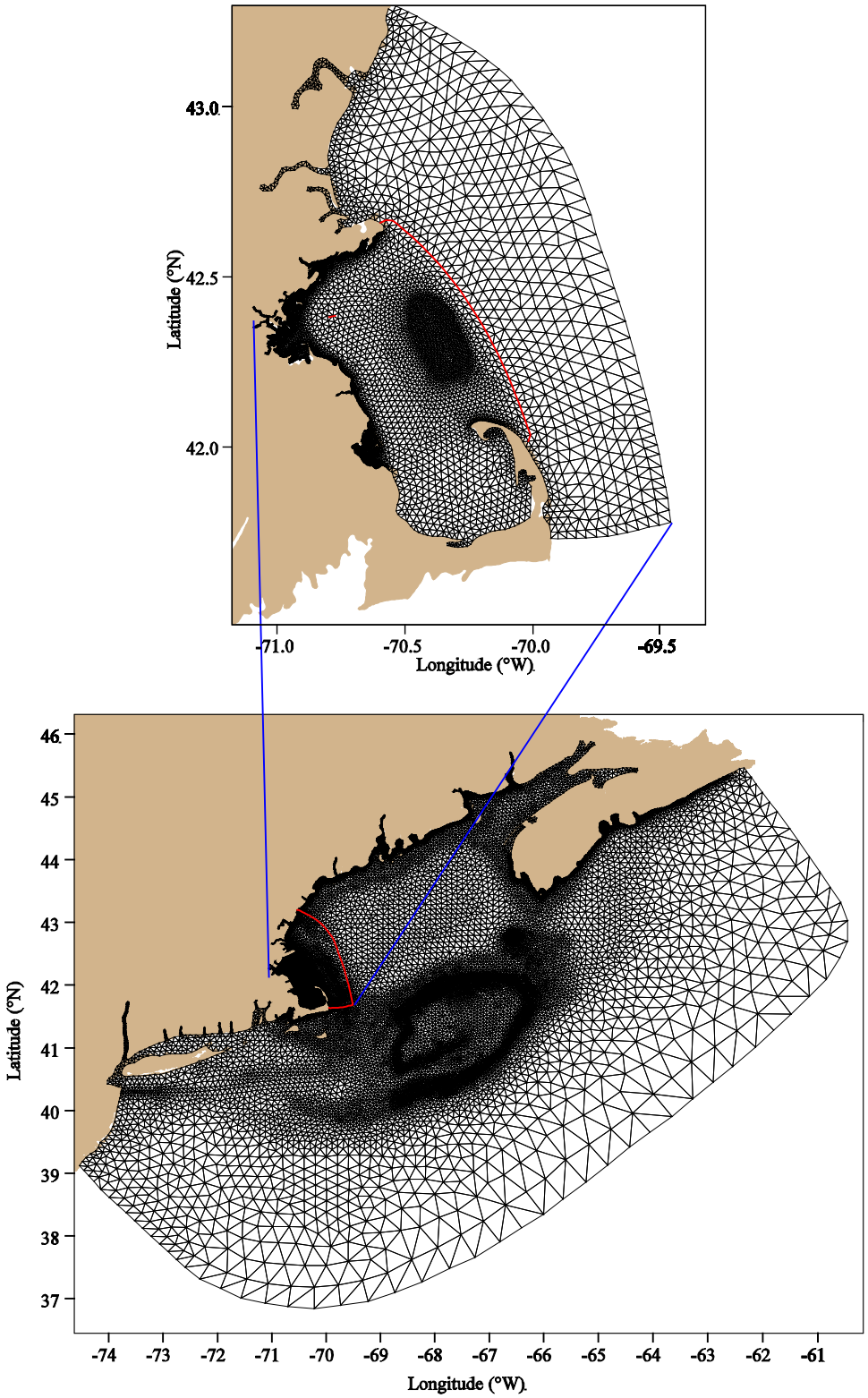

Figure 2. 2 Grid for Gulf-of-Maine FVCOM (lower panel); the red line shows the nested domain of Massachusetts Bay FVCOM. The upper panel shows the higher-resolution grid for MB-FVCOM; the red line shows the domain of the water quality model UG-RCA.

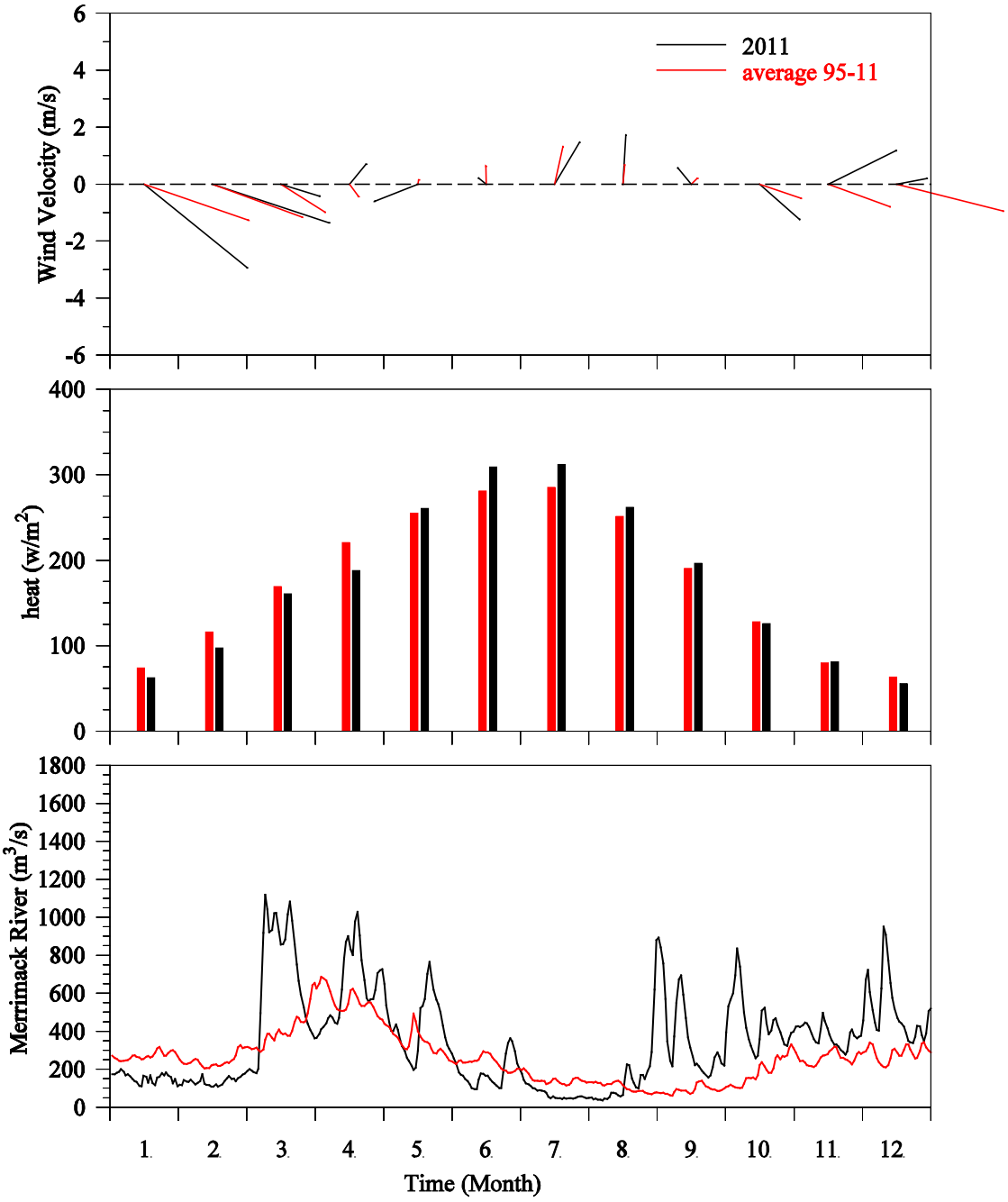

Figure 2. 3 Monthly-averaged wind (upper panel) and heat flux (mid panel) and daily-averaged discharge from Merrimack River in 2011 (black) and the 17-year (1995-2011) average (red).

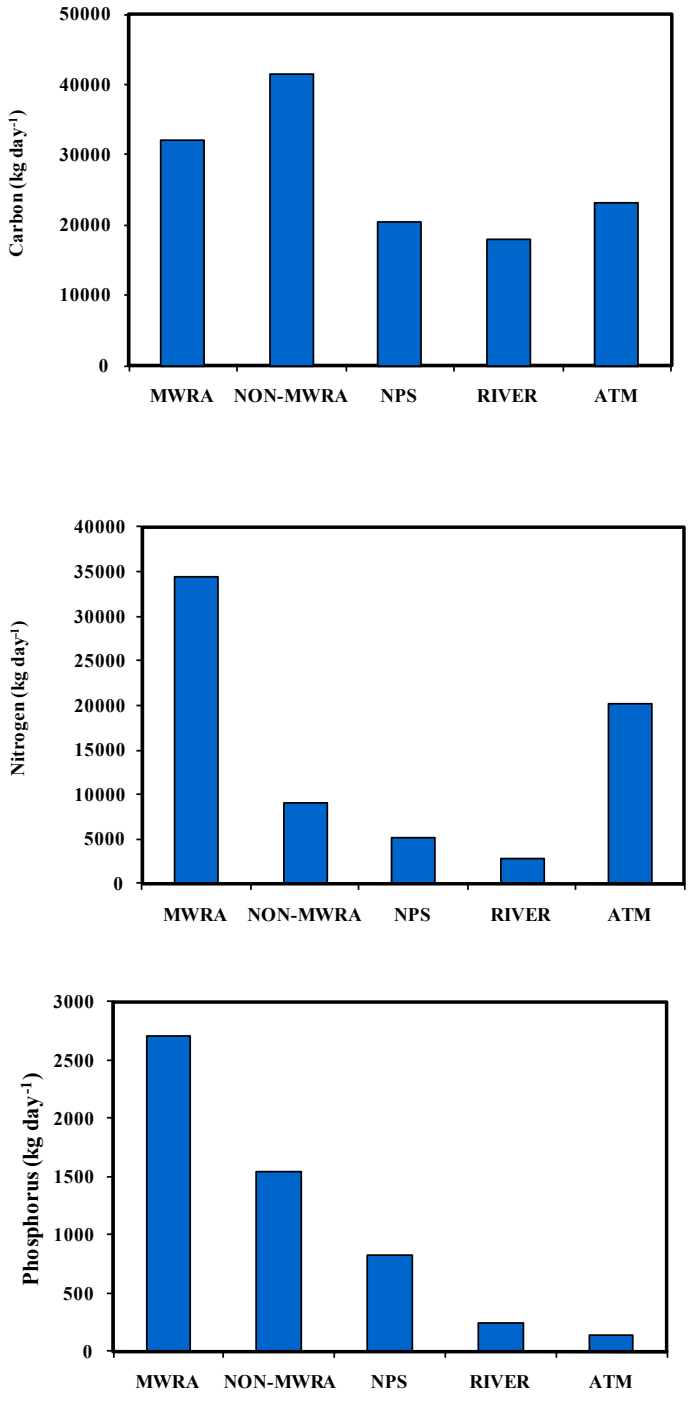

Figure 2. 4 Mean daily loads of carbon, nitrogen and phosphorus from different anthropogenic sources in 2011. MWRA: MWRA outfall; Non-MWRA: Non MWRA point sources; NPS: Non-point sources; River: River loadings; ATM: Atmospheric input.

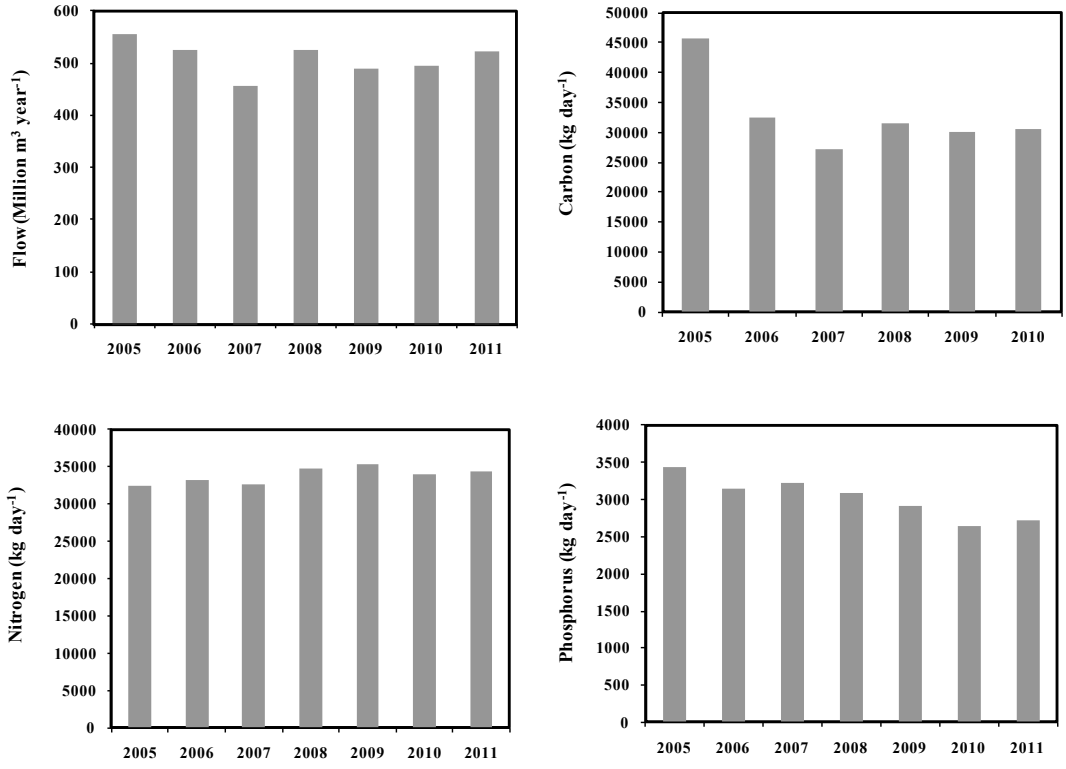

Figure 2. 5 Mean annual flow and mean daily loads of carbon, nitrogen and phosphorus from the MWRA outfall, 2005-2011.

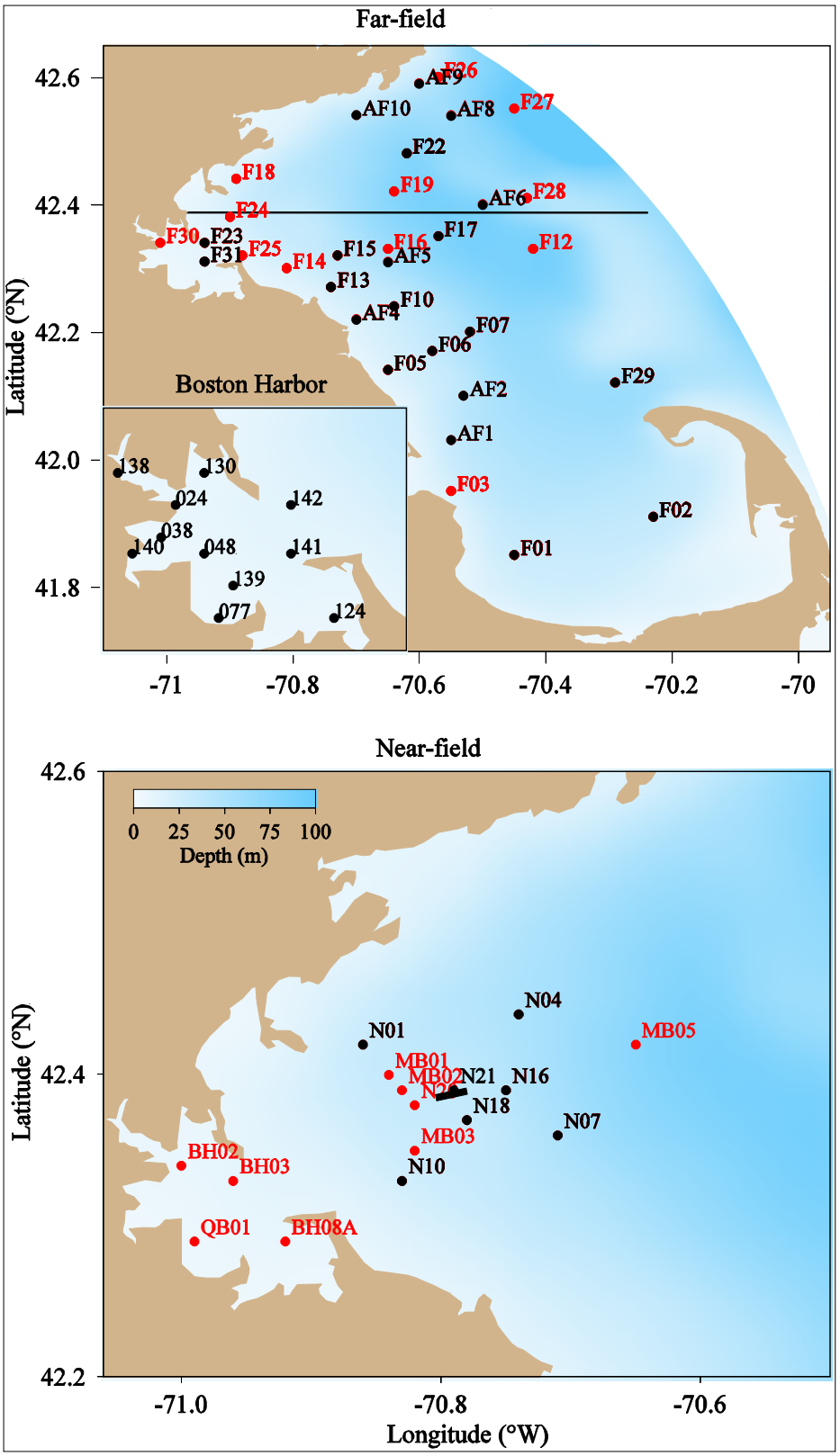

Figure 2.6 Station locations: farfield (denoted with "F"), *Alexandrium* Rapid Response Study (denoted with "AF") and harbor stations in the upper panel; the horizontal line is the transect used in Fig. 4.8. The nearfield stations are denoted with "N". The stations in red were sampled in the past but not in 2011.

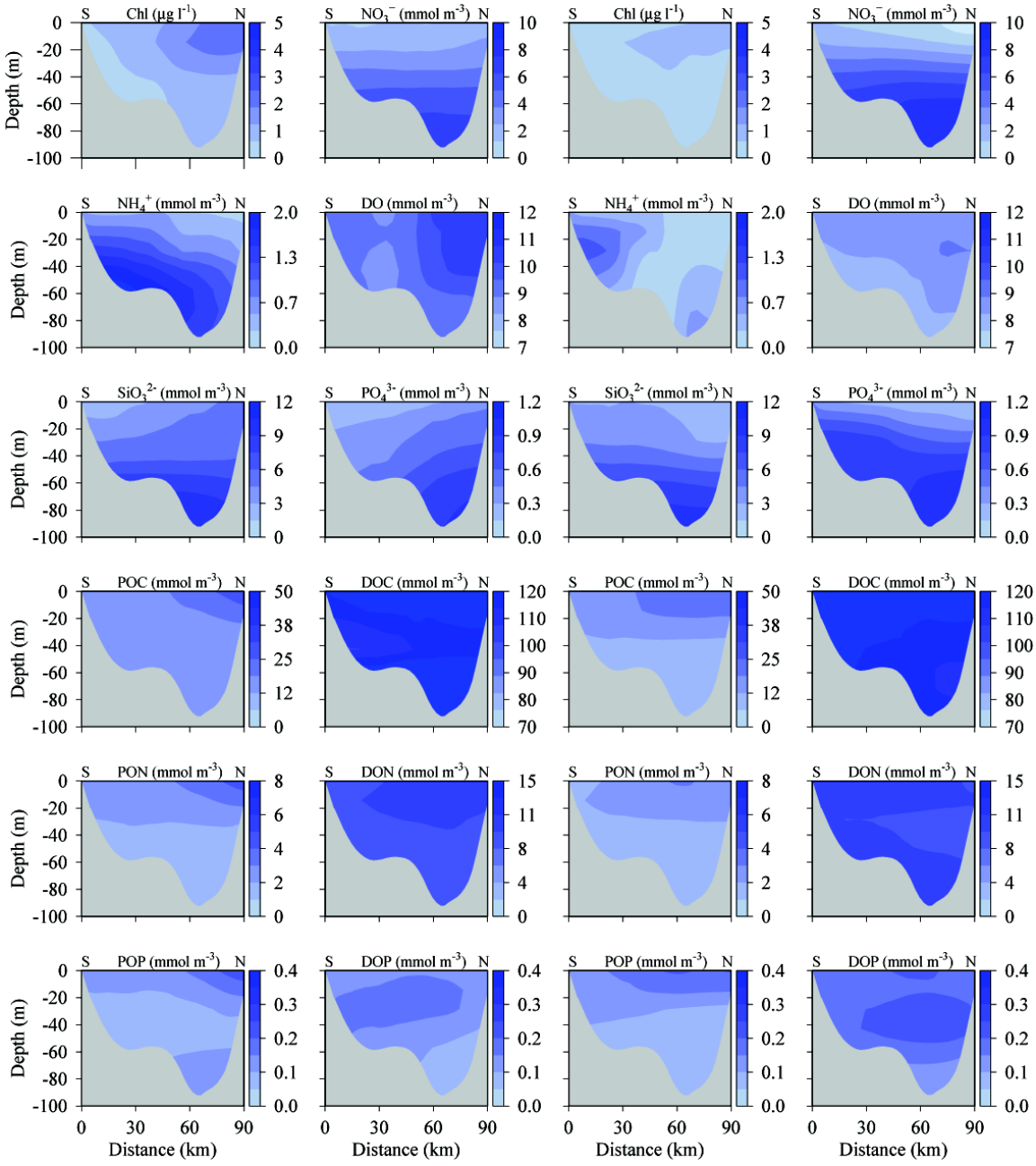

Figure 2. 7 Open boundary condition transects from Cape Cod (south S) to Cape Ann (north N) of chlorophyll, nutrients, DO and organic components on April 15 (left 12 panels) and August 15 (right 12 panels), 2011.

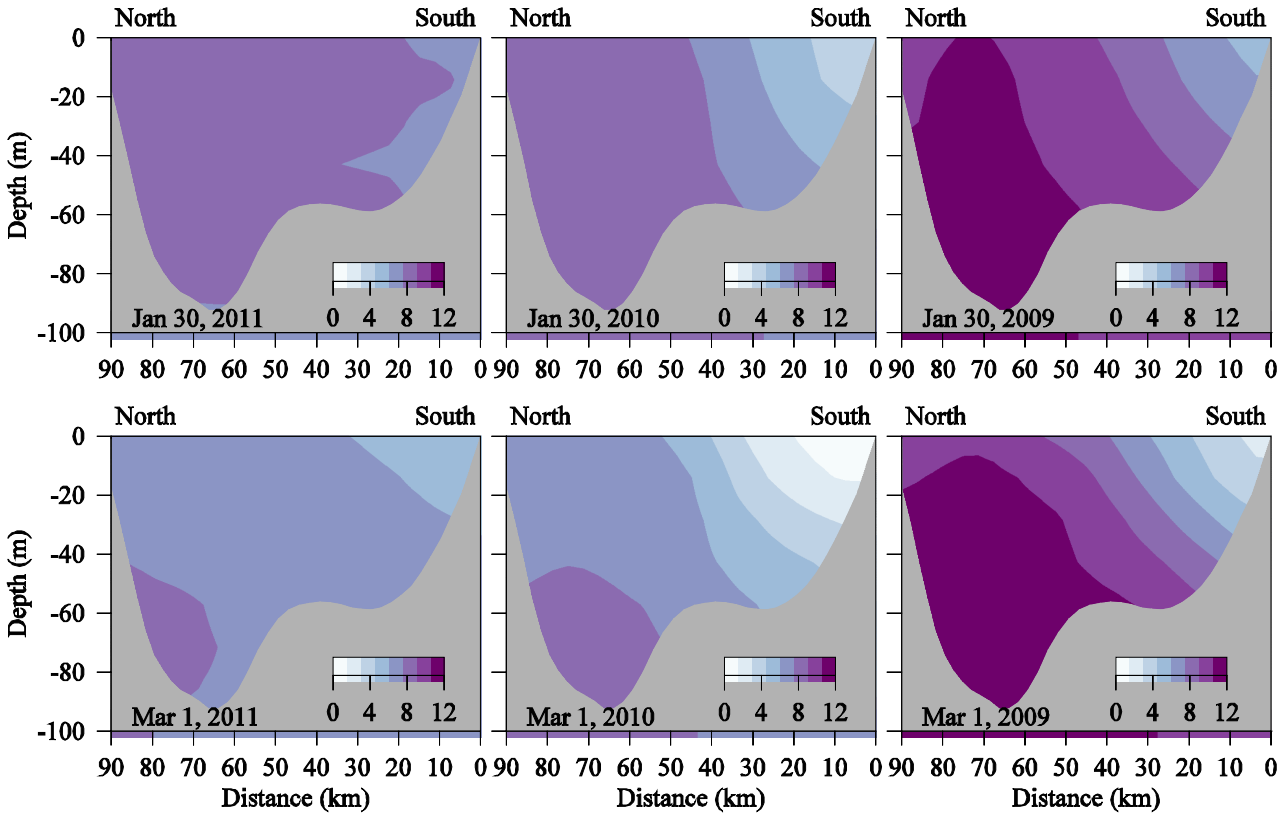

Figure 2. 8. Comparison of nitrate open boundary condition among 2011 (left panels) 2010 (middle panels) and 2009 (right panels) in winter on Jan. 30 (upper panels) and Mar. 1 (lower panels).

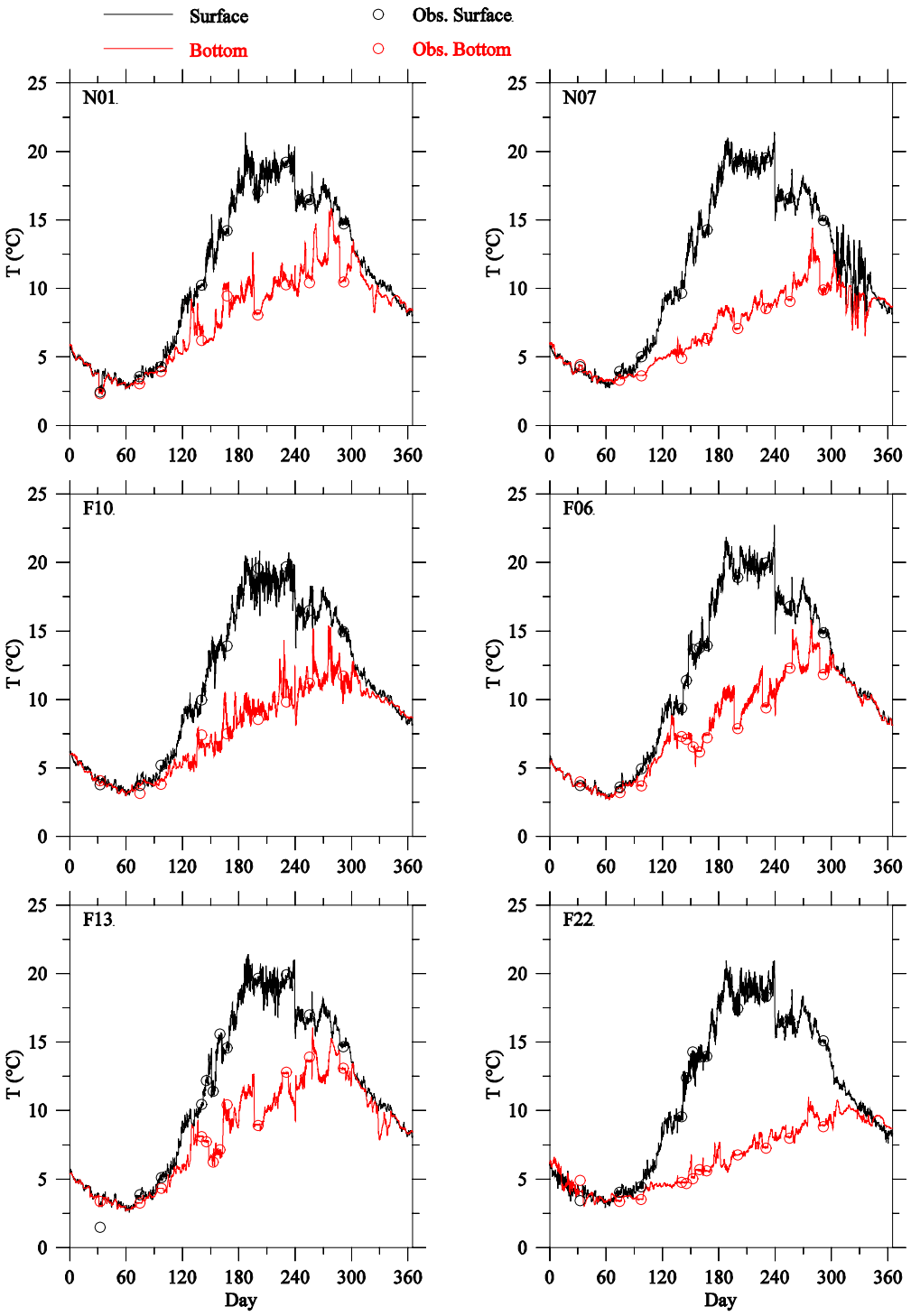

Figure 3. 1 Comparison of temperature observed (circles) and modeled (lines) time series at selected Massachusetts Bay monitoring stations in 2011.

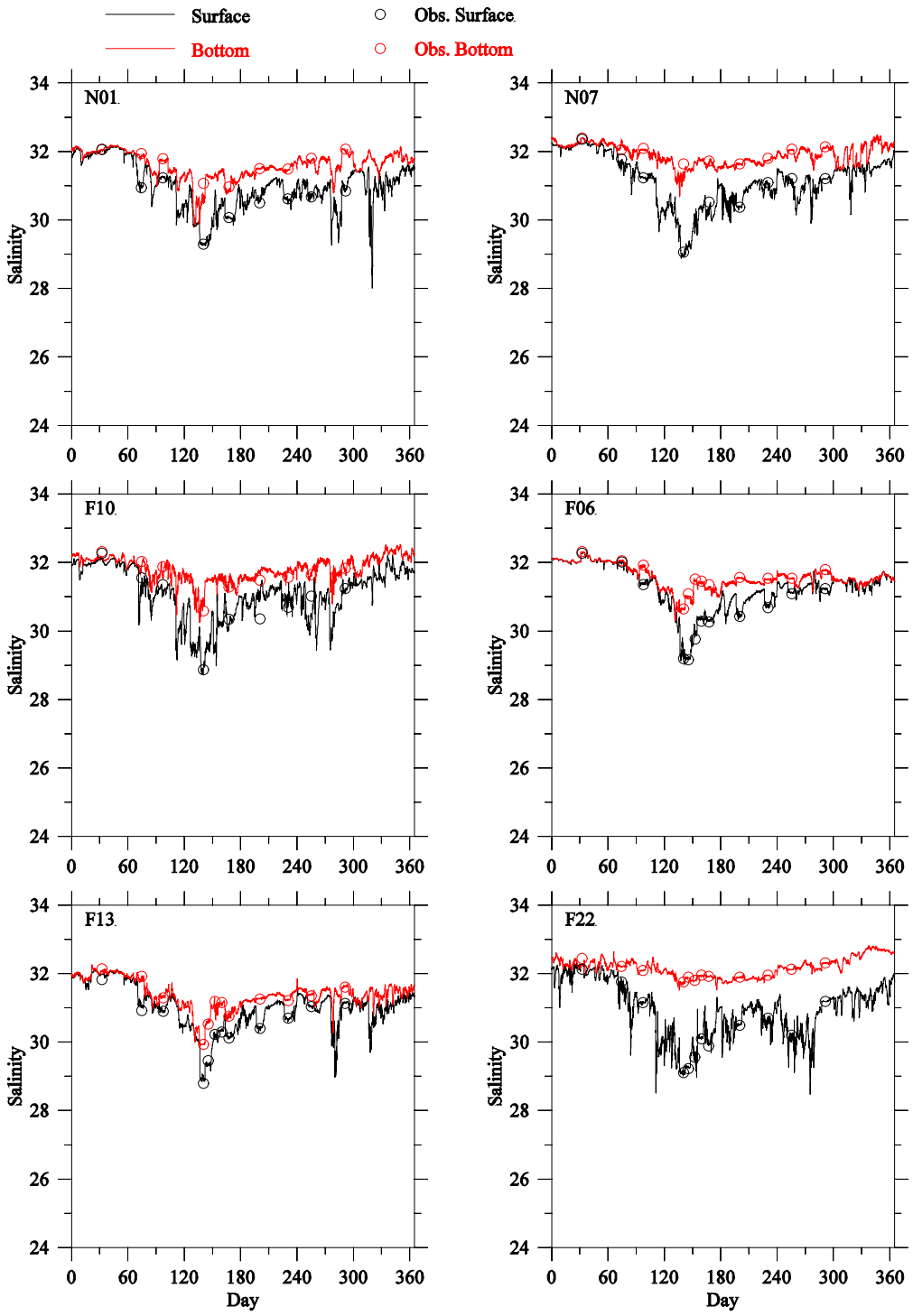

Figure 3. 2 Comparison of salinity observed (circles) and modeled (lines) time-series at selected Massachusetts Bay monitoring stations in 2011.

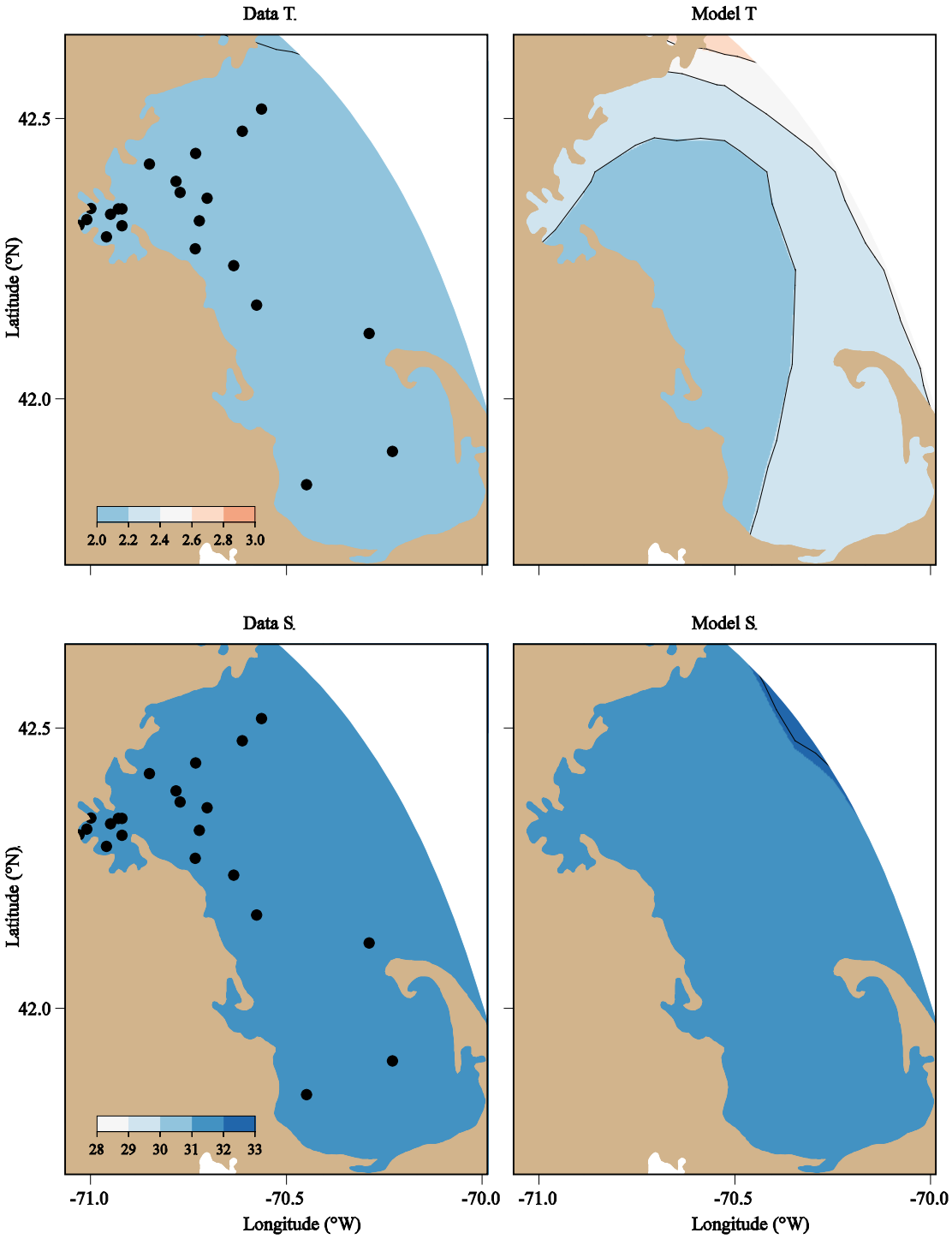

Figure 3. 3 Comparison between observed (left) and model-computed (right) near-surface temperatures (upper panels) and salinities (lower panels) in February 2011.

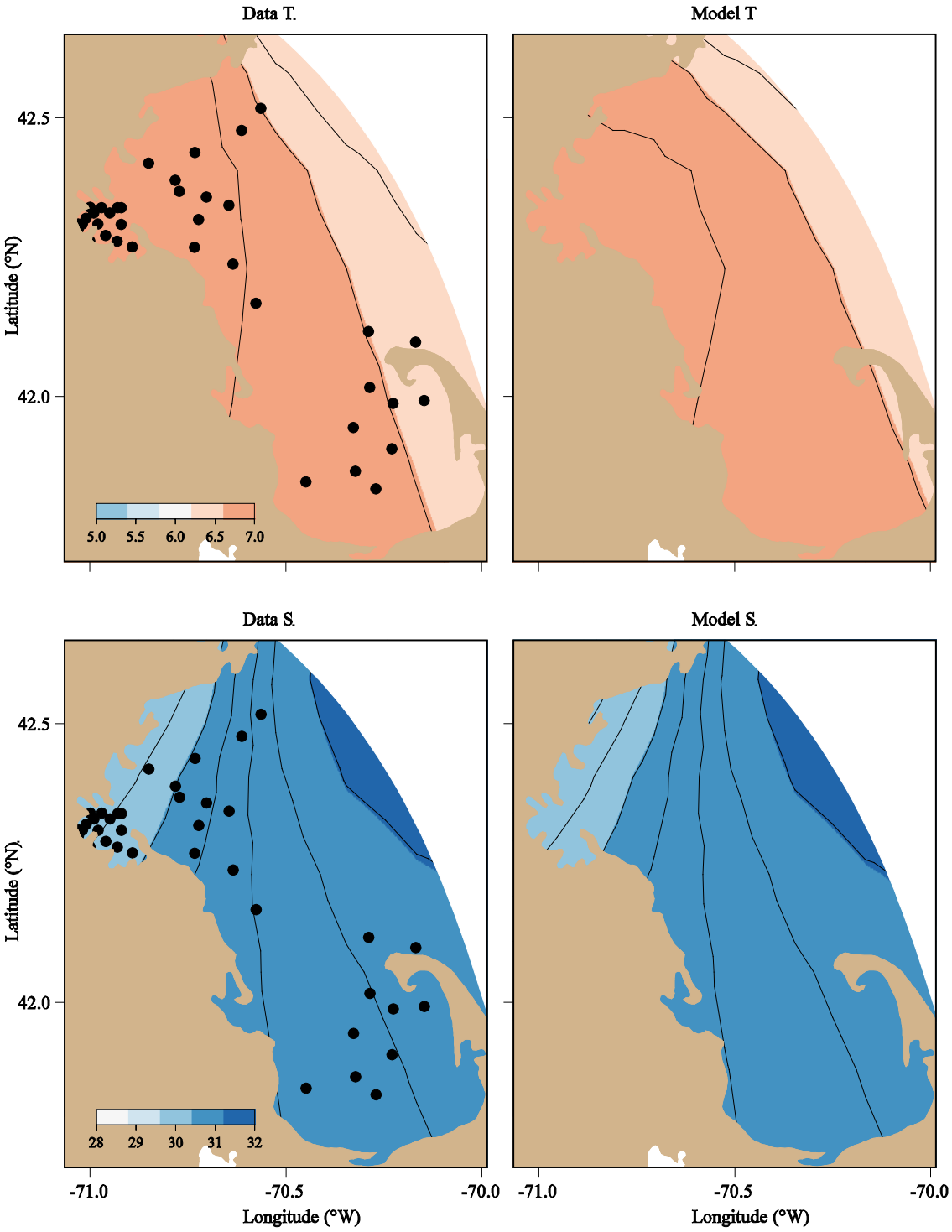

Figure 3. 4 Comparison between observed (left) and model-computed (right) near-surface temperatures (upper panels) and salinities (lower panels) in April 2011.

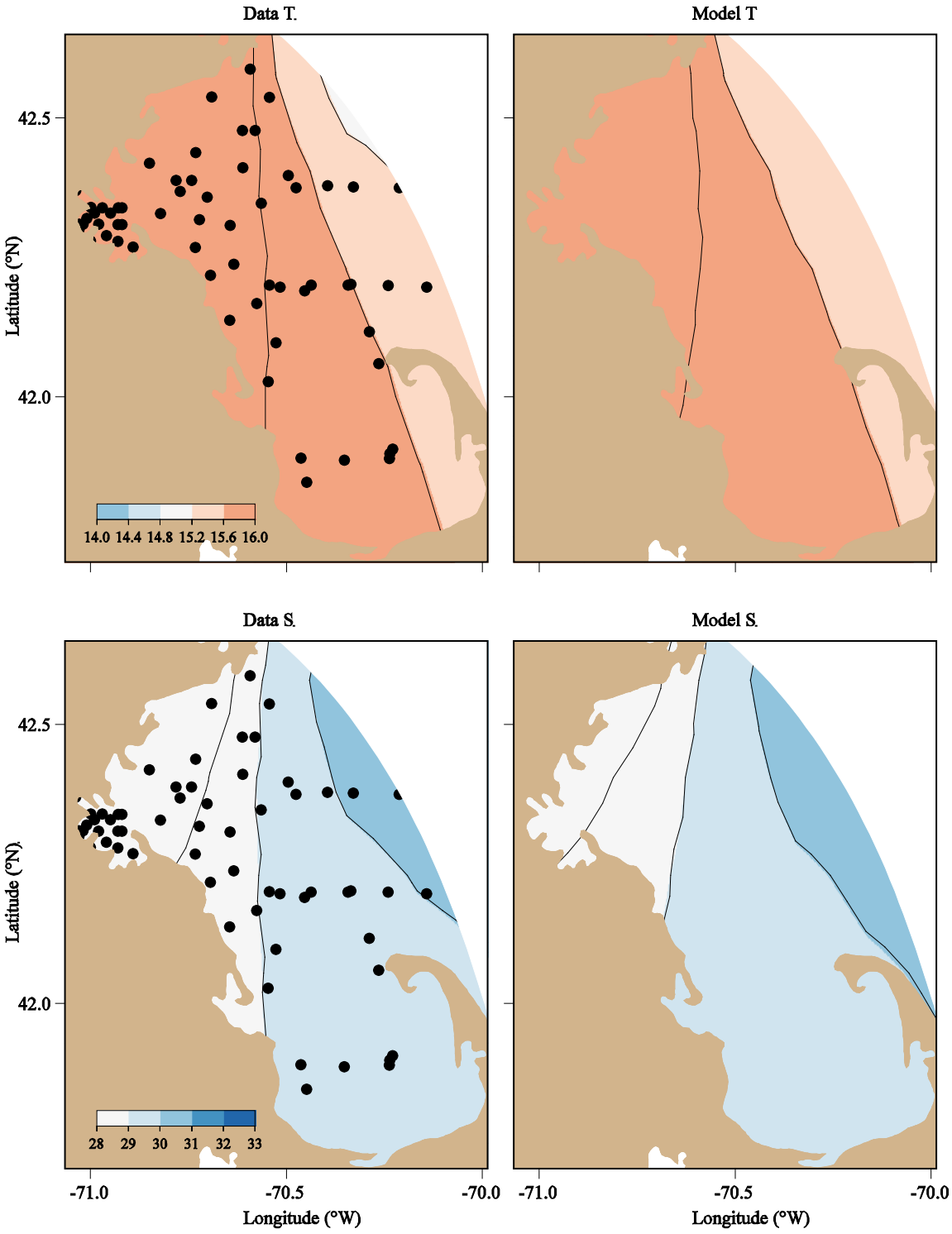

Figure 3. 5 Comparison between observed (left) and model-computed (right) near-surface temperatures (upper panels) and salinities (lower panels) in June 2011.

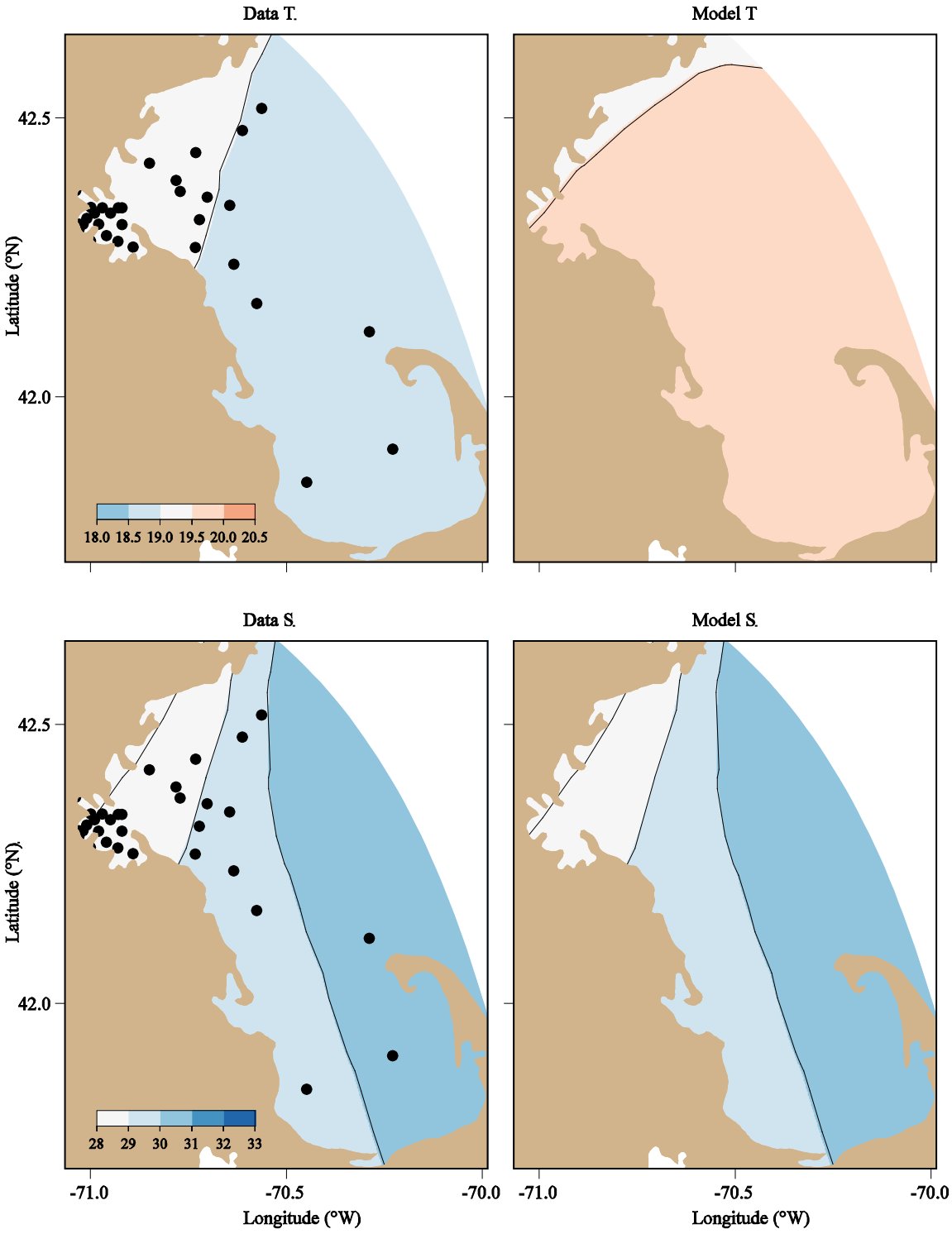

Figure 3. 6 Comparison between observed (left) and model-computed (right) near-surface temperatures (upper panels) and salinities (lower panels) in August 2011.

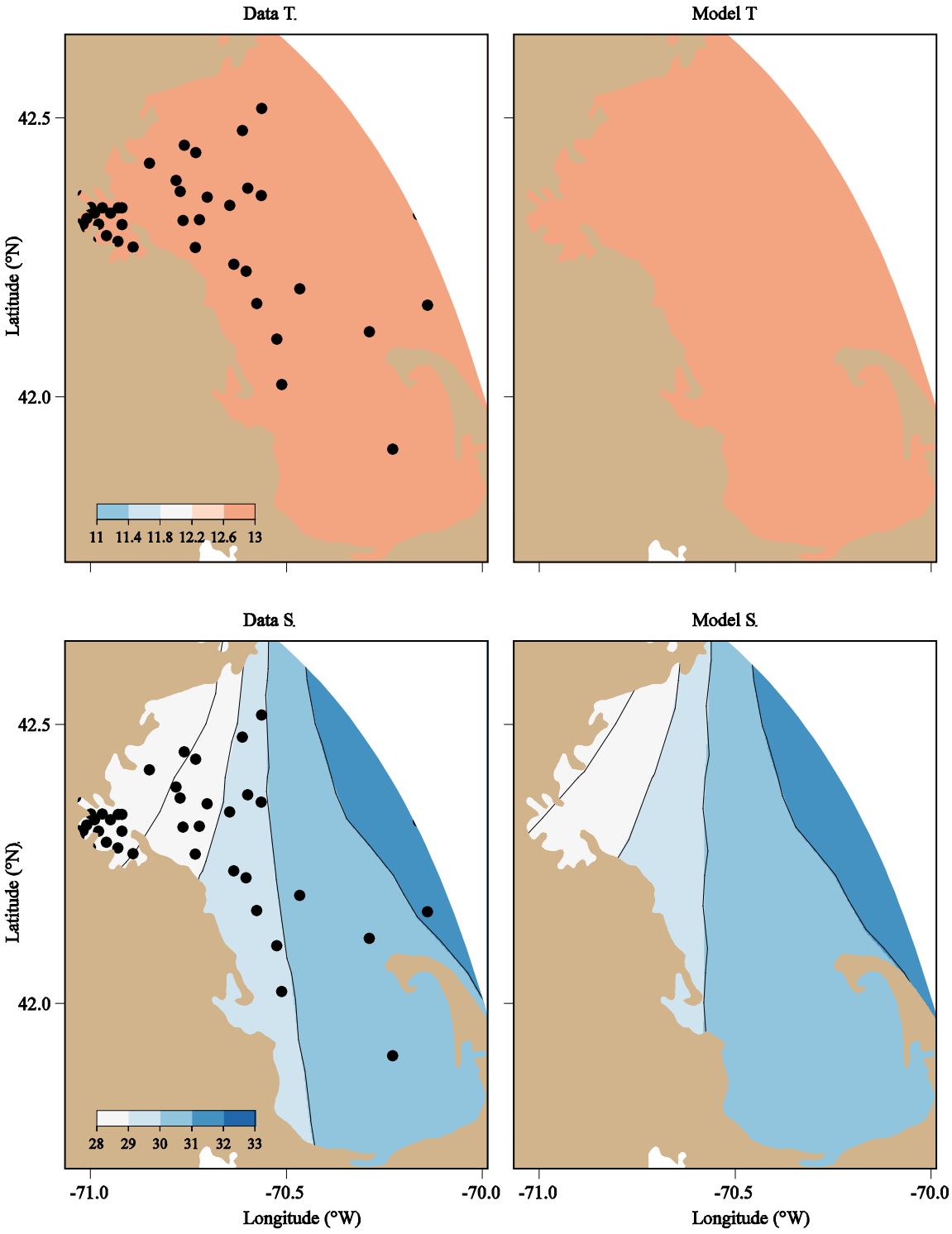

Figure 3. 7 Comparison between observed (left) and model-computed (right) near-surface temperatures (upper panels) and salinities (lower panels) in October 2011.

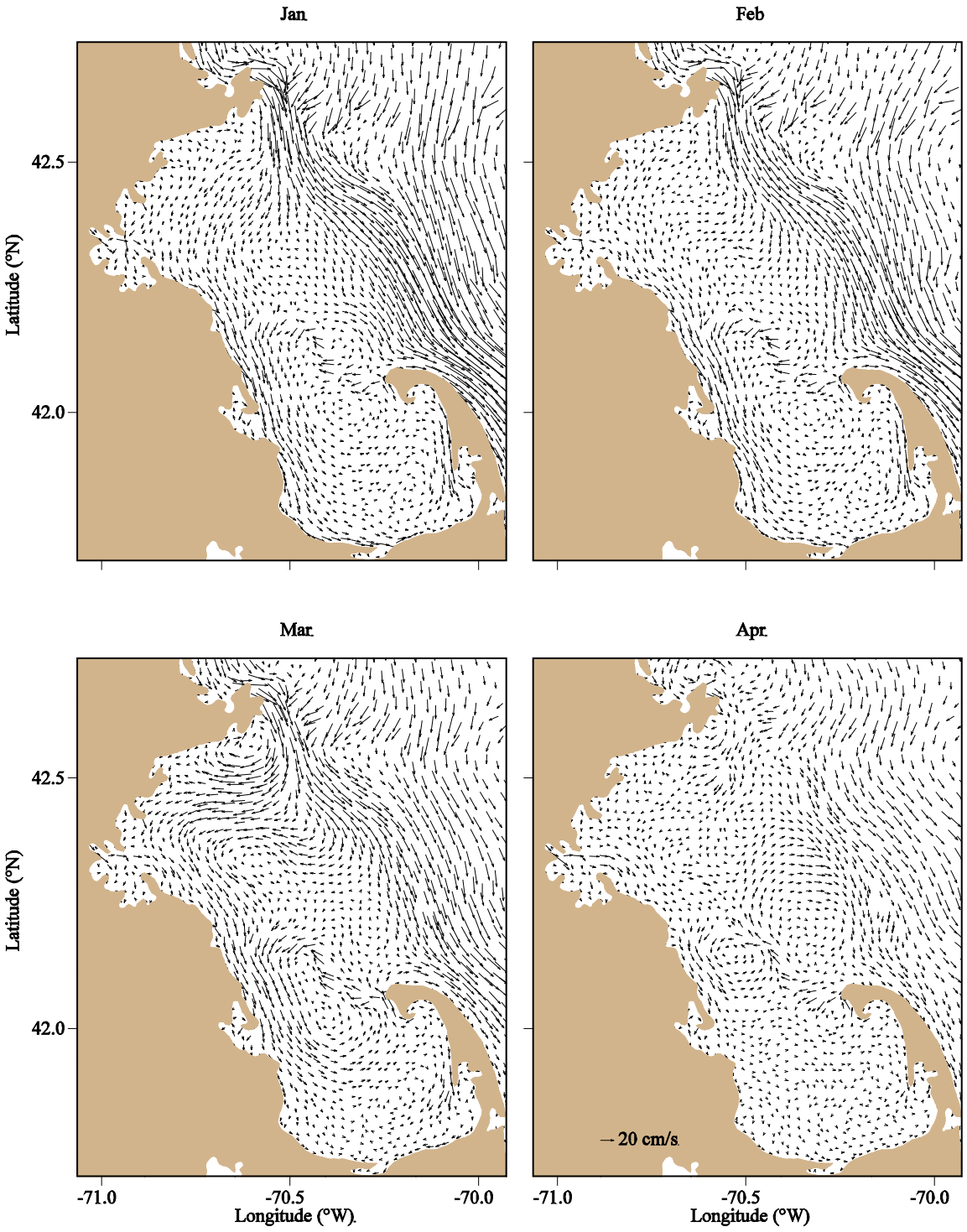

Figure 3. 8 Monthly-averaged surface current from January through April 2011 predicted by FVCOM.

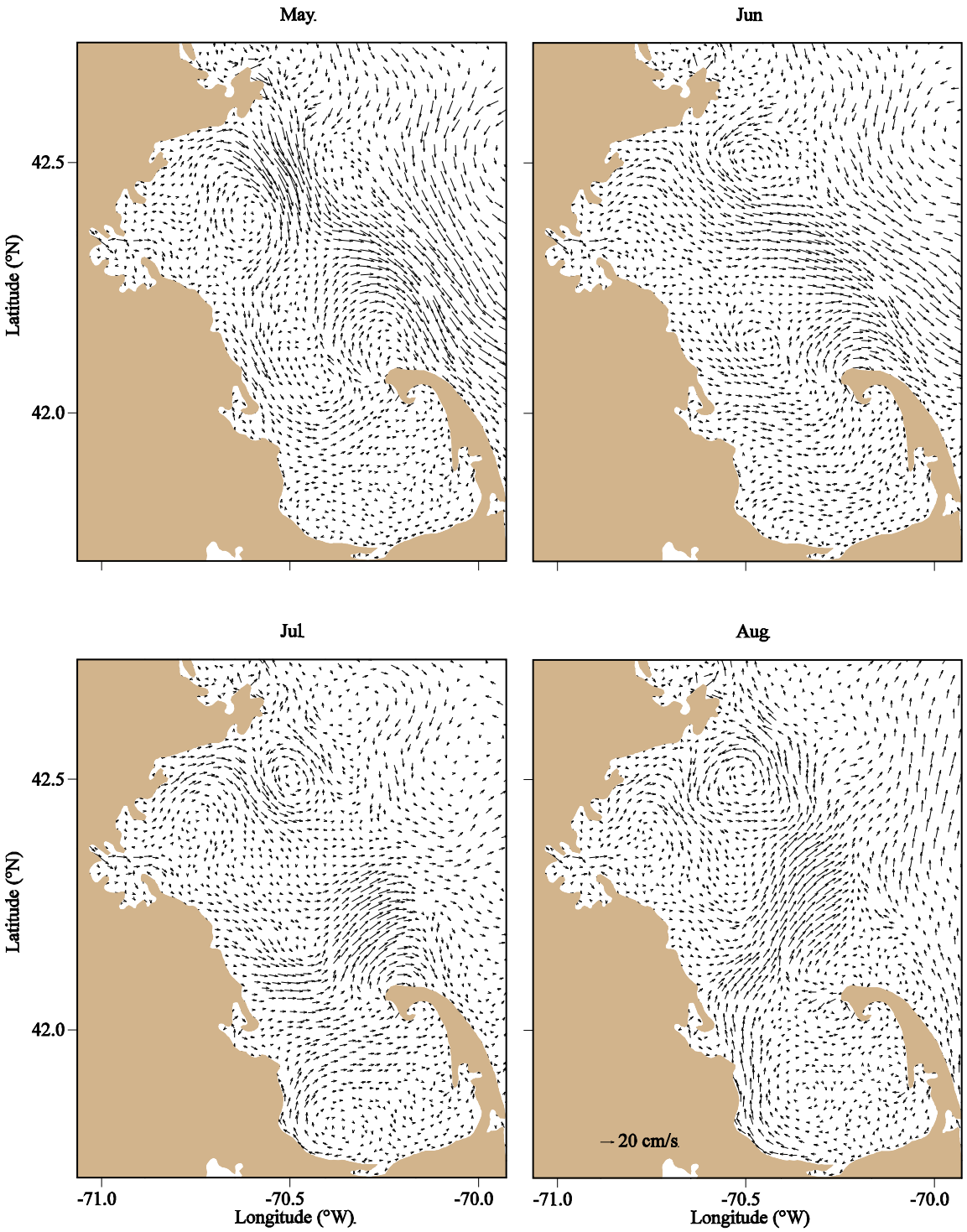

Figure 3. 9 Monthly-averaged surface current from May through August 2011 predicted by FVCOM.

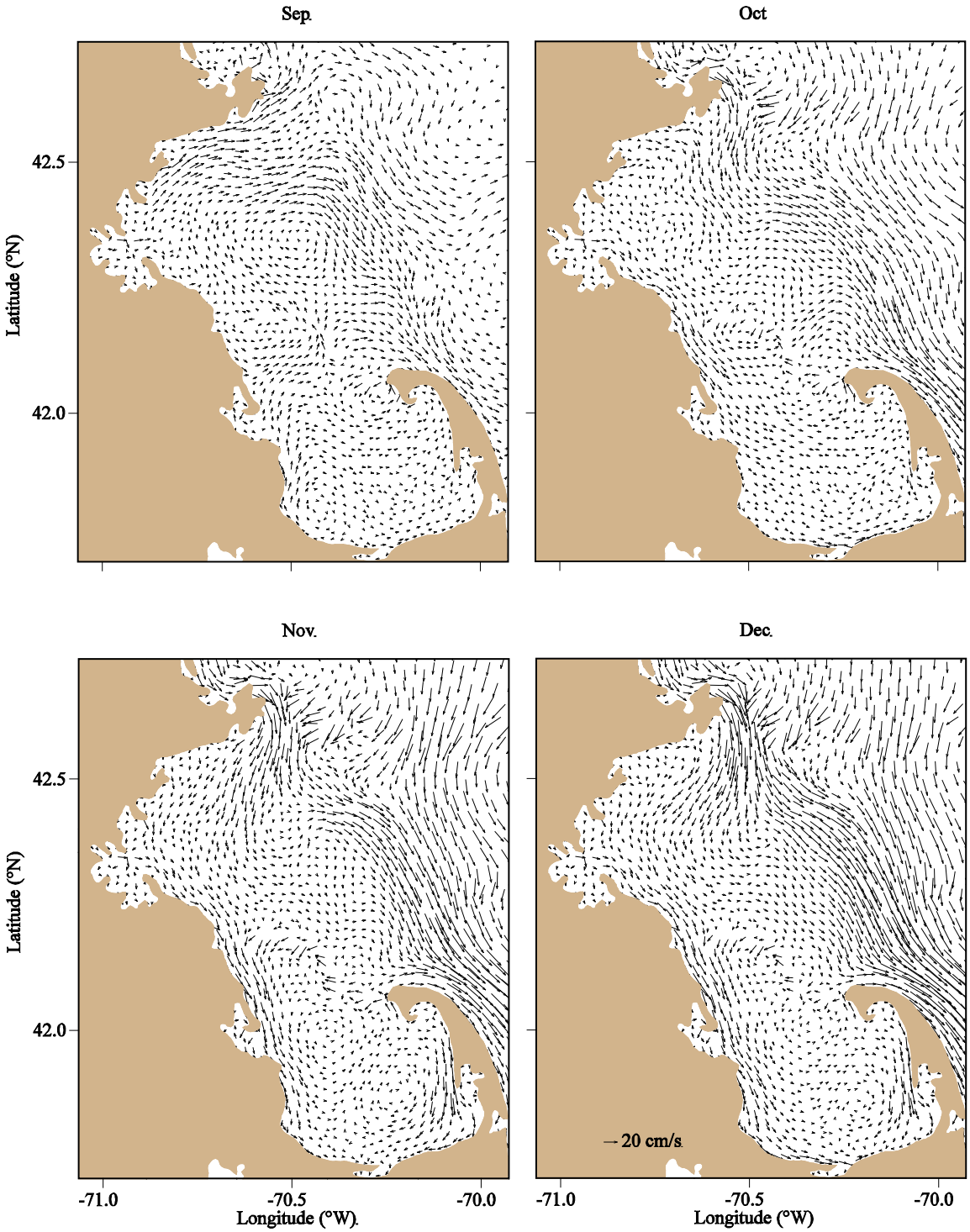

Figure 3. 10 Monthly-averaged surface current from September through December 2011 predicted by FVCOM.

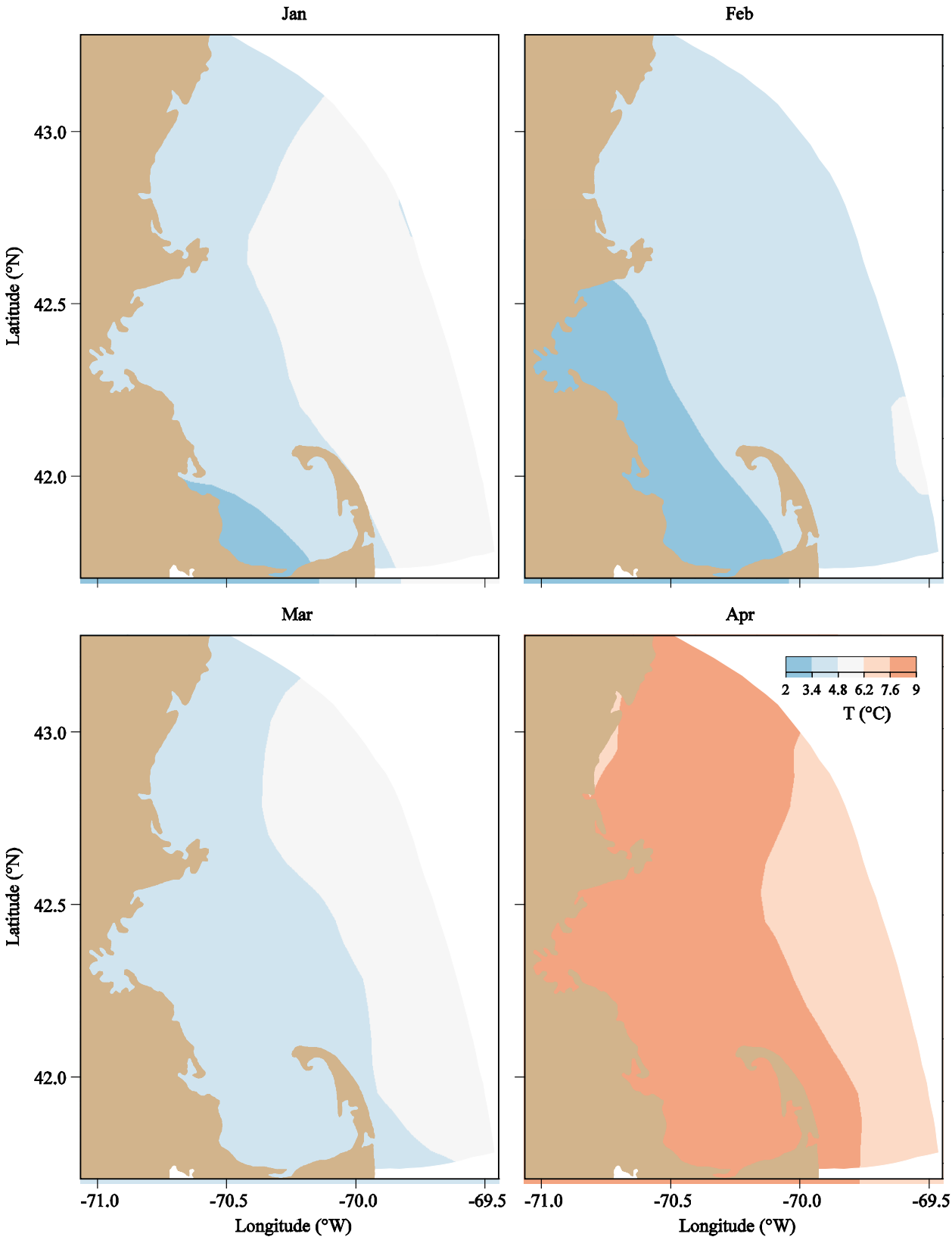

Figure 3. 11 Surface temperature at the end of January, February, March, and April, 2011 predicted by FVCOM.

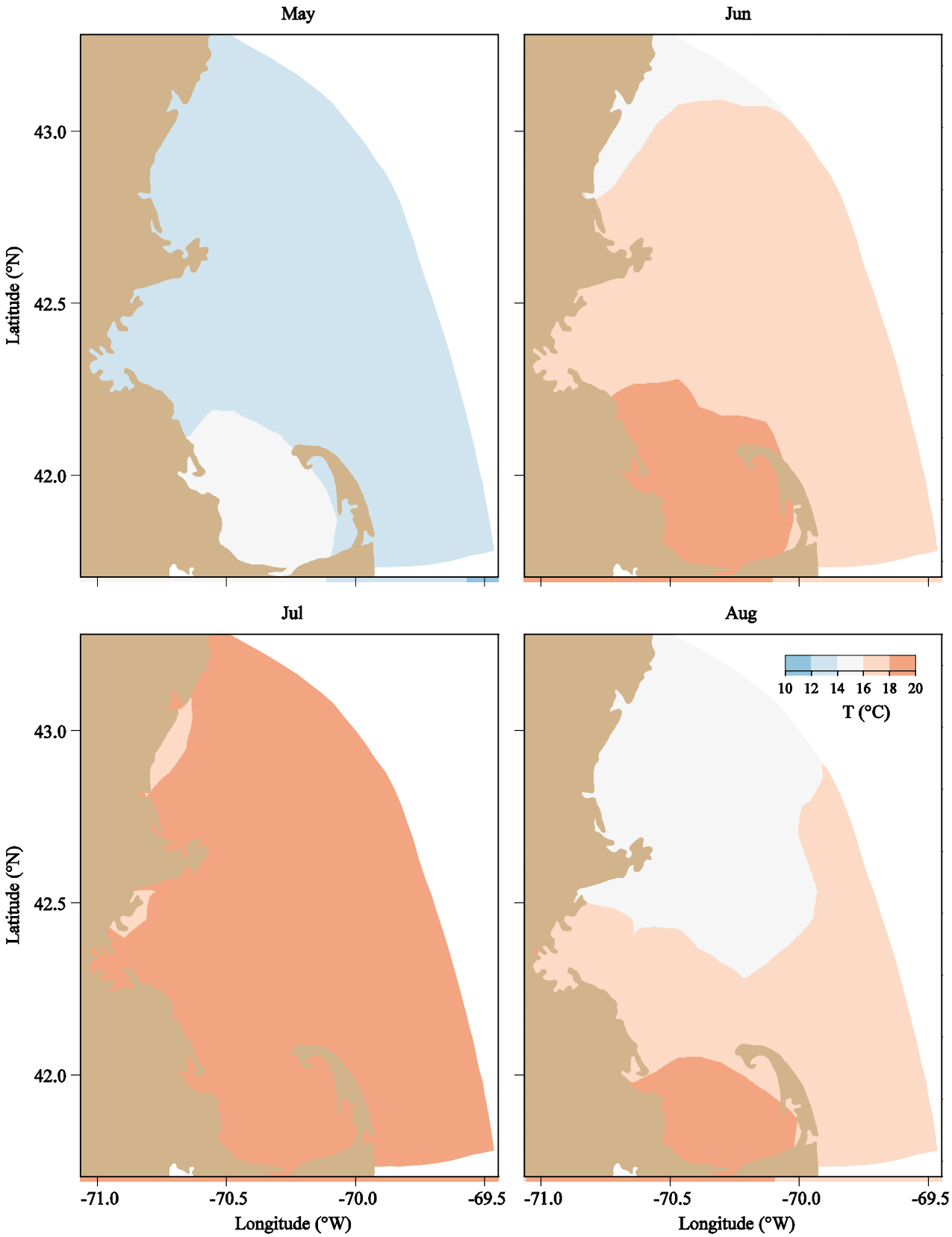

Figure 3. 12 Surface temperature at the end of May, June, July, and August, 2011 predicted by FVCOM.

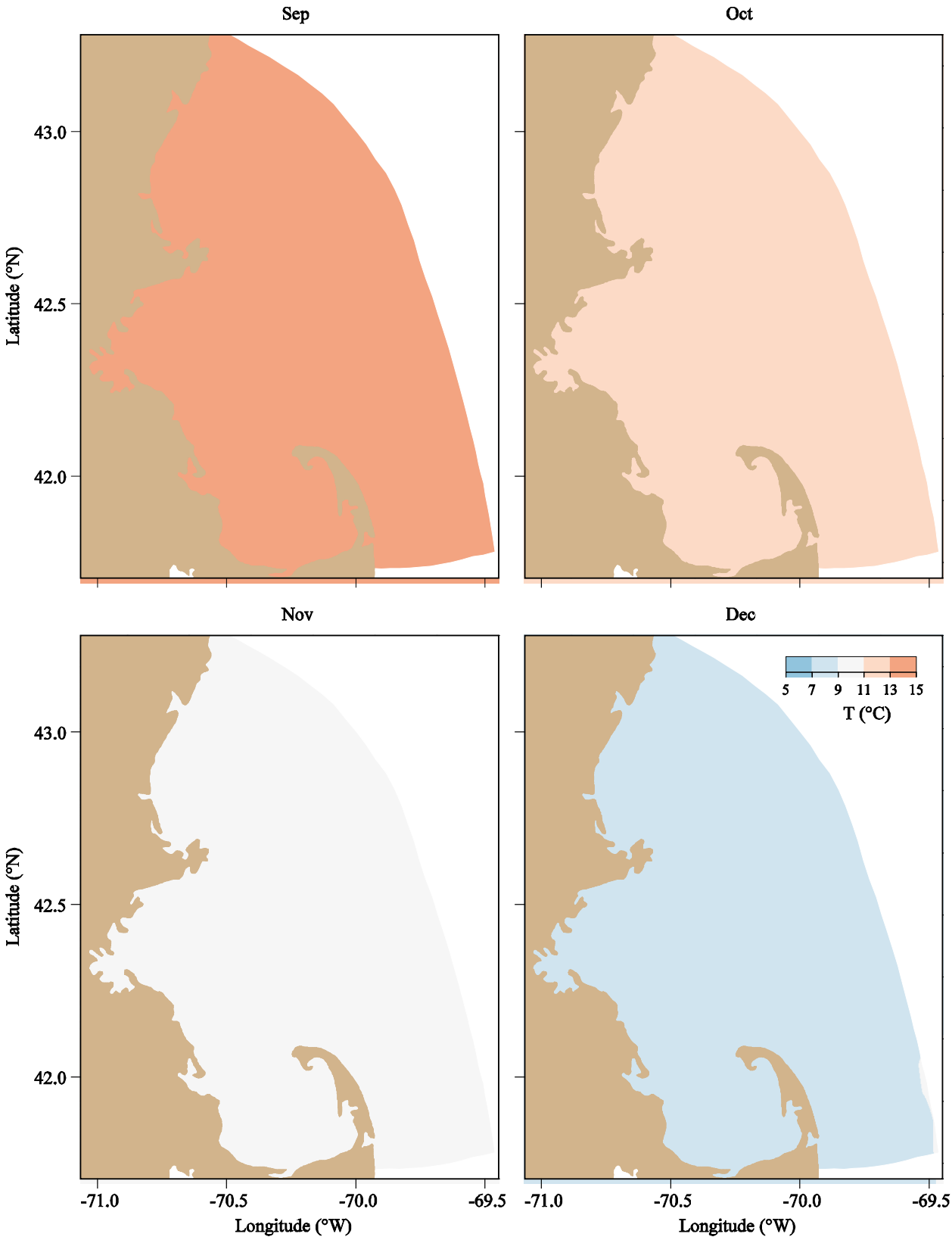

Figure 3. 13 Surface temperature at the end of September, October, November, and December, 2011 predicted by FVCOM.

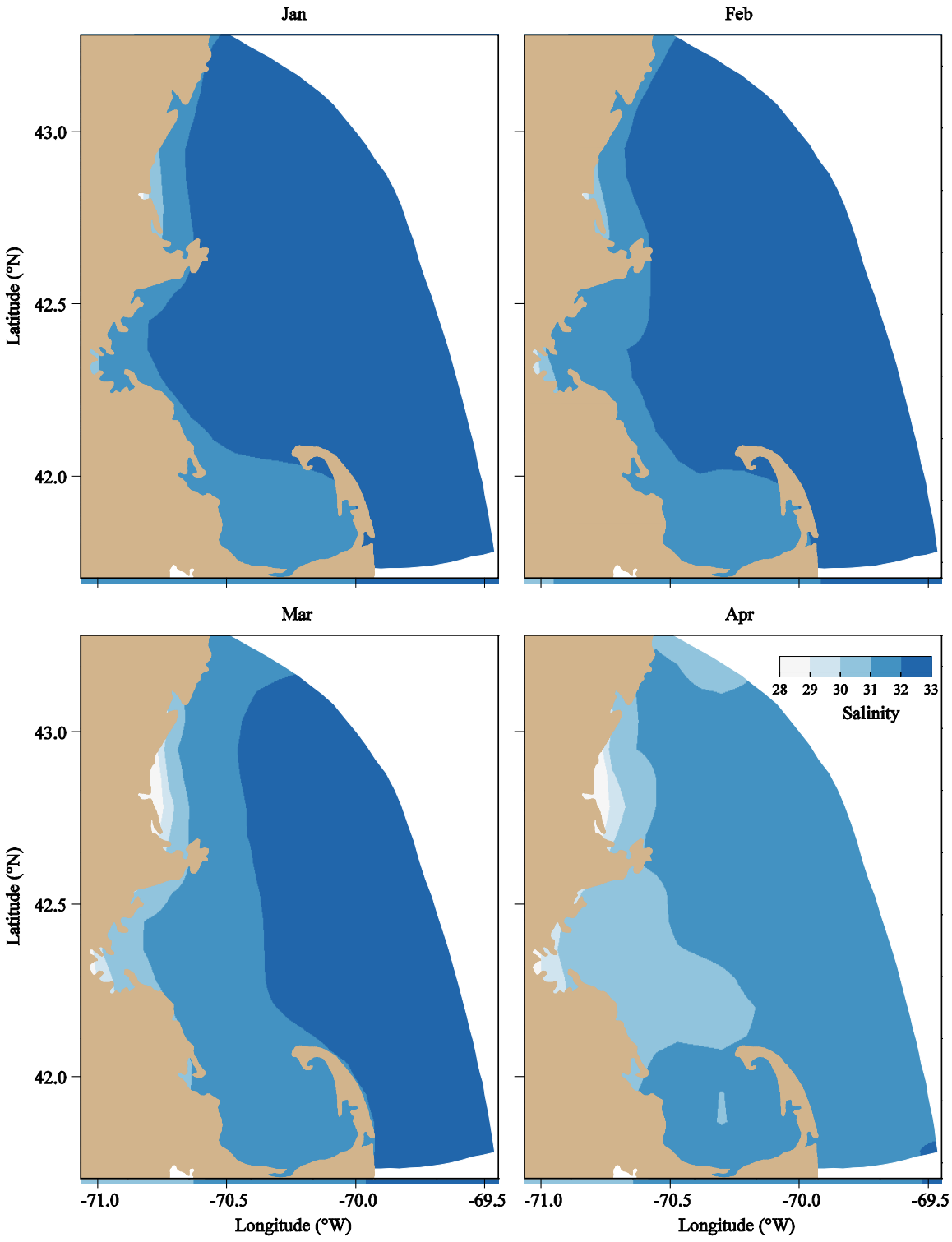

Figure 3. 14 Surface salinity at the end of January, February, March, and April, 2011 predicted by FVCOM.

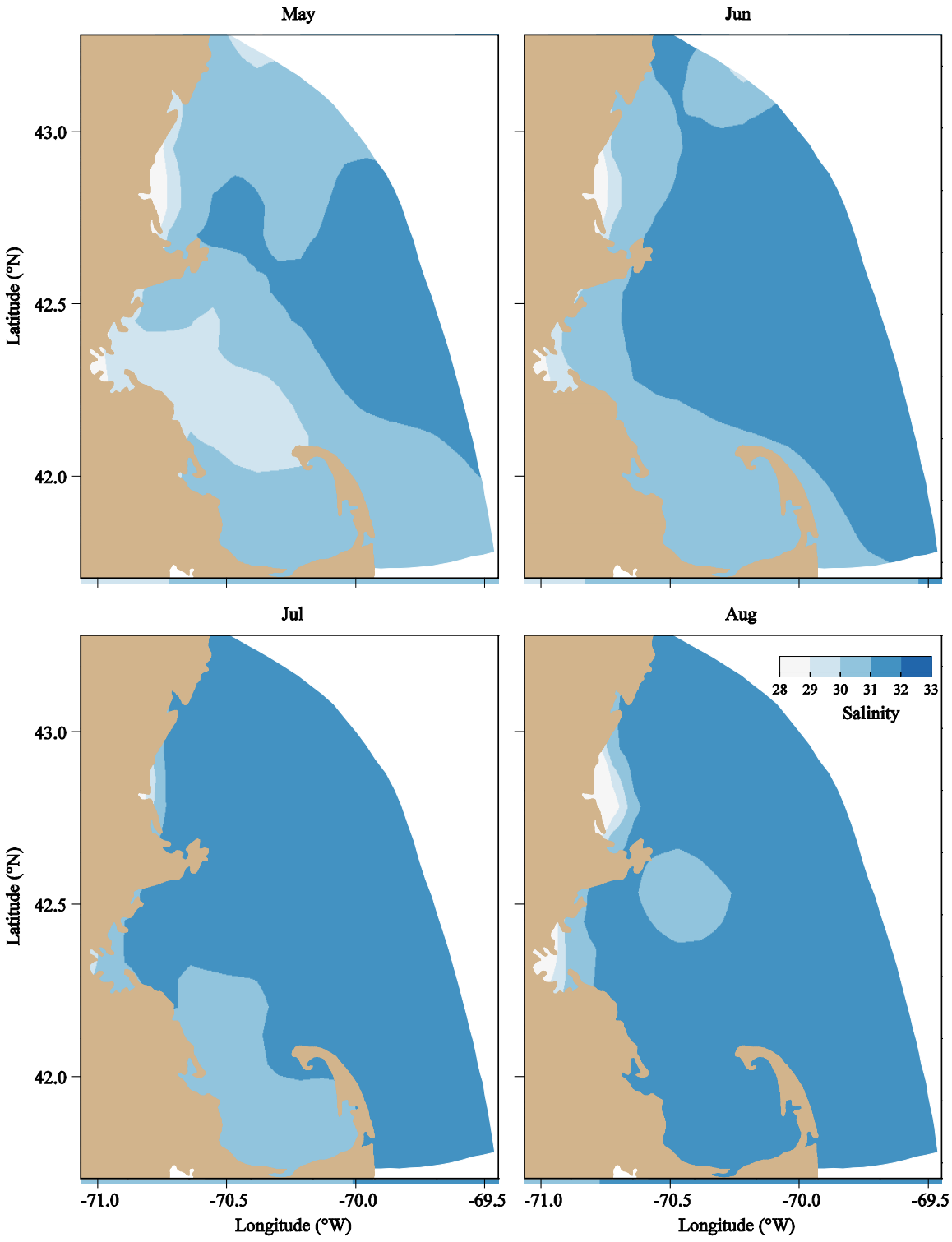

Figure 3. 15 Surface salinity at the end of May, June, July, and August, 2011 predicted by FVCOM.

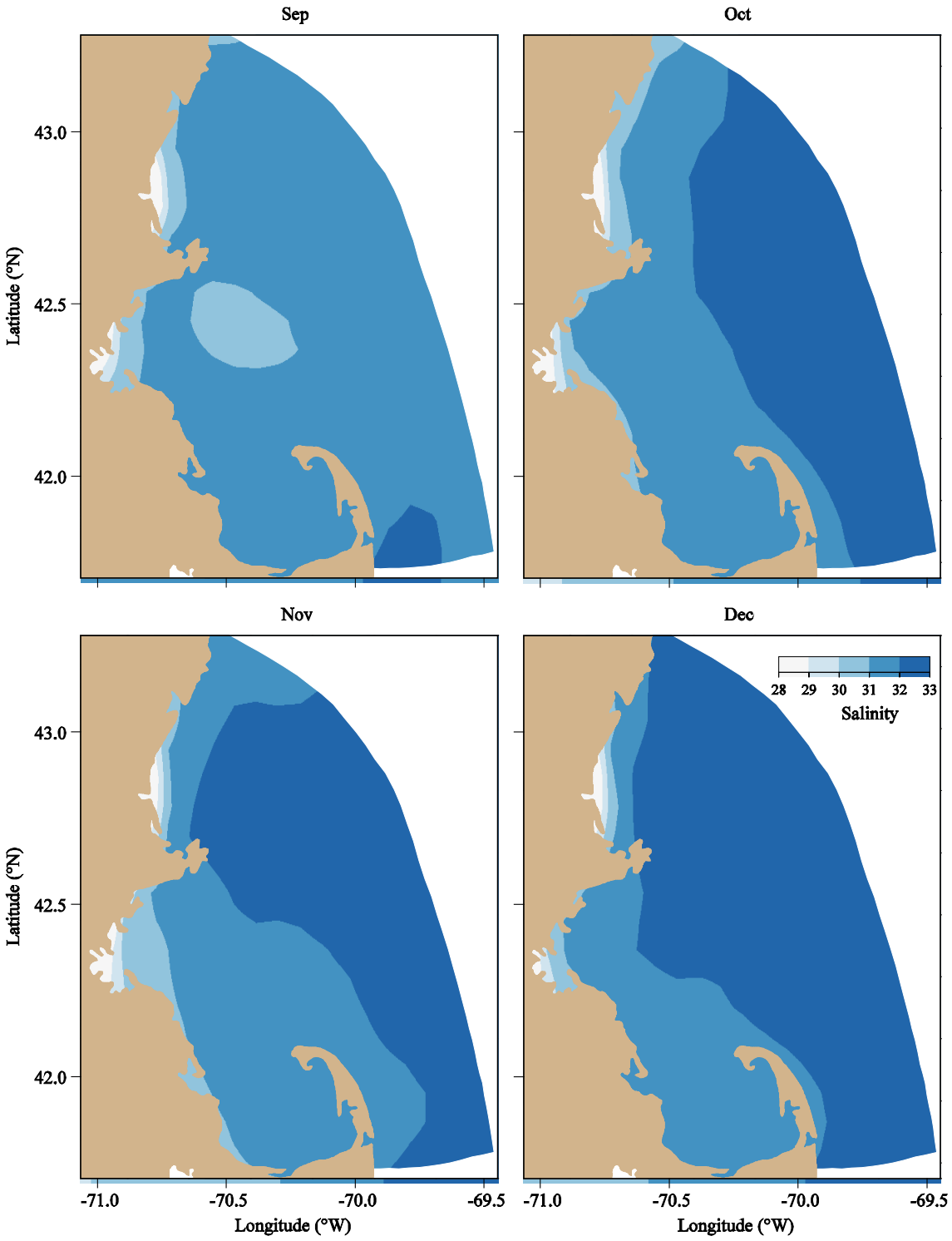

Figure 3. 16 Surface salinity at the end of September, October, November, and December, 2011 predicted by FVCOM.

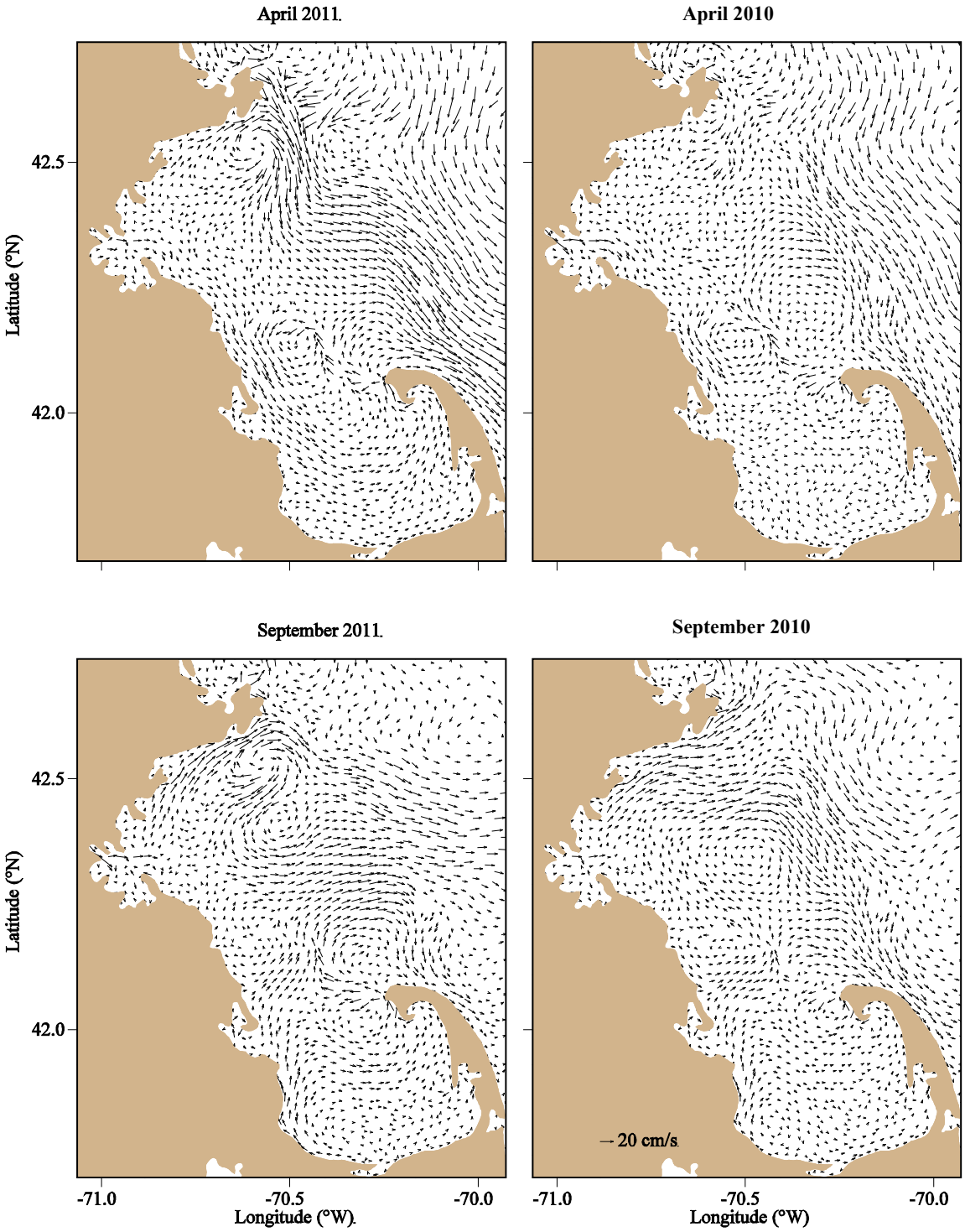

Figure 3. 17 Monthly-averaged surface current of 2011 (left panels) and 2010 (right panels) in April (upper panels) and September (lower panels).

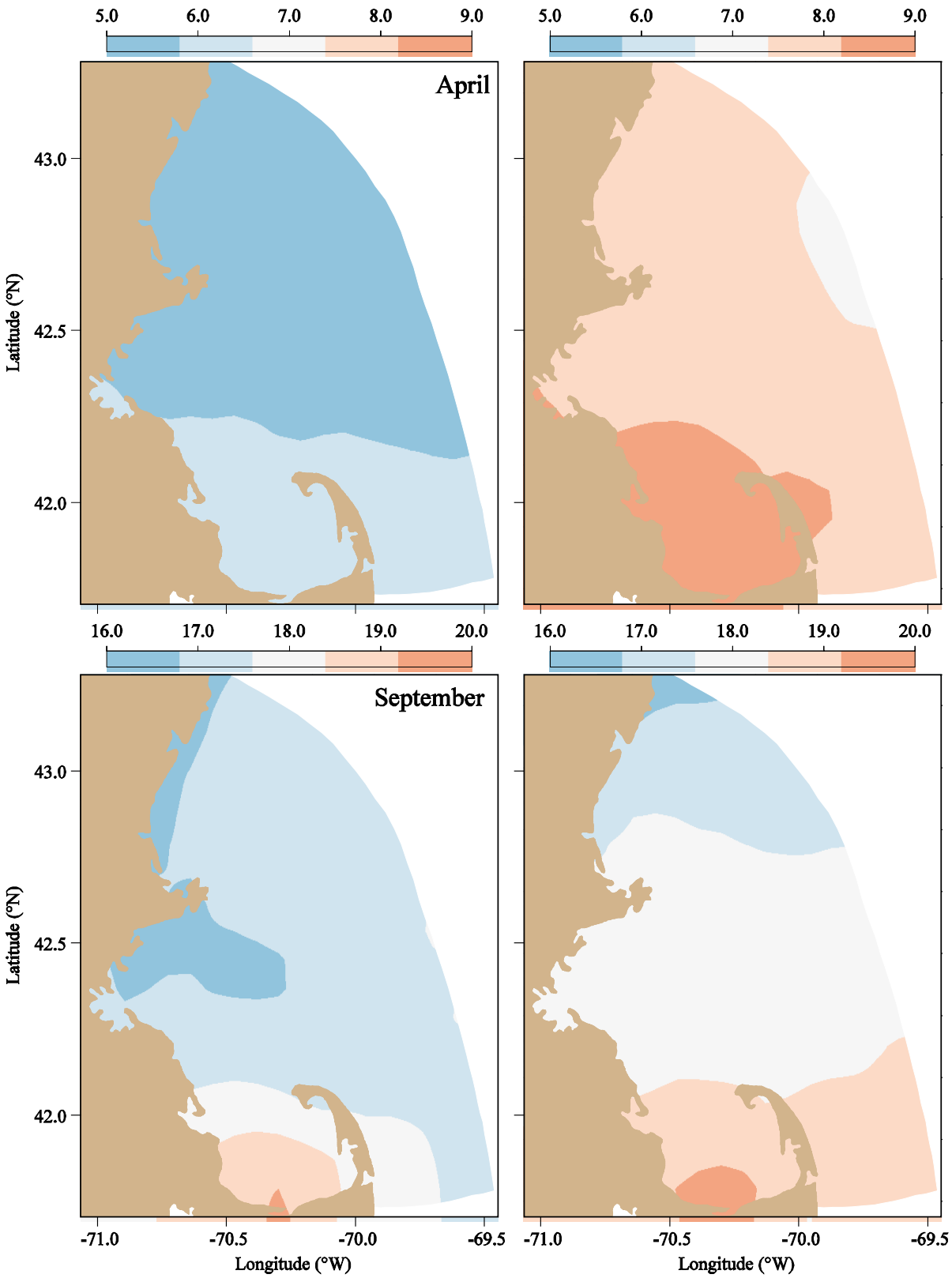

Figure 3. 18 Monthly-averaged surface temperature of 2011 (left panels) and 2010 (right panels) in April (upper panels) and September (lower panels).

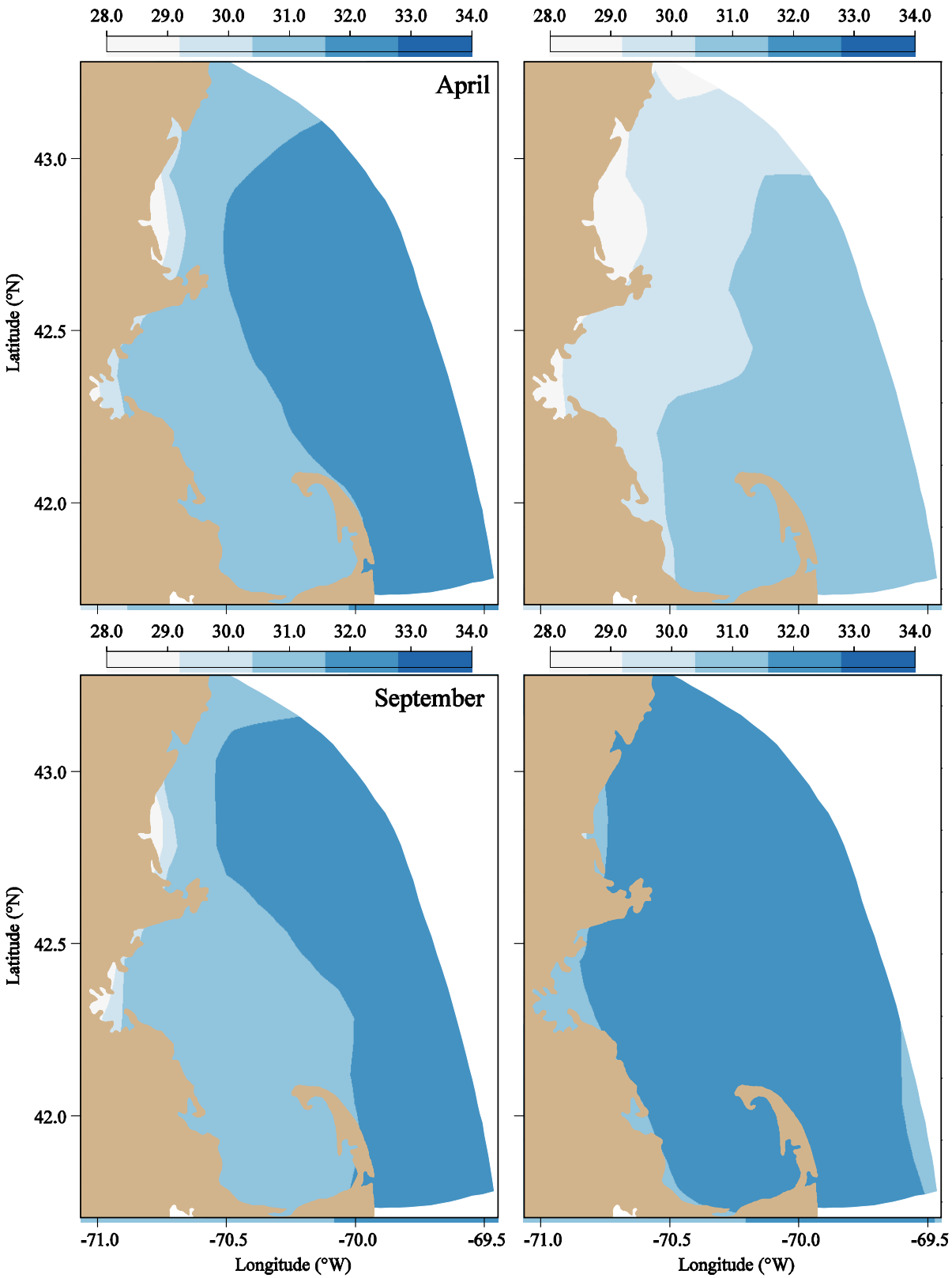

Figure 3. 19 Monthly-averaged surface salinity of 2011 (left panels) and 2010 (right panels) in April (upper panels) and September (lower panels).

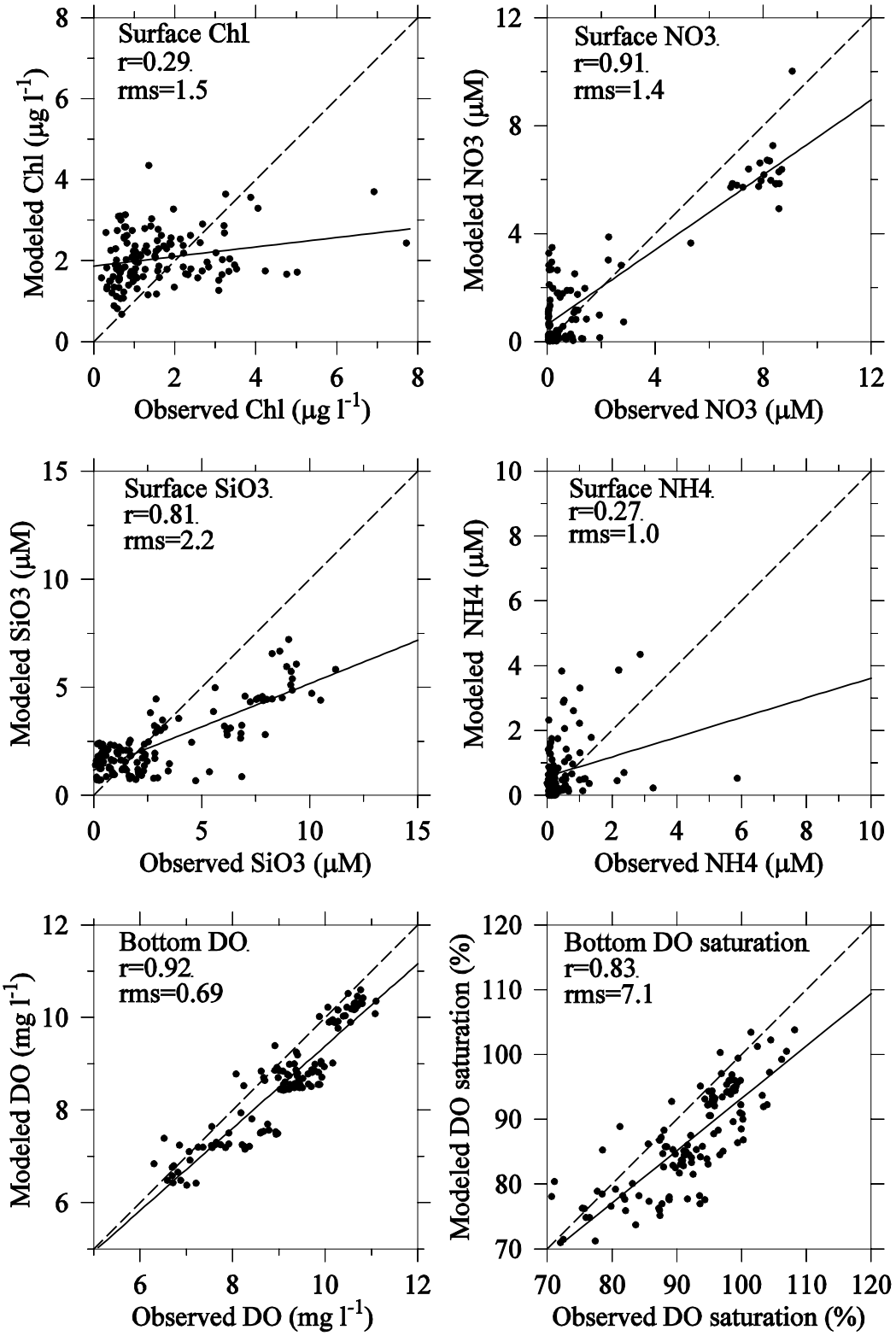

Figure 3. 20 Overall correlation and regression (solid lines) between observed and modeled results of key parameters in 2011. The dashed lines indicate equality between observed and modeled results. All stations are included.

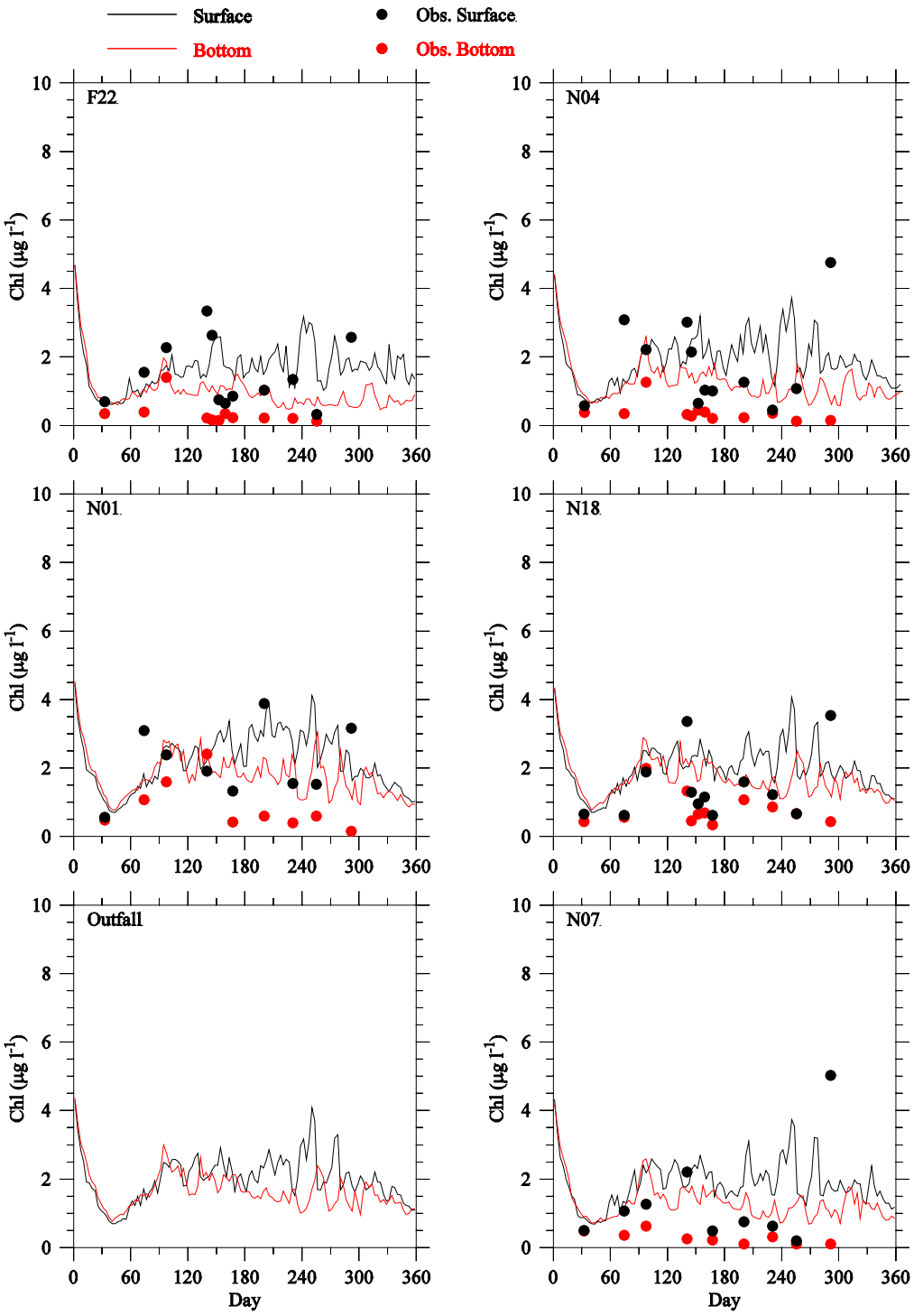

Figure 3. 21 Comparison of chlorophyll observed (dots) and modeled (lines) time-series at the outfall site and selected Massachusetts Bay monitoring stations F22, N04, N01, N18, and N07 for 2011. No chlorophyll data are available at the outfall site.

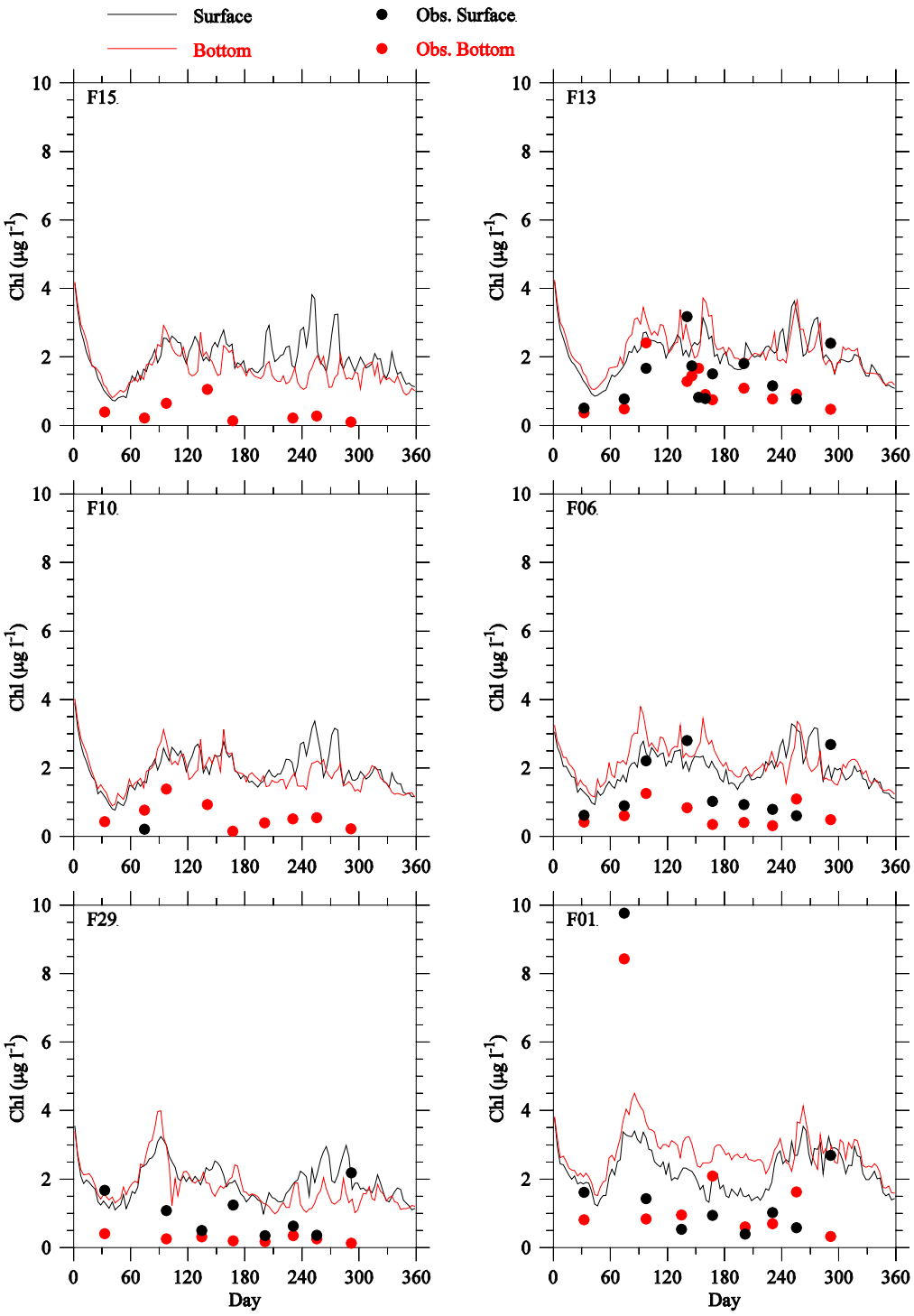

Figure 3. 22 Comparison of chlorophyll observed (dots) and modeled (lines) time-series at selected Massachusetts Bay monitoring stations F15, F13, F10, F06, F29 and F01 for 2010. (Results for stations F15, F10 and F29 are calibrated fluorescence rather than extracted chlorophyll.)

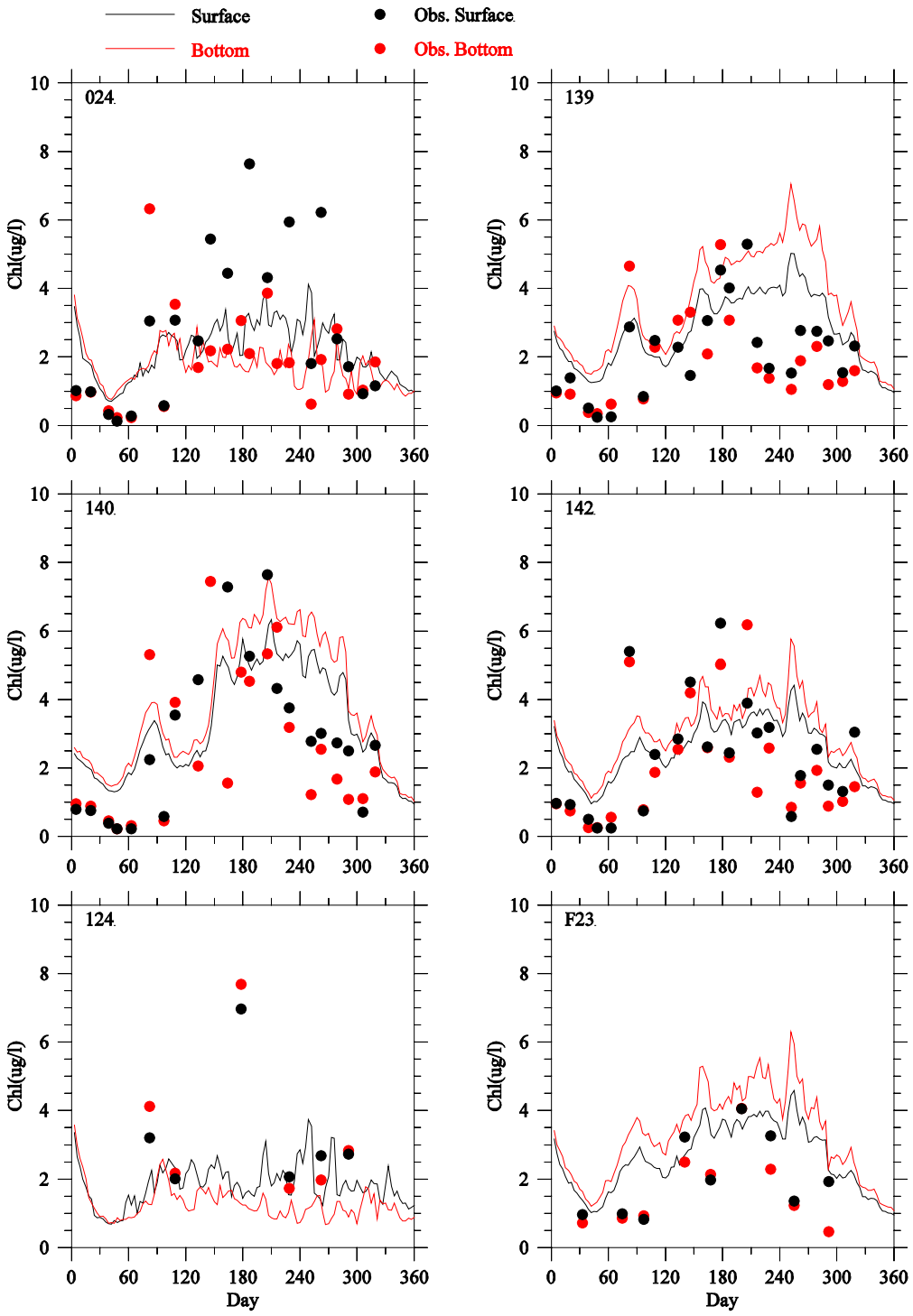

Figure 3. 23 Comparison of chlorophyll observed (dots) and modeled (lines) time-series at selected Boston Harbor stations for 2011.

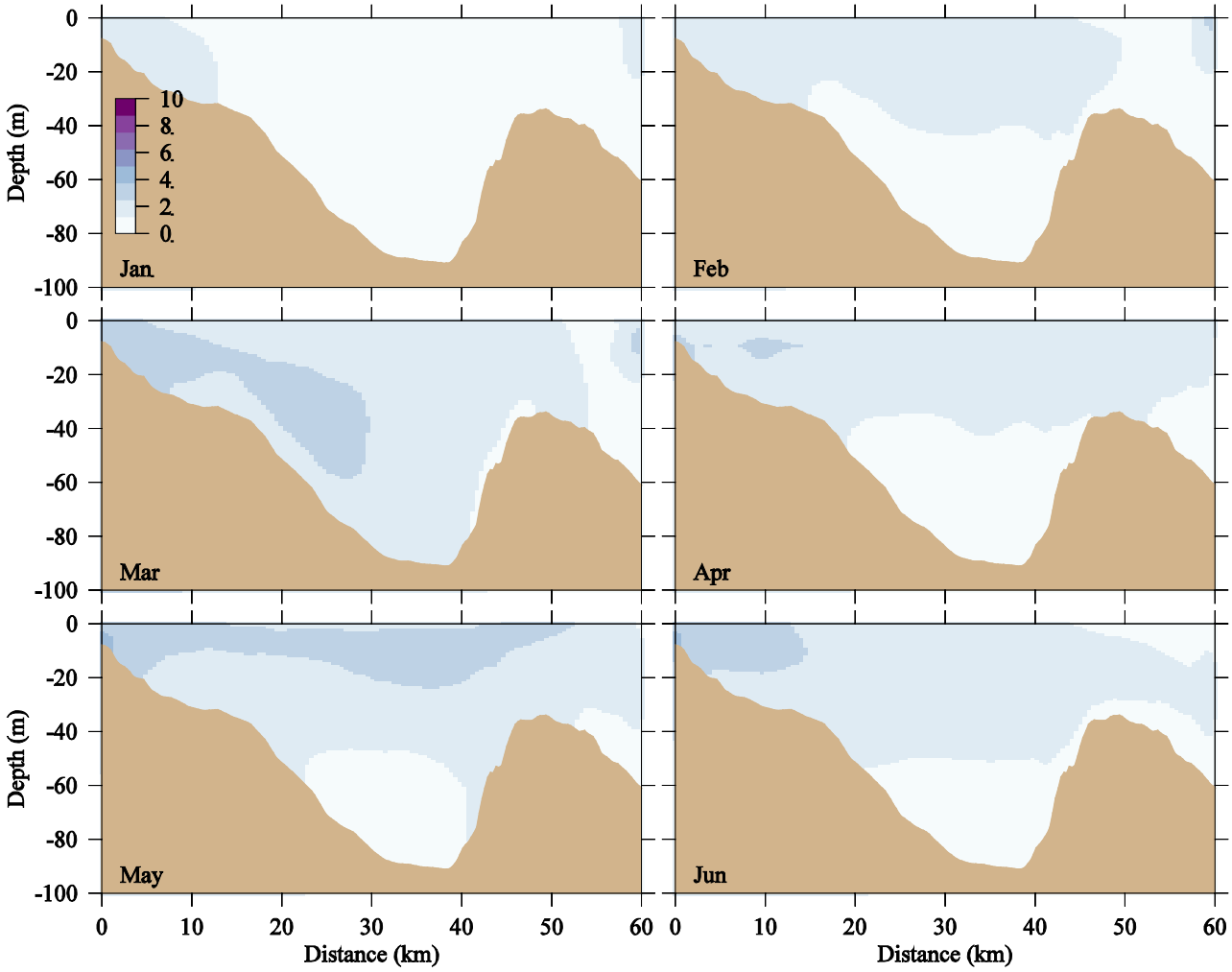

Figure 3. 24 Chlorophyll concentration (ug/l) on the east-west transect across the MWRA outfall at the end of each month from January through June in 2011.

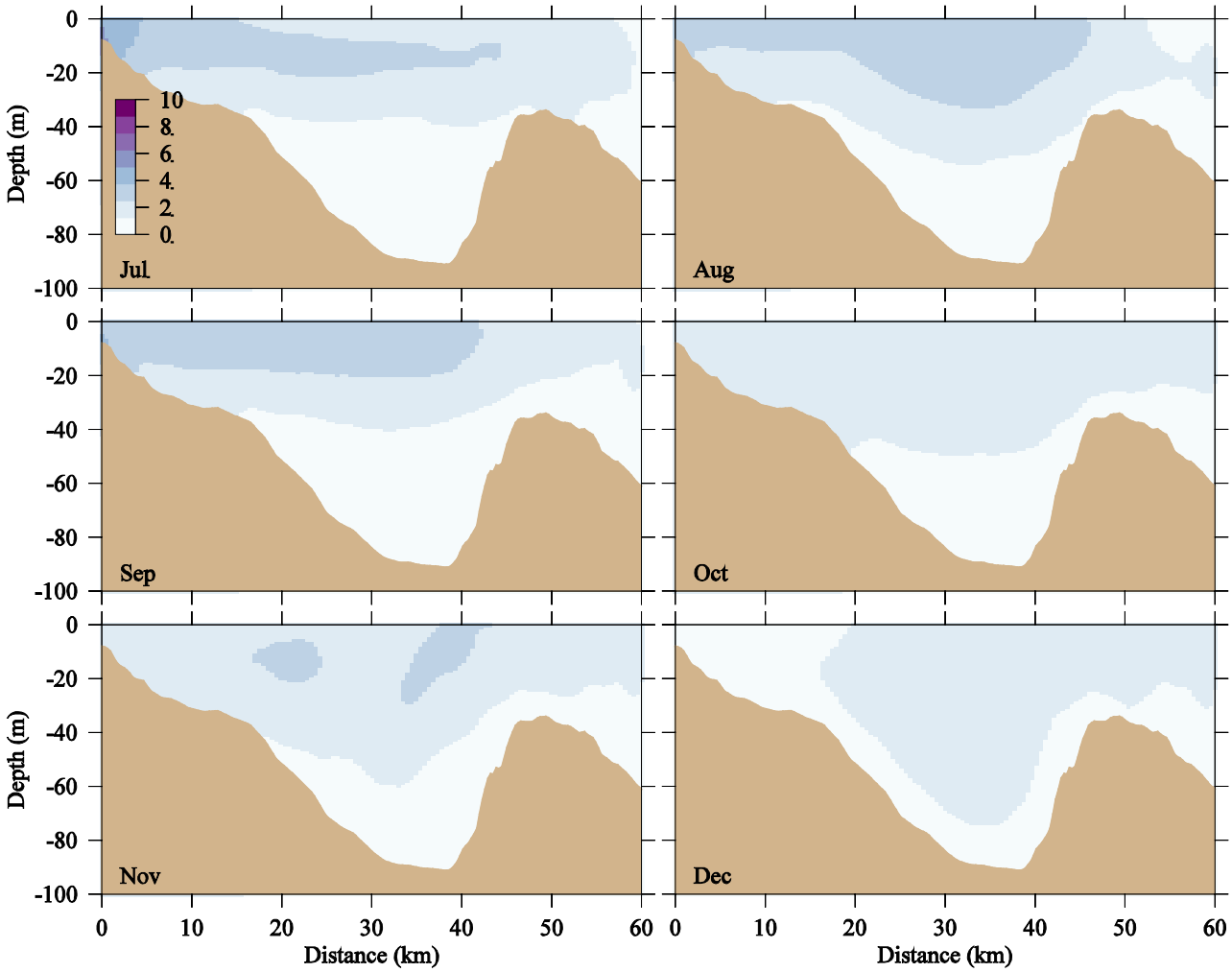

Figure 3. 25 Chlorophyll concentration (ug/l) on the east-west transect across the MWRA outfall at the end of each month from July through December in 2011

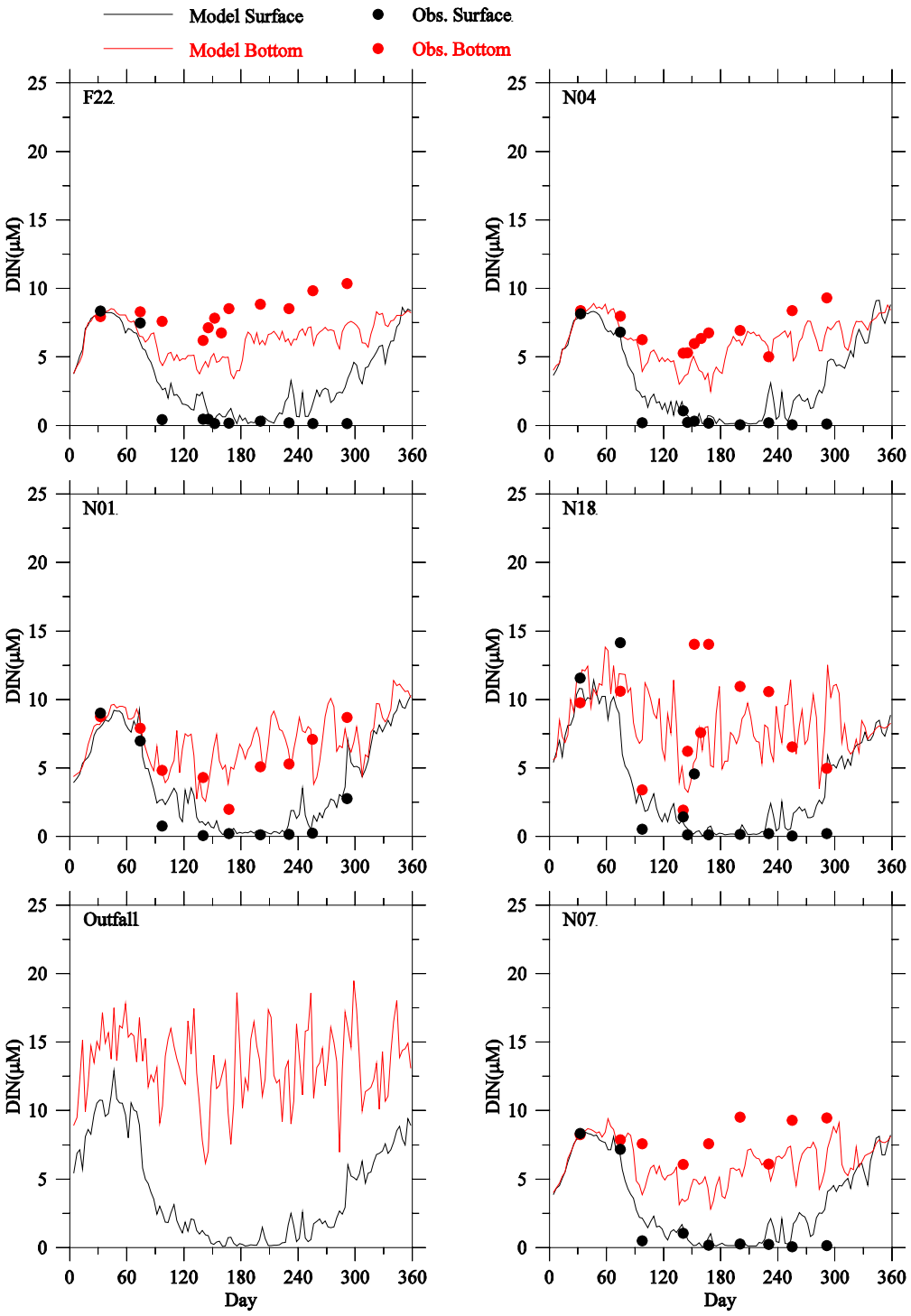

Figure 3. 26 Comparison of DIN observed (dots) and modeled (lines) time-series at the outfall site and selected Massachusetts Bay monitoring stations F22, N04, N01, N18, and N07 for 2011. No DIN data are available at the outfall site.

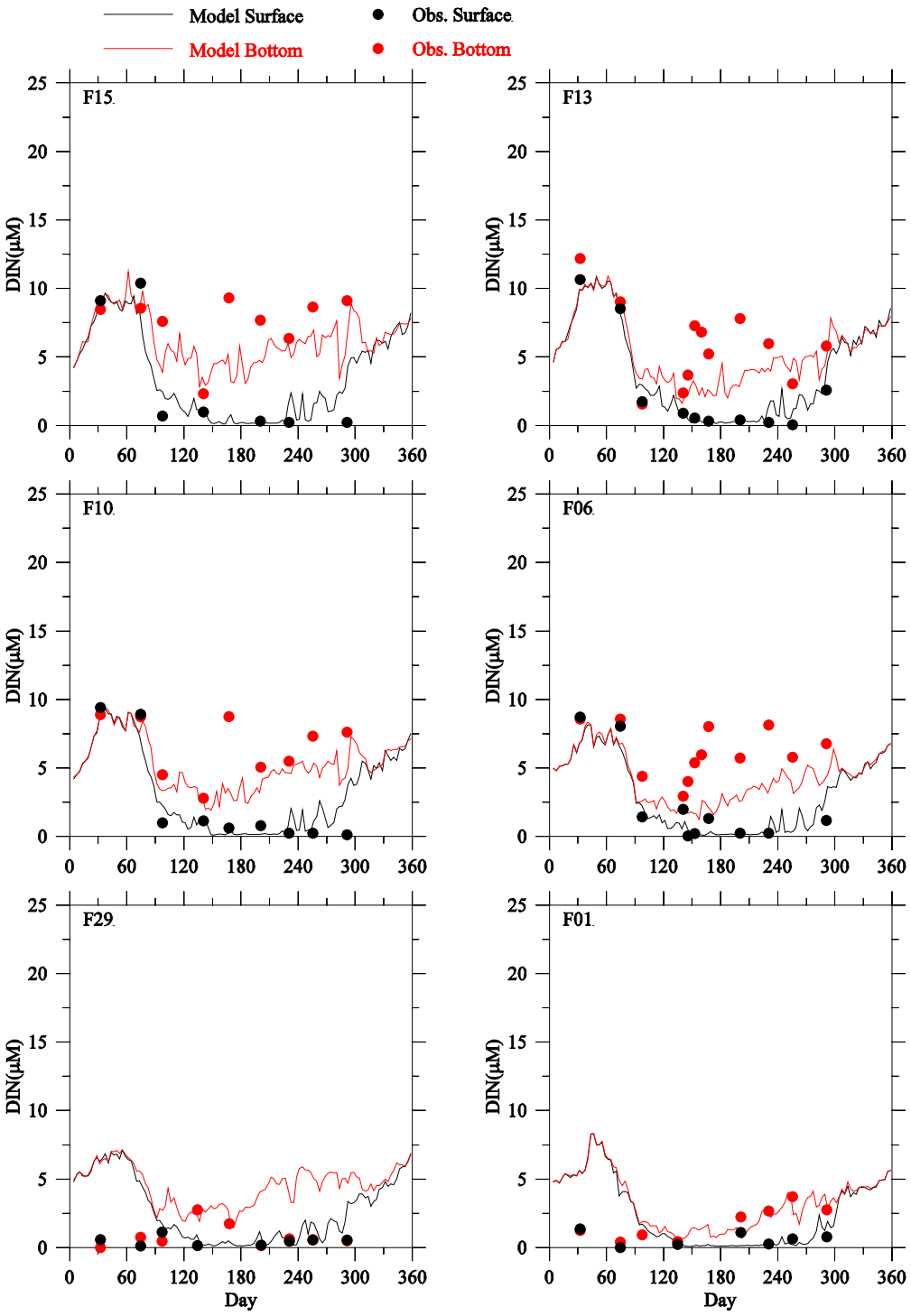

Figure 3. 27 Comparison of DIN observed (dots) and modeled (lines) time-series at selected Massachusetts Bay monitoring stations F15, F13, F10, F06, F29 and F01 for 2011.

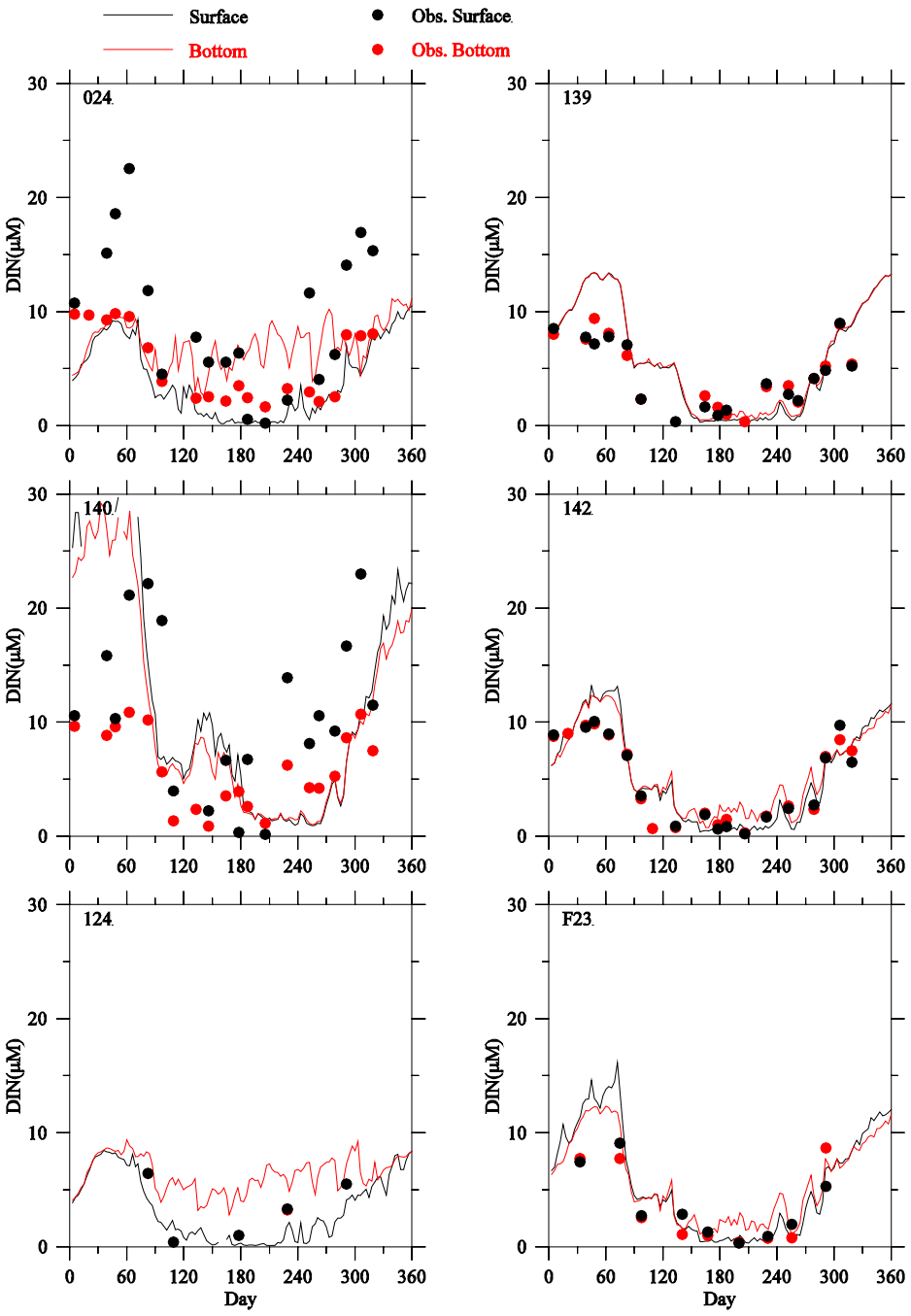

Figure 3. 28 Comparison of DIN observed (dots) and modeled (lines) time-series at selected Boston Harbor stations for 2011.

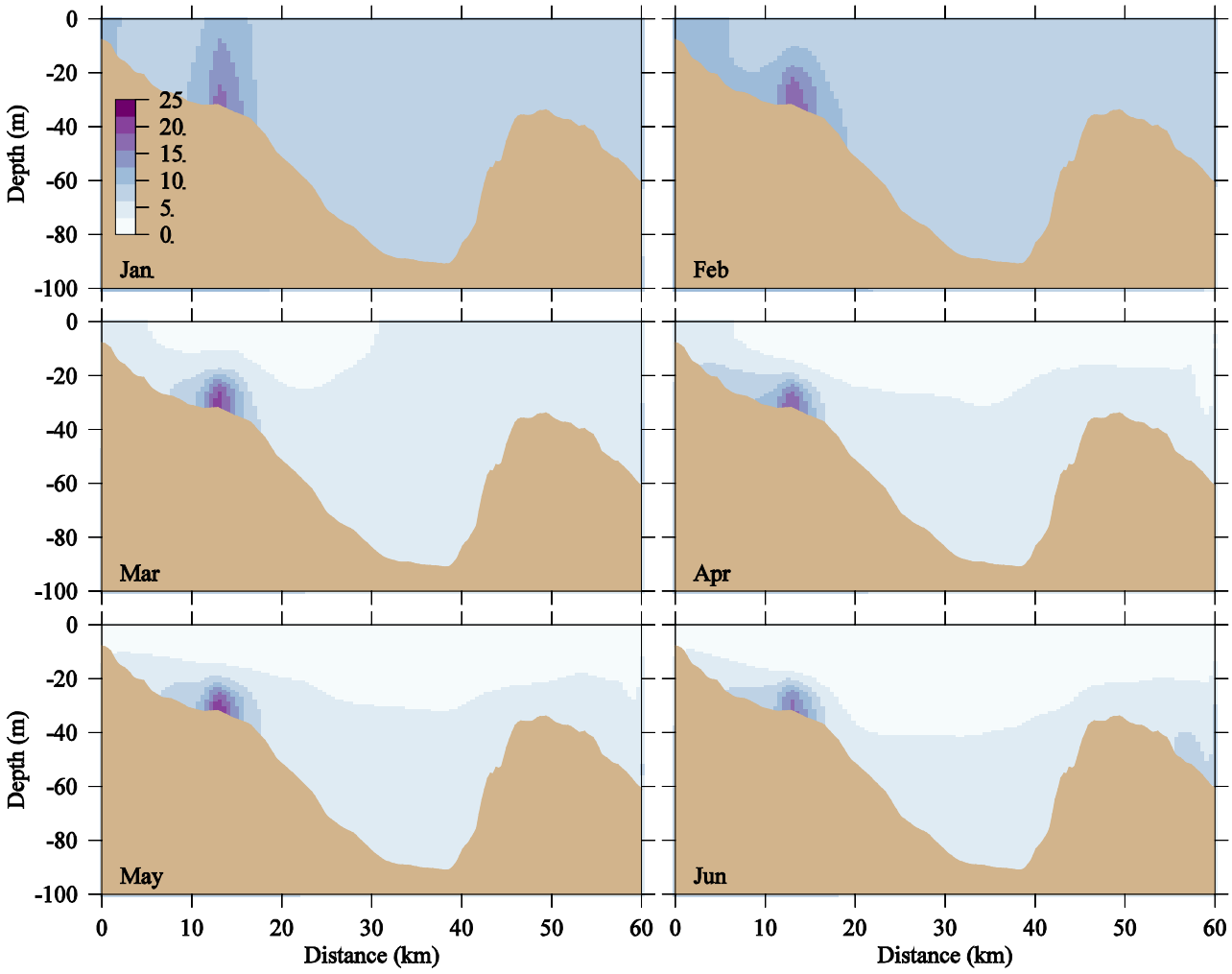

Figure 3. 29 DIN concentrations (μM) on the east-west transect across the MWRA outfall at the end of each month from January through June in 2011.

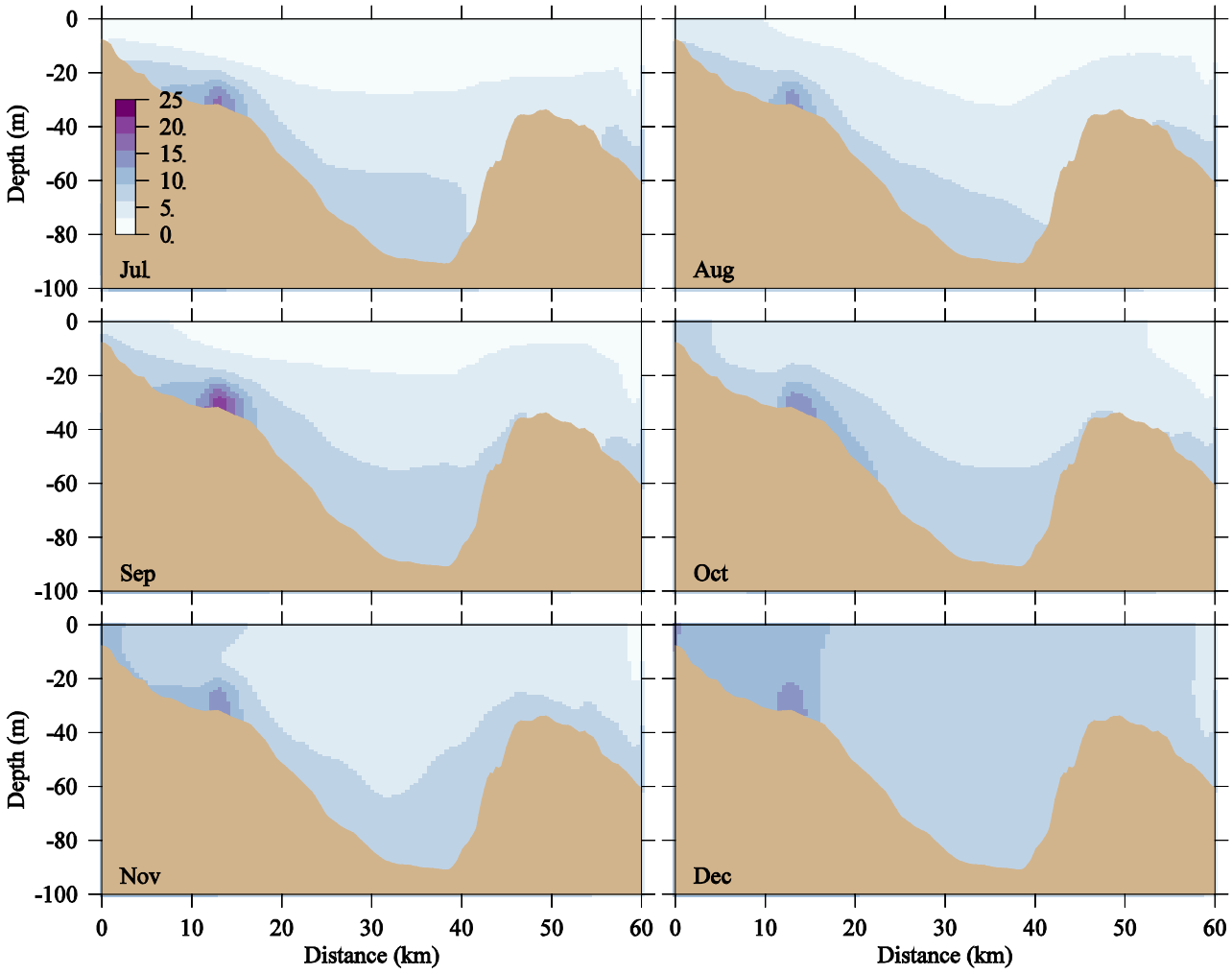

Figure 3. 30 DIN concentrations (μM) on the east-west transect across the MWRA outfall at the end of each month from July through December in 2011.

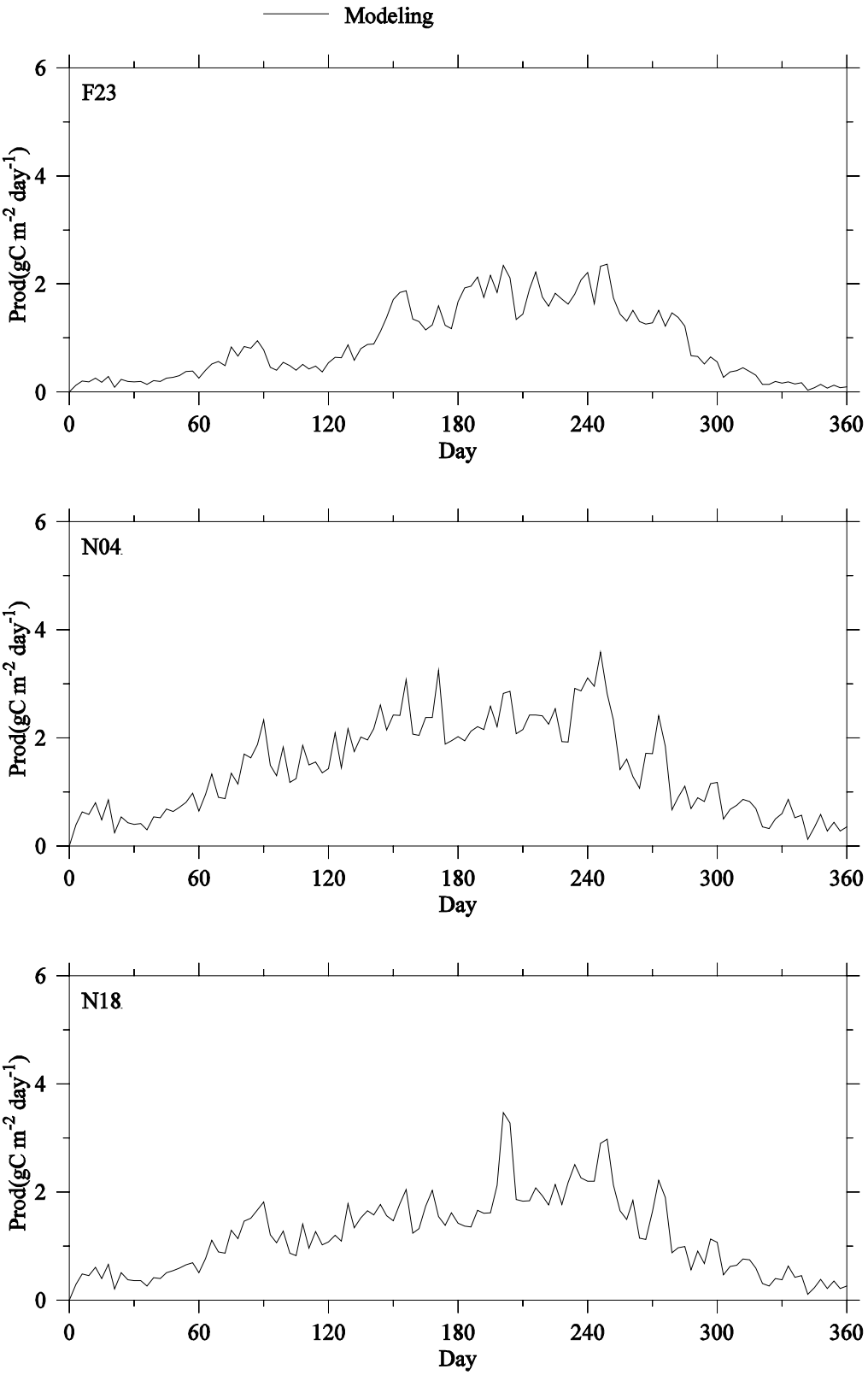

Figure 3. 31 Vertically integrated primary production time series at the MWRA monitoring stations in 2011.

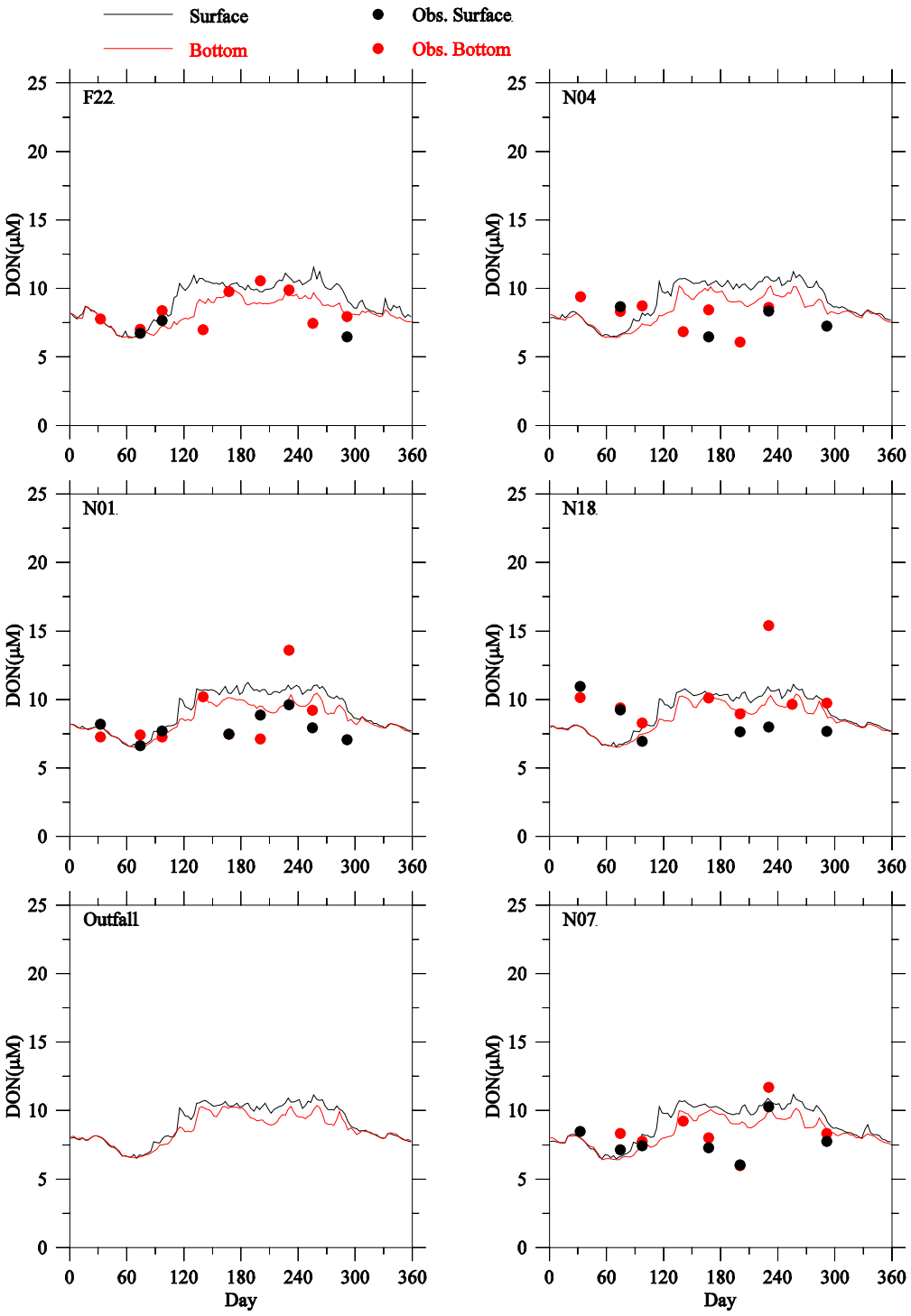

Figure 3. 32 Comparison of DON observed (dots) and modeled (lines) time-series at the outfall site and selected Massachusetts Bay monitoring stations F22, N04, N01, N18, and N07 for 2011. No DON data are available at the outfall site.

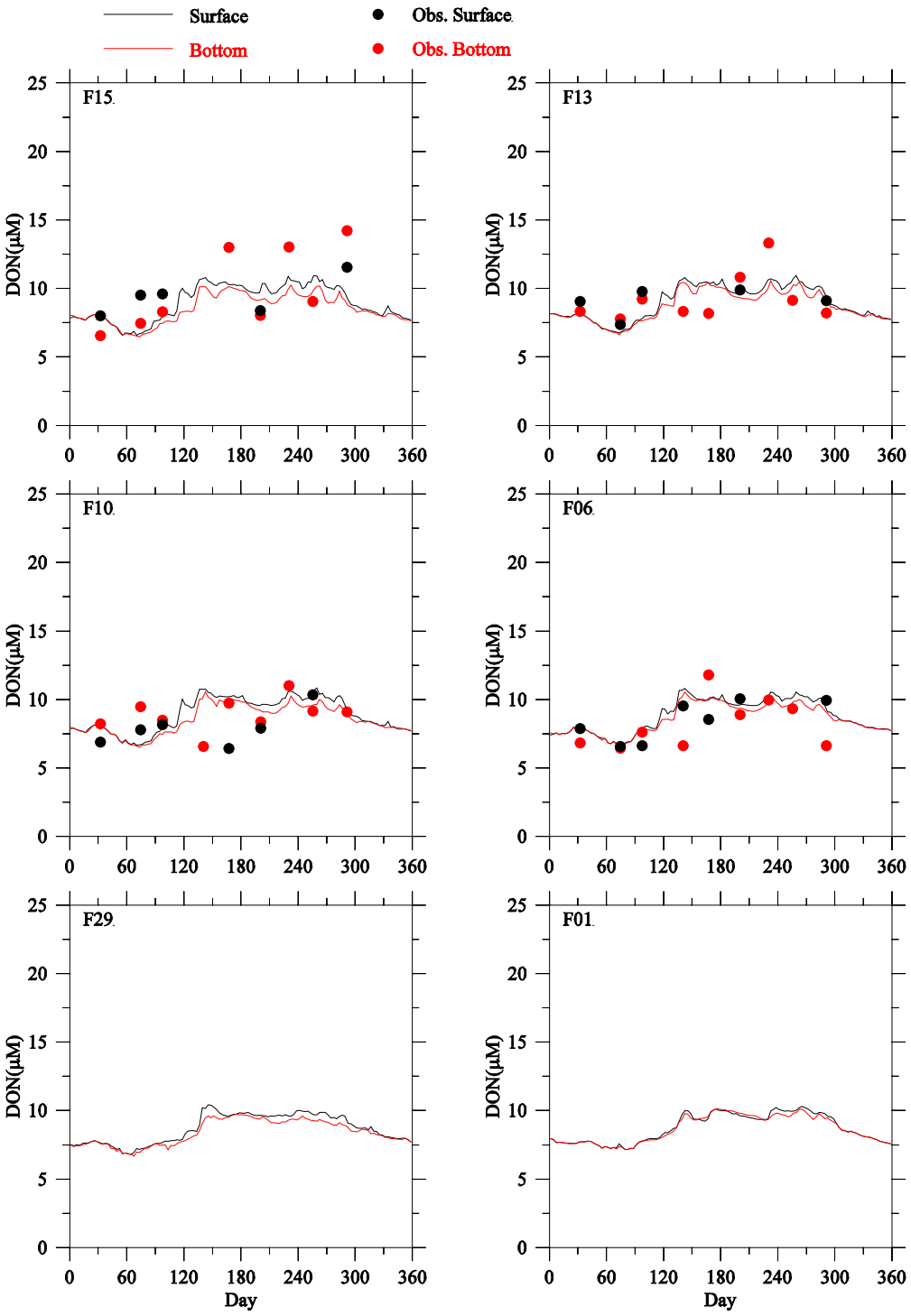

Figure 3. 33 Comparison of DON observed (dots) and modeled (lines) time-series at selected Massachusetts Bay monitoring stations F15, F13, F10, F06, F29 and F01 for 2011. No DON data are available at stations F01 and F29.

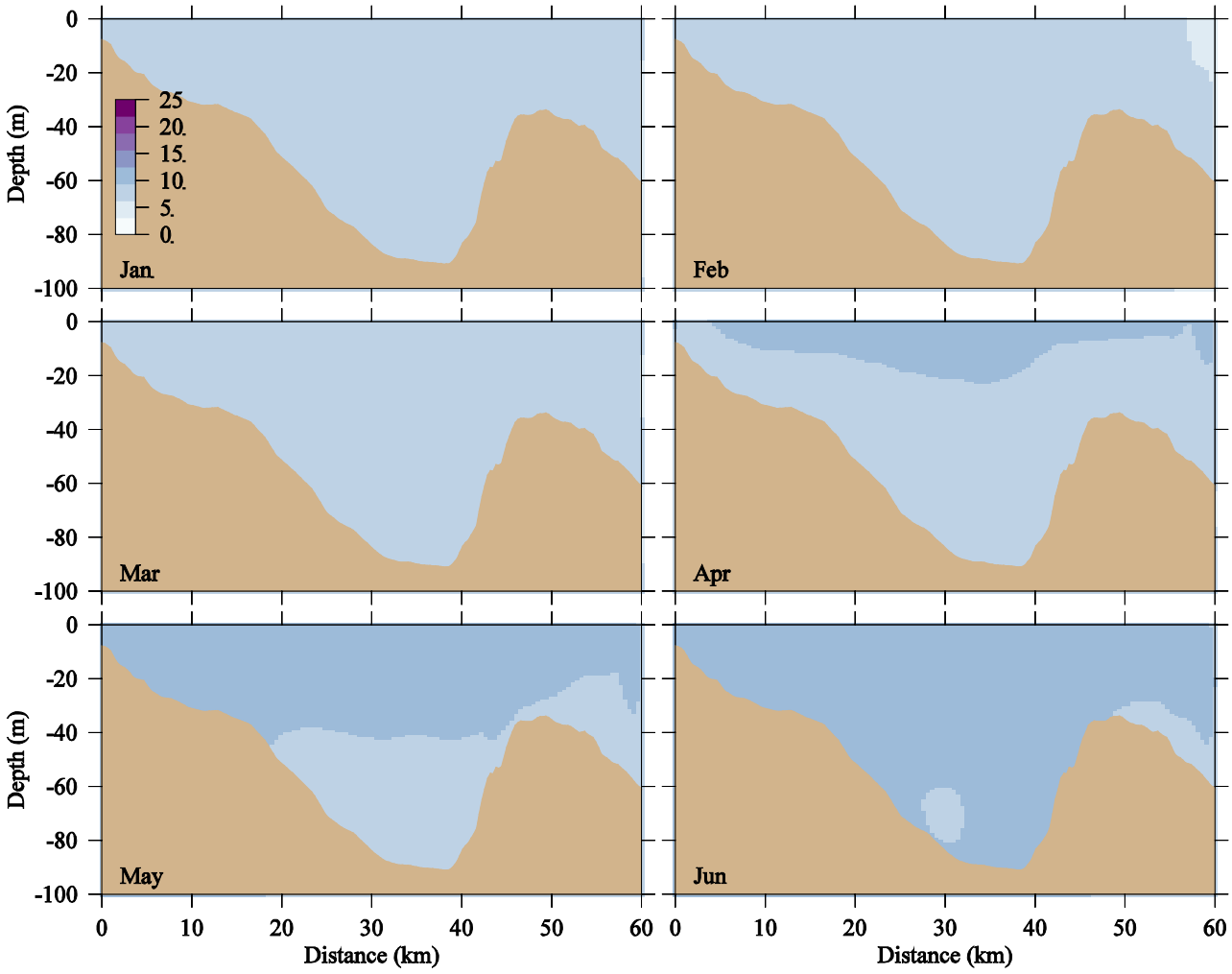

Figure 3. 34 DON concentration (μM) on the east-west transect across the MWRA outfall at the end of each month from January through June in 2011.

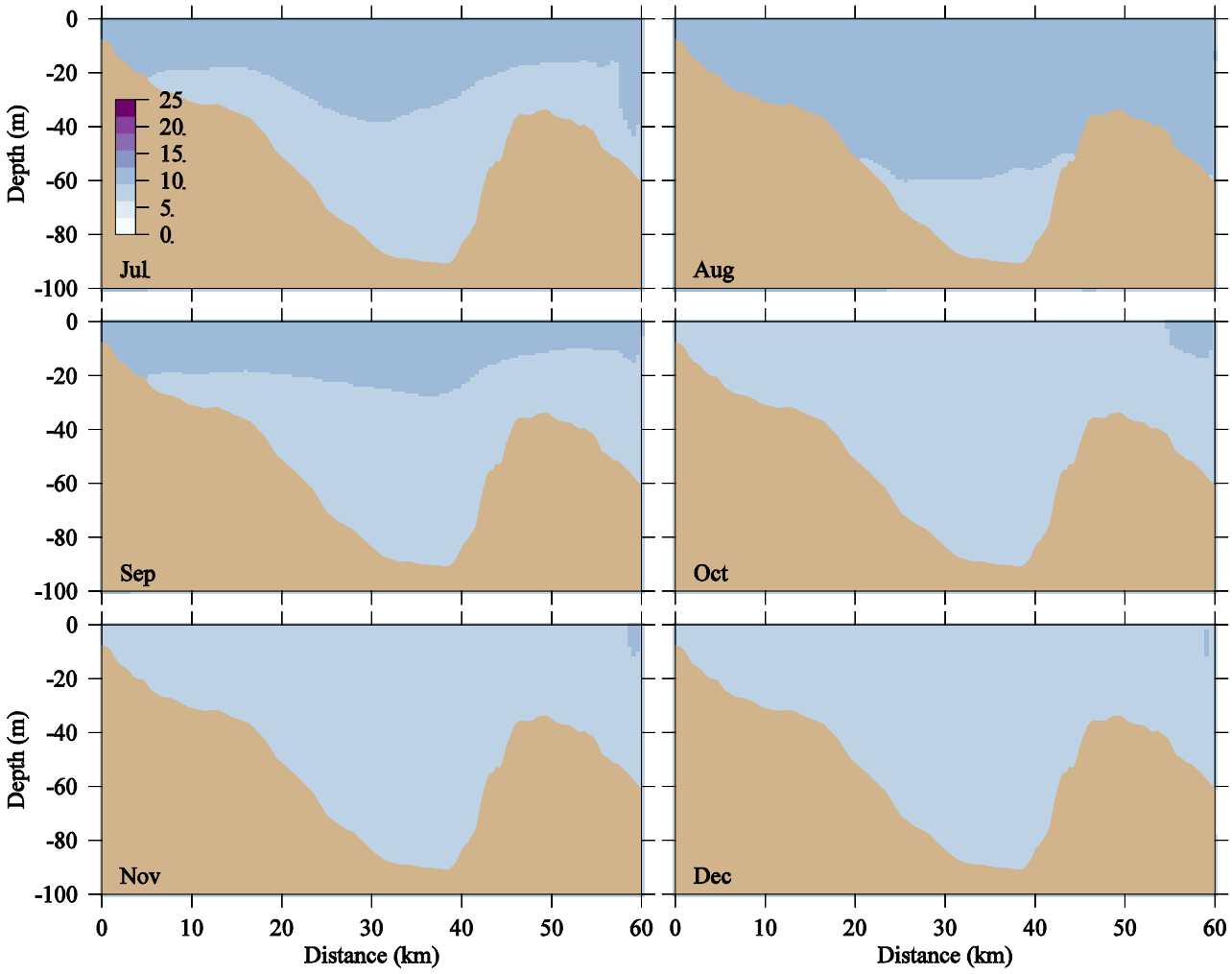

Figure 3. 35 DON concentration (μM) on the east-west transect across the MWRA outfall at the end of each month from July through December in 2011.

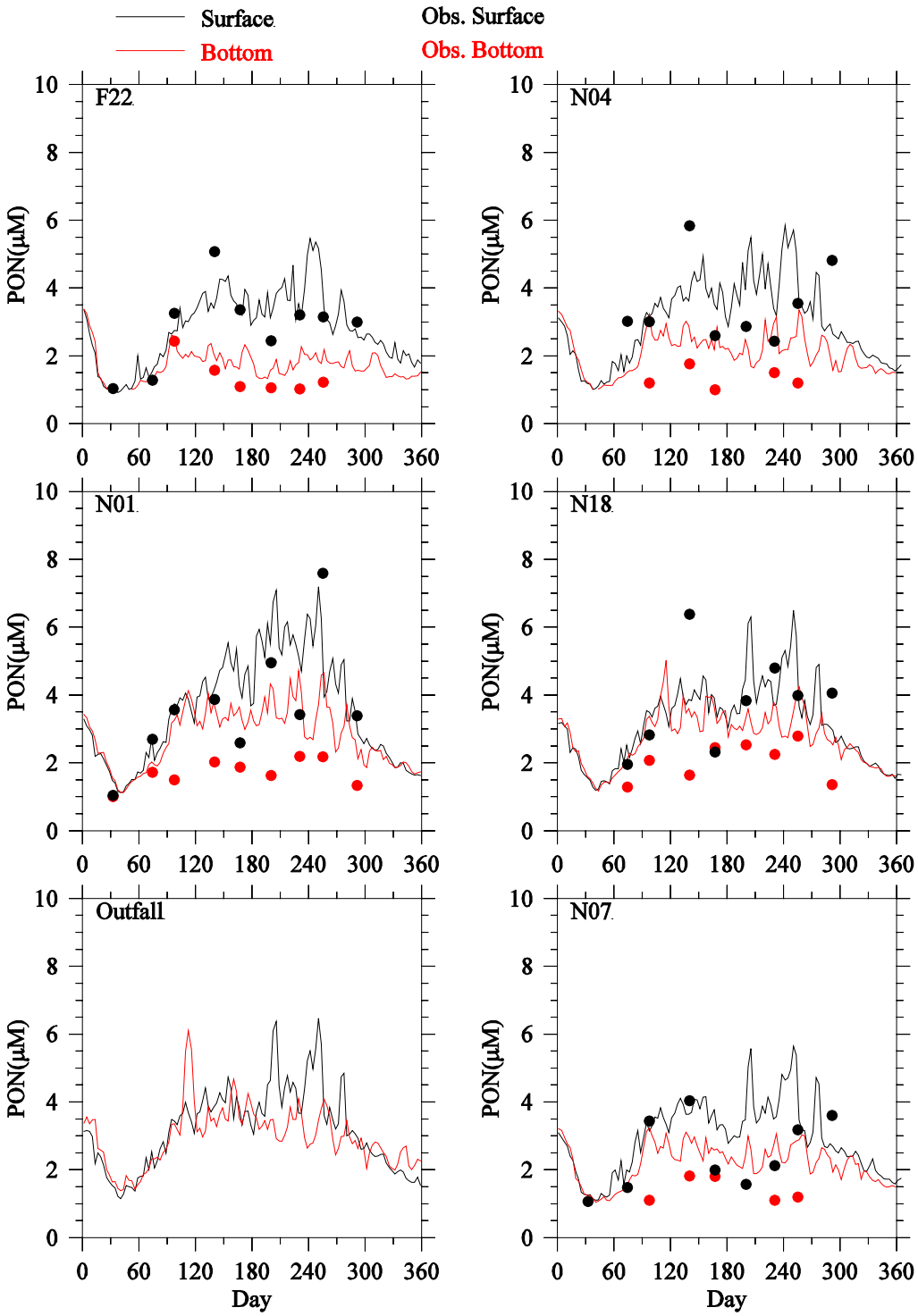

Figure 3. 36 Comparison of PON observed (dots) and modeled (lines) time-series at the outfall site and selected Massachusetts Bay monitoring stations F22, N04, N01, N18, and N07 for 2011. No PON data are available at the outfall site.

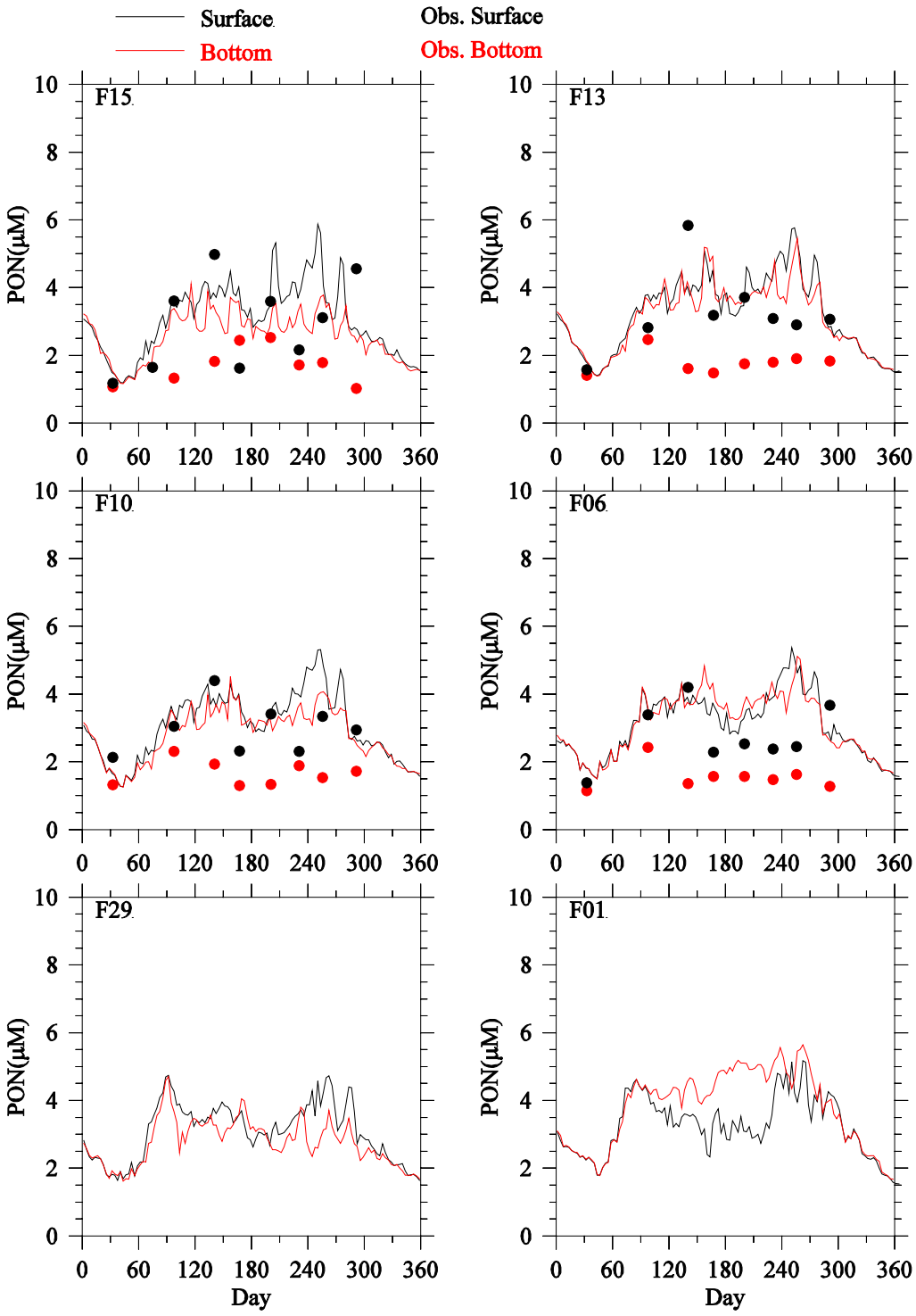

Figure 3. 37 Comparison of PON observed (dots) and modeled (lines) time-series at selected Massachusetts Bay monitoring stations F15, F13, F10, F06, F29 and F01 for 2011. No PON data are available at stations F15, F10 and F29.

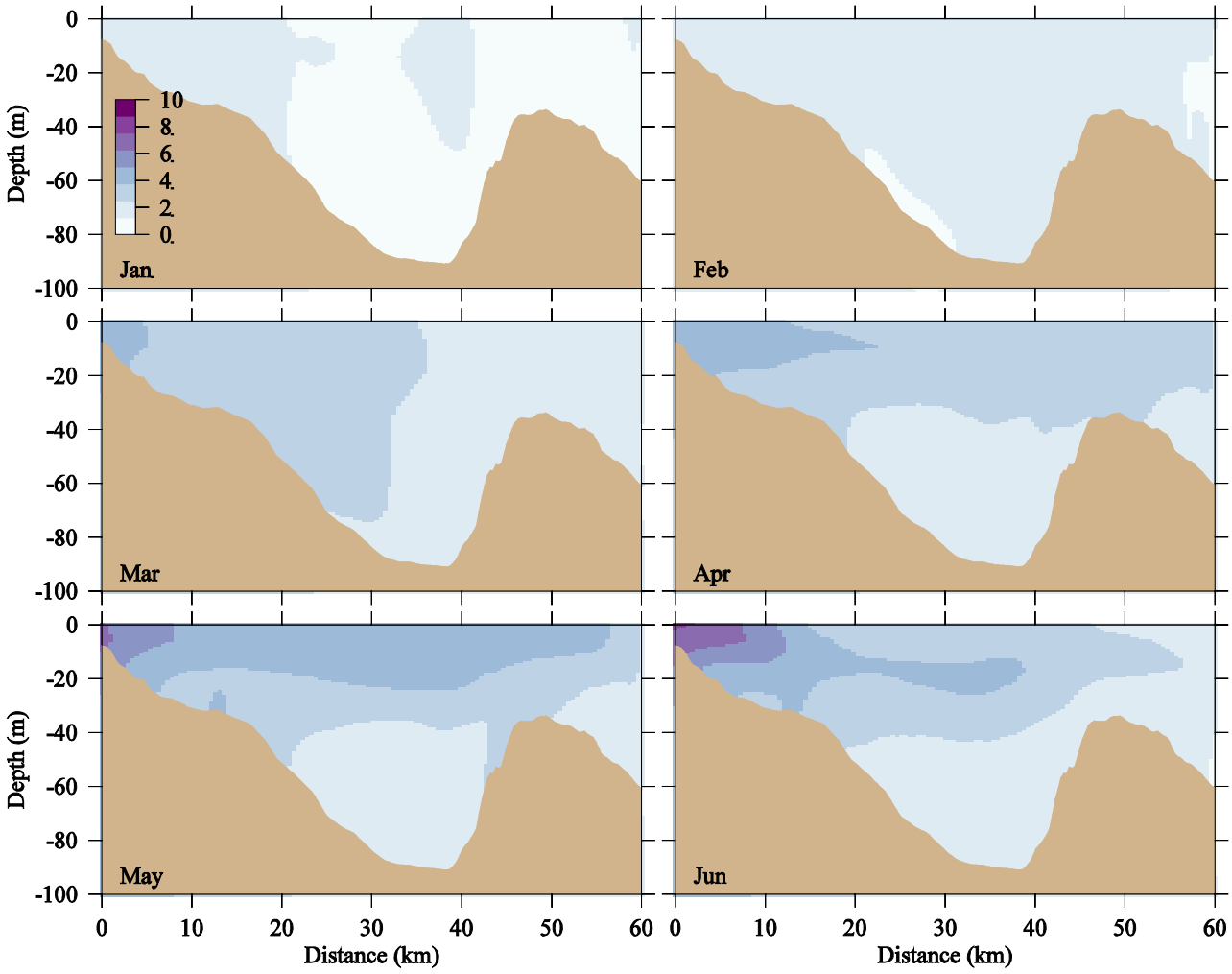

Figure 3. 38 PON concentration (μM) on the east-west transect across the MWRA outfall at the end of each month from January through June in 2011.

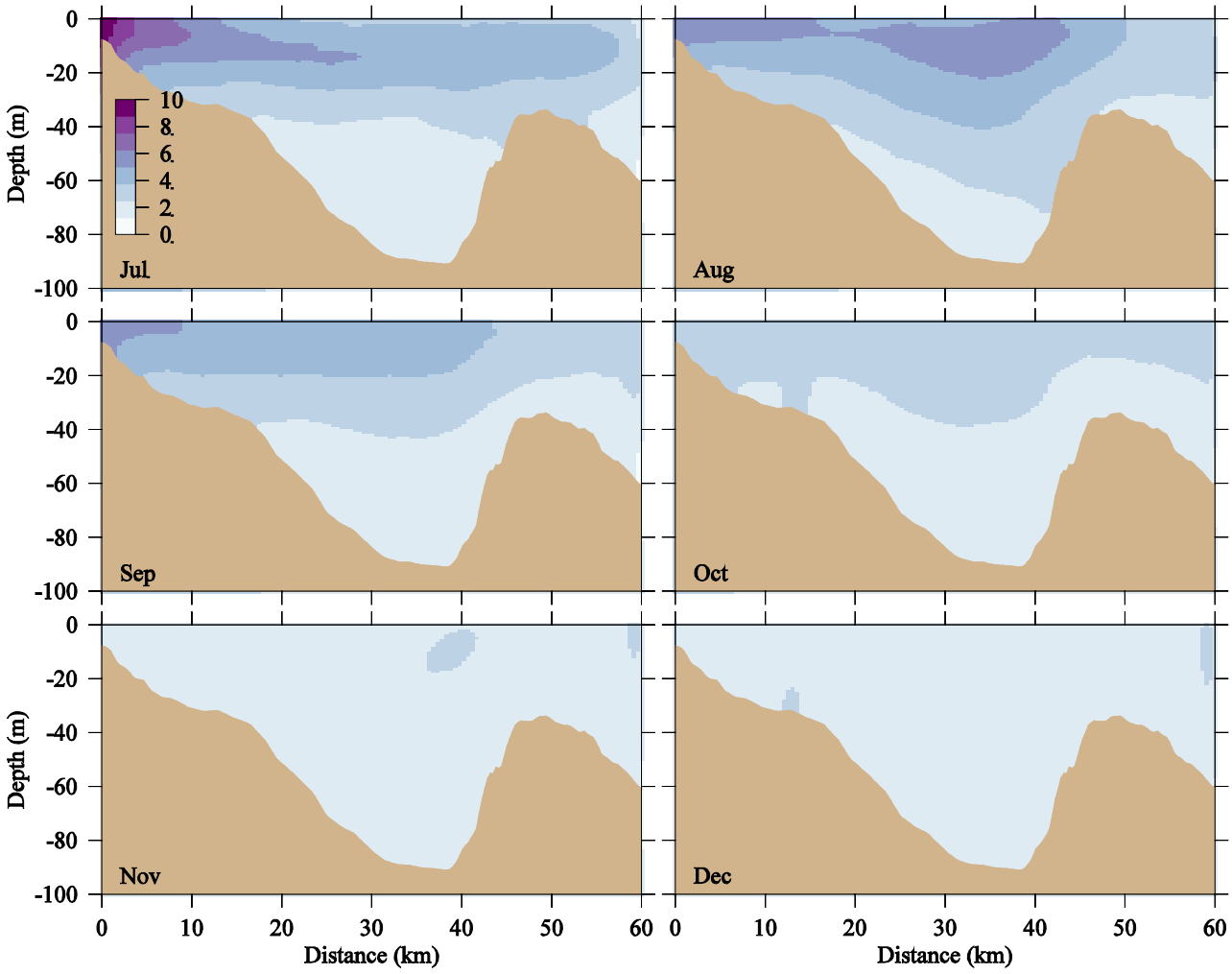

Figure 3. 39 PON concentration (μM) on the east-west transect across the MWRA outfall at the end of each month from July through December in 2011.

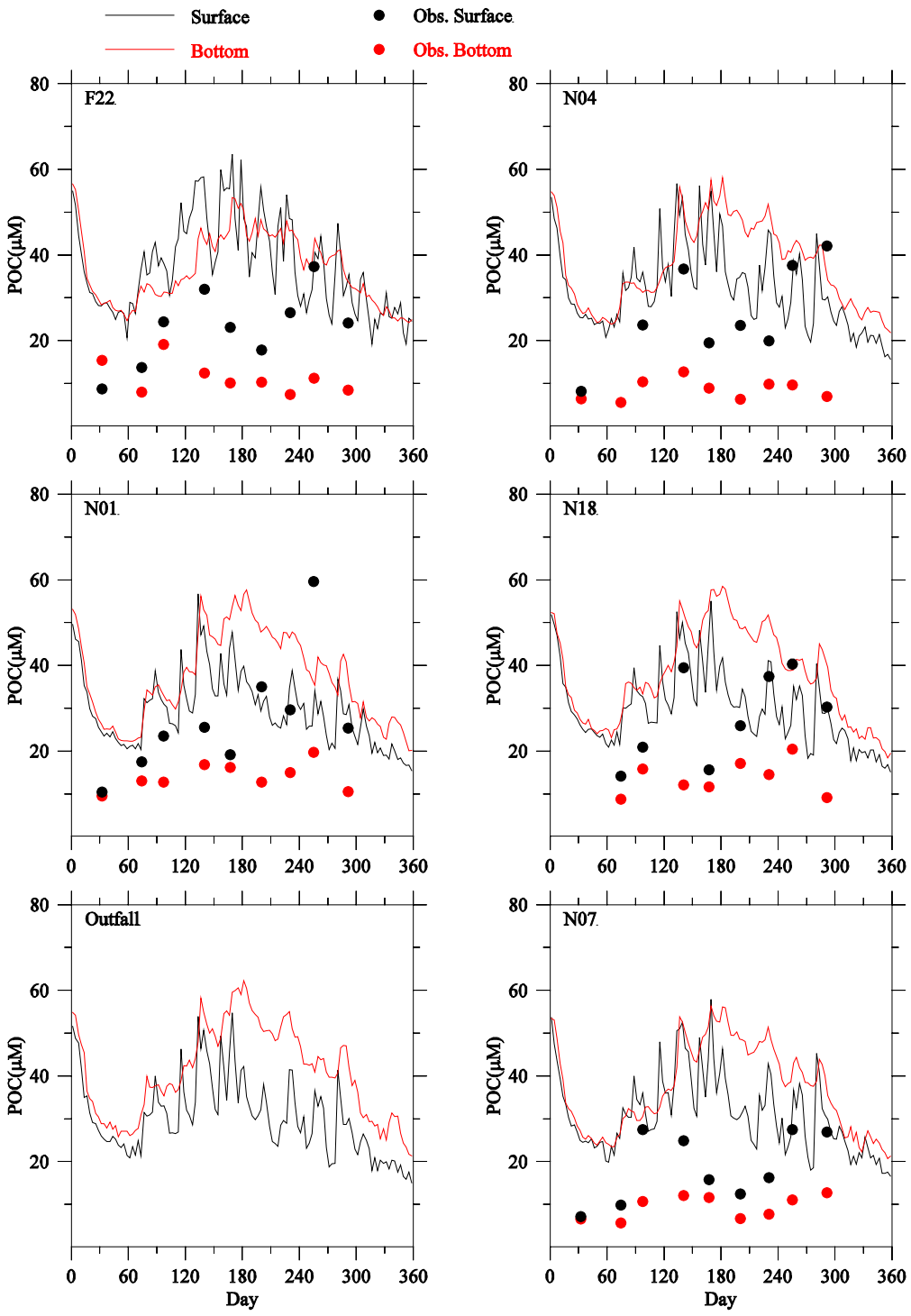

Figure 3. 40 Comparison of POC observed (dots) and modeled (lines) time-series at the outfall site and selected Massachusetts Bay monitoring stations F22, N04, N01, N18, and N07 for 2011. No POC data are available at the outfall site.

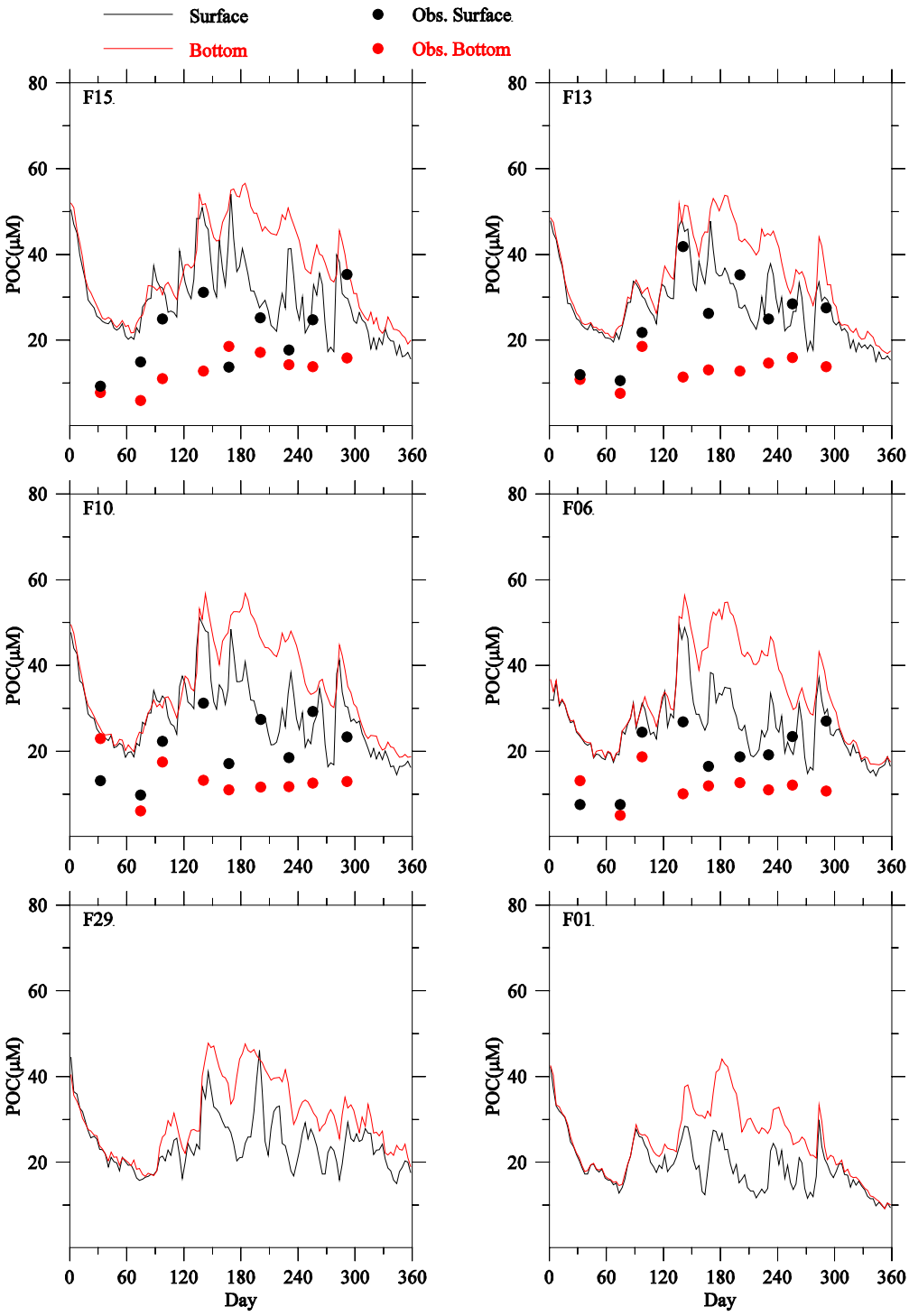

Figure 3. 41 Comparison of POC observed (dots) and modeled (lines) time-series at selected Massachusetts Bay monitoring stations F15, F13, F10, F06, F29 and F01 for 2010. No POC data are available at stations F01 and F29.

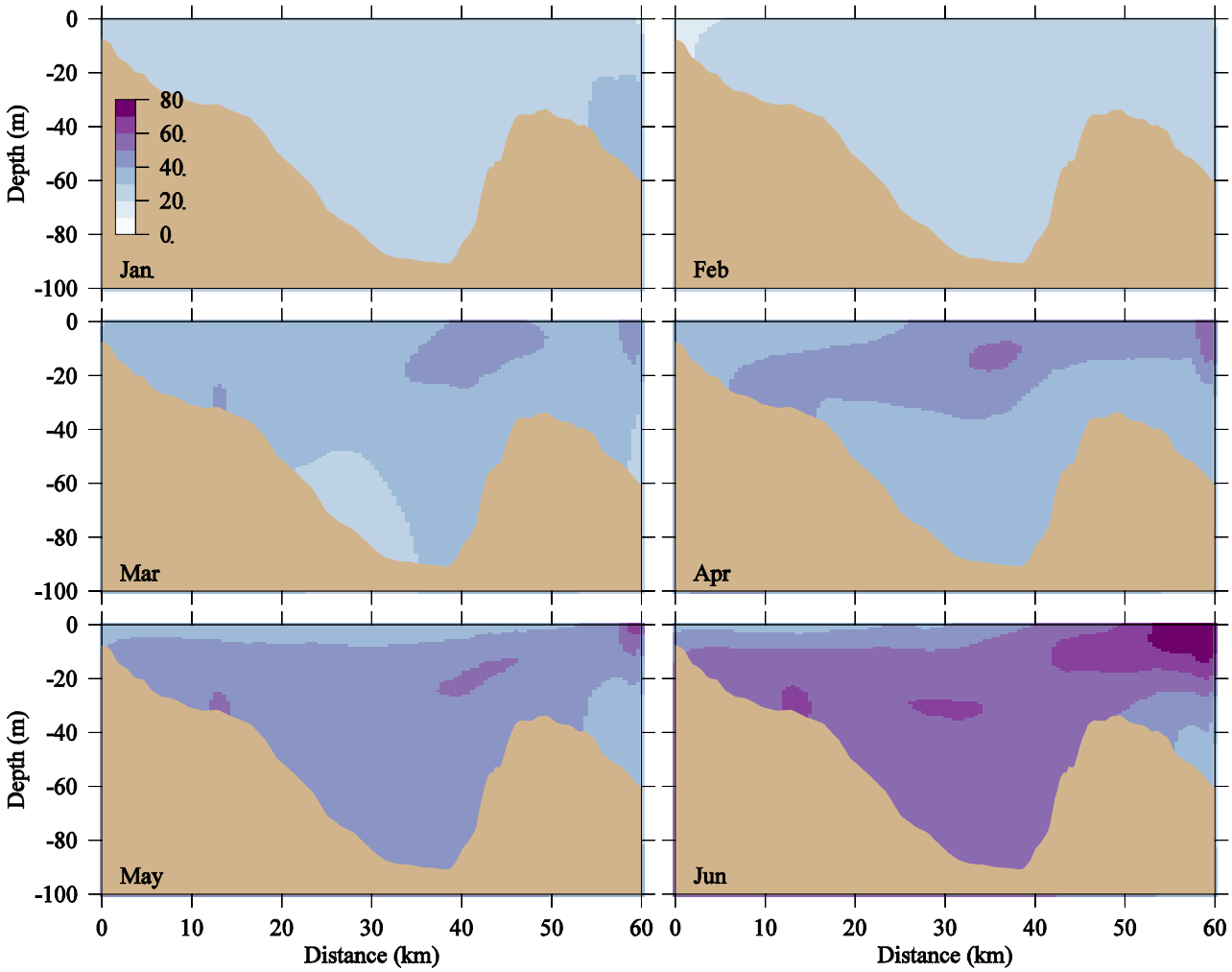

Figure 3. 42 POC concentration (µM) on the east-west transect across the MWRA outfall at the end of each month from January through June in 2011.

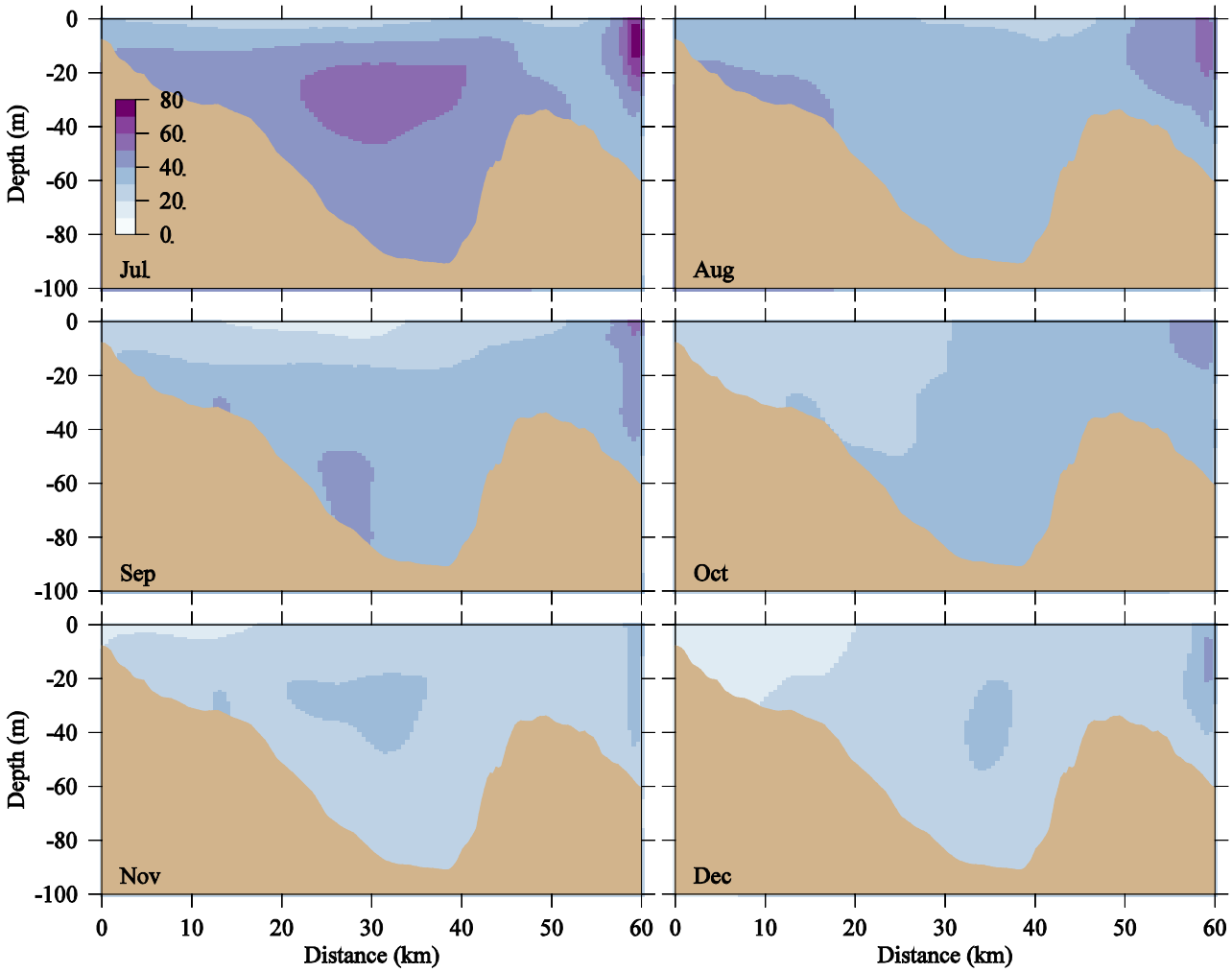

Figure 3. 43 POC concentration (μM) on the east-west transect across the MWRA outfall at the end of each month from July through December in 2011.

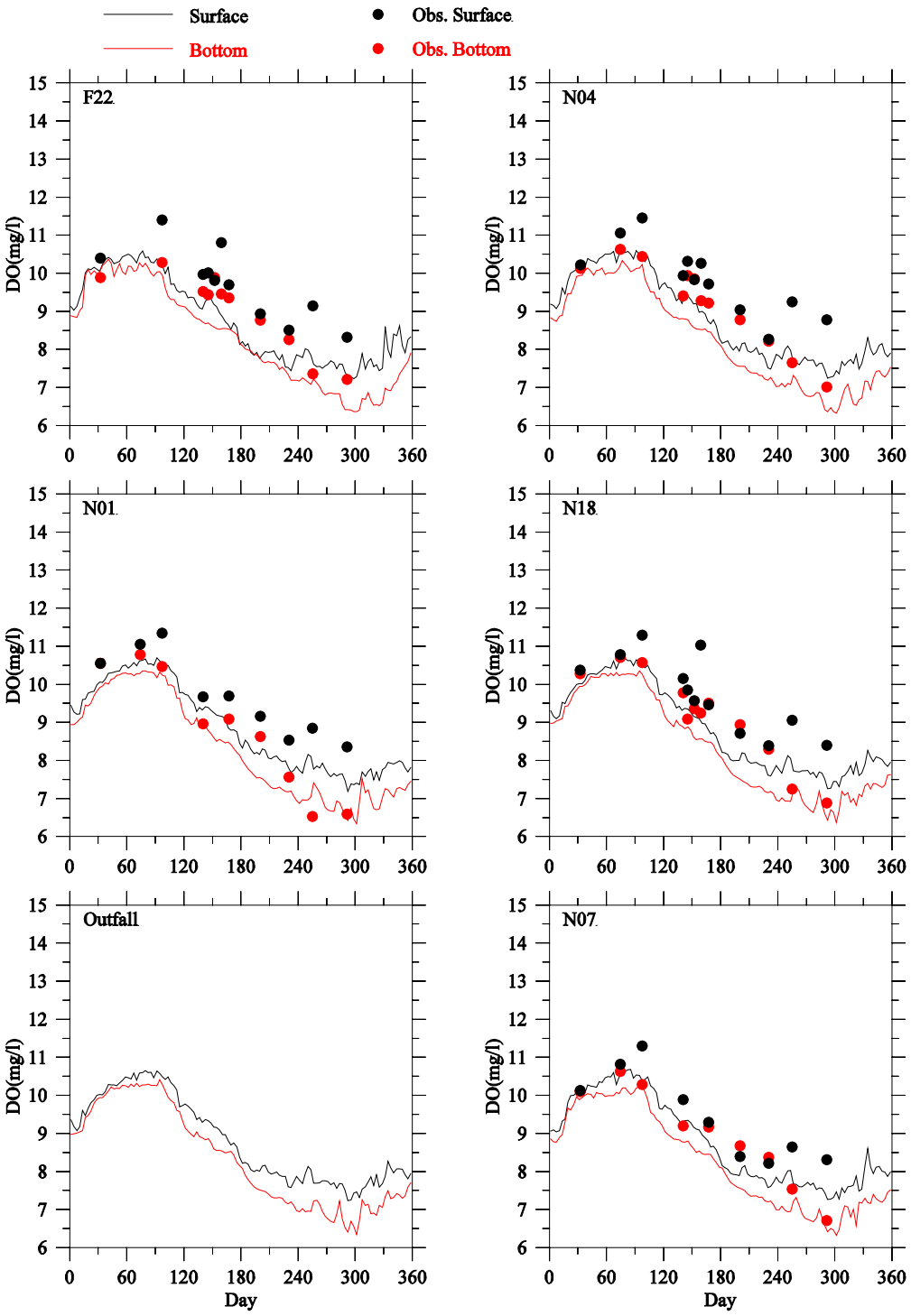

Figure 3. 44 Comparison of DO observed (dots) and modeled (lines) time-series at the outfall site and selected Massachusetts Bay monitoring stations F22, N04, N01, N18, and N07 for 2011. No DO data are available at the outfall site.

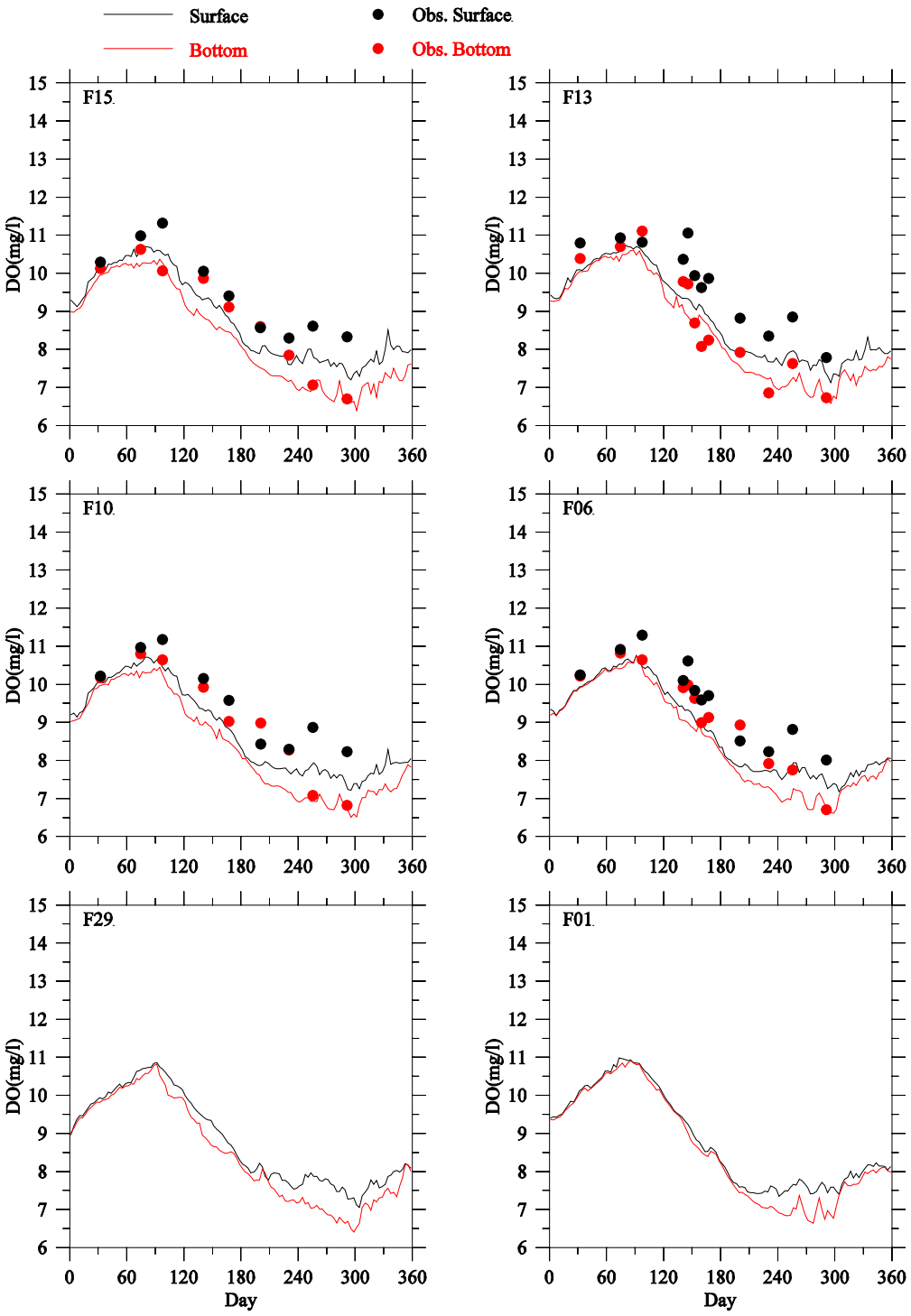

Figure 3. 45 Comparison of DO observed (dots) and modeled (lines) time-series at selected Massachusetts Bay monitoring stations F15, F13, F10, F06, F29 and F01 for 2011.

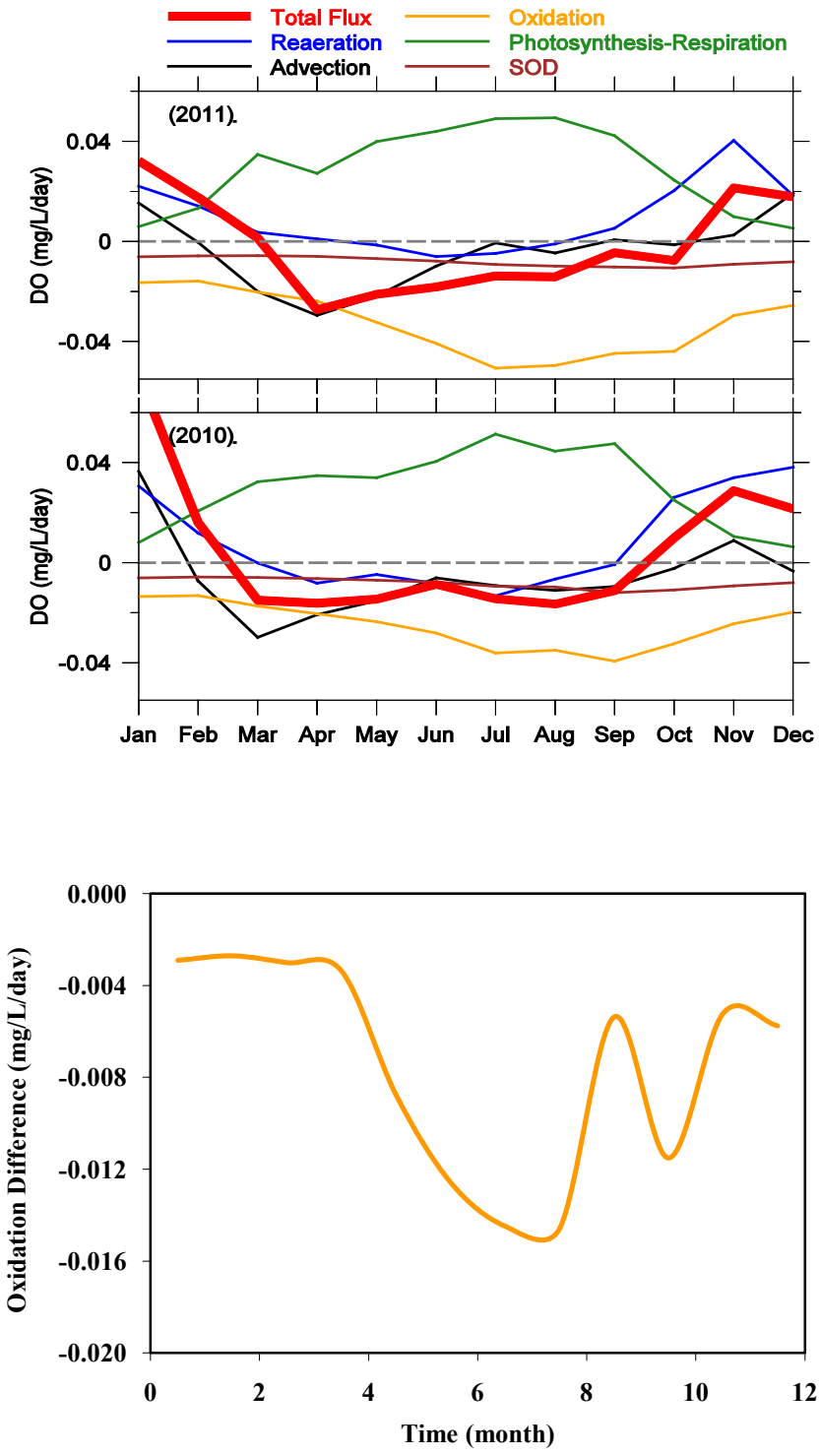

Figure 3. 46 Monthly mean of DO flux terms for vertical averaged 2-D balance in simulation domain for 2011 (upper panel) and 2010 (middle panel). Lower panel shows the difference in oxidation between 2011 and 2010.

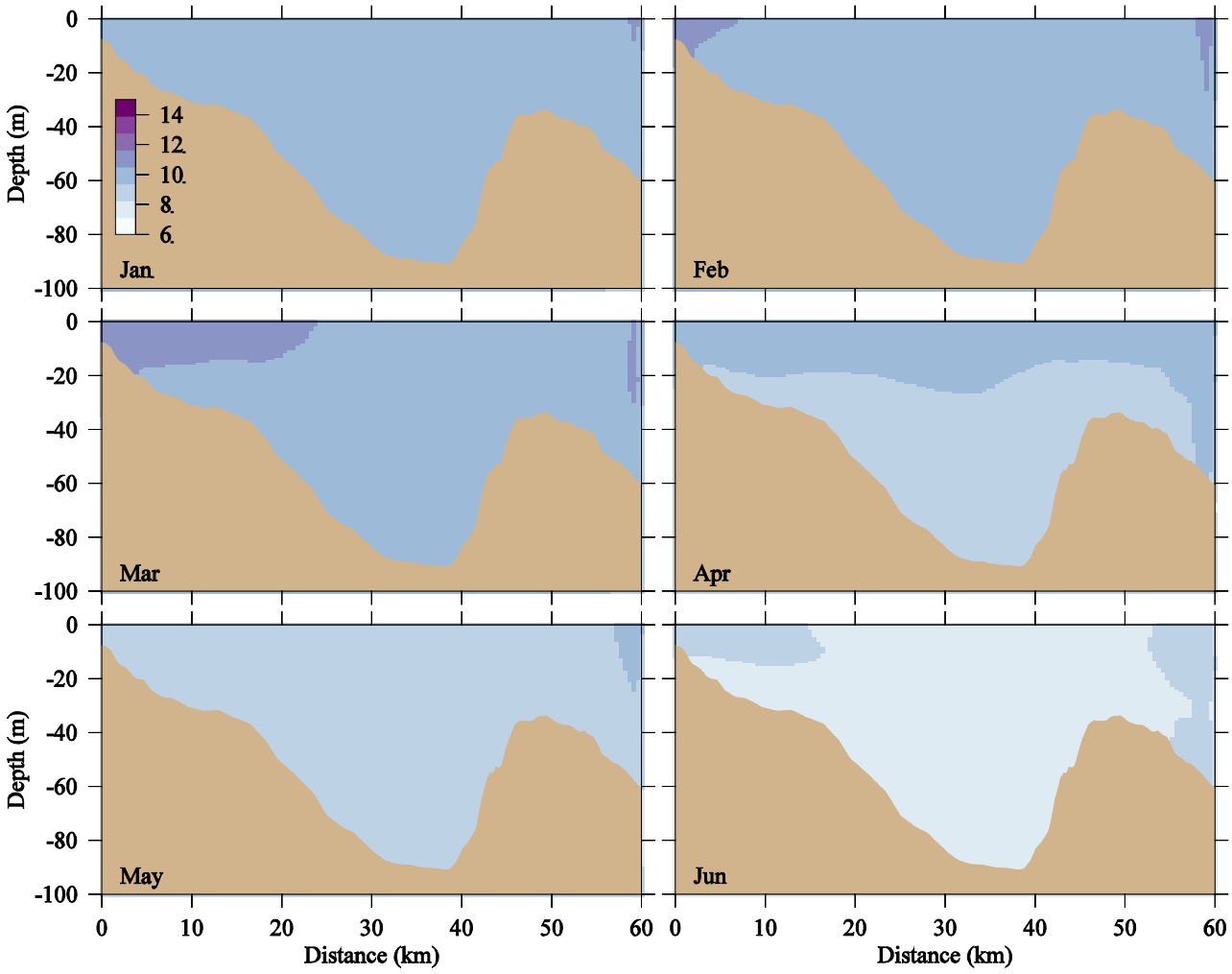

Figure 3. 47 DO concentration (mg/l) on the east-west transect across the MWRA outfall at the end of each month from January through June in 2011.

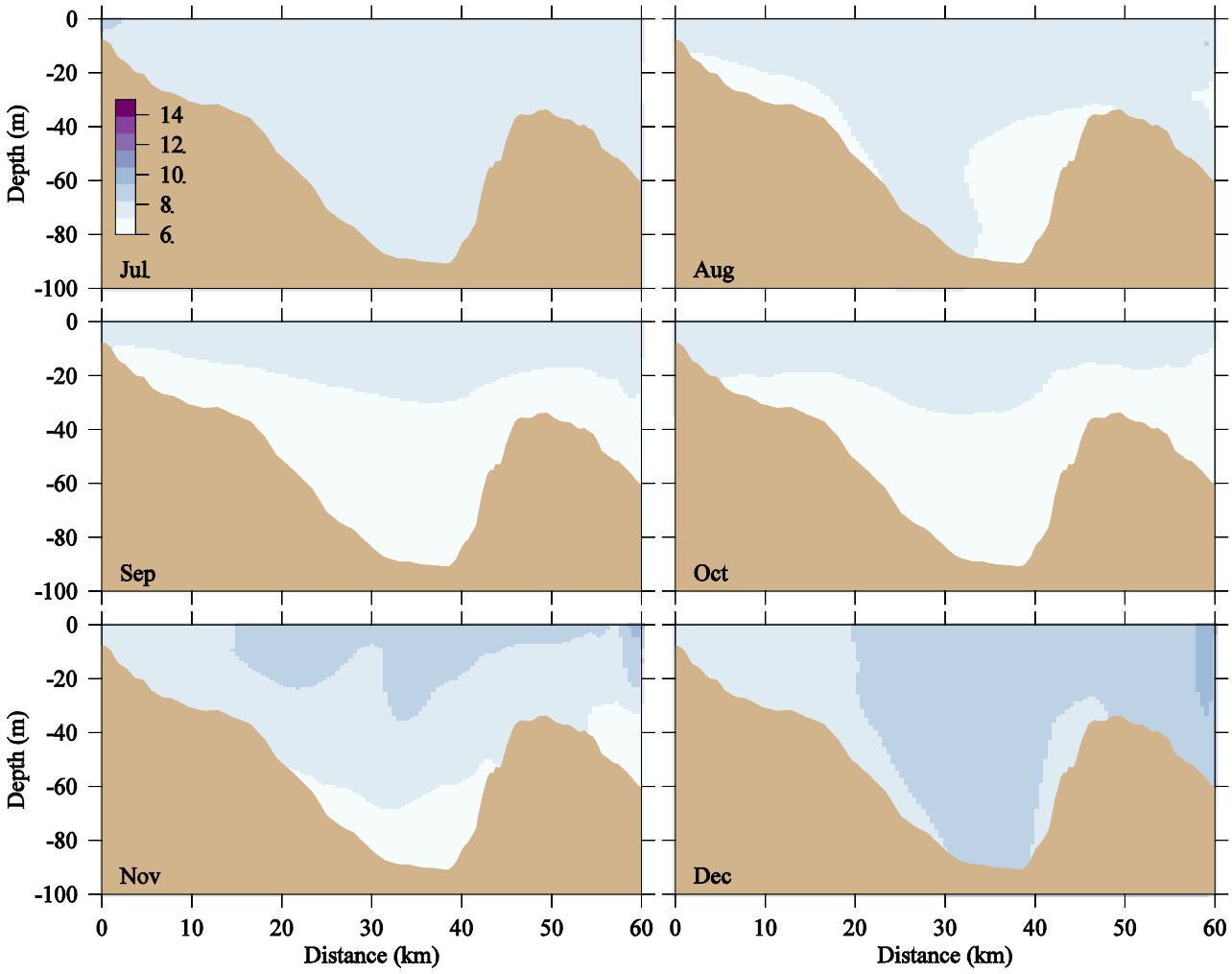

Figure 3. 48 DO concentration (mg/l) on the east-west transect across the MWRA outfall at the end of each month from July through December in 2011.

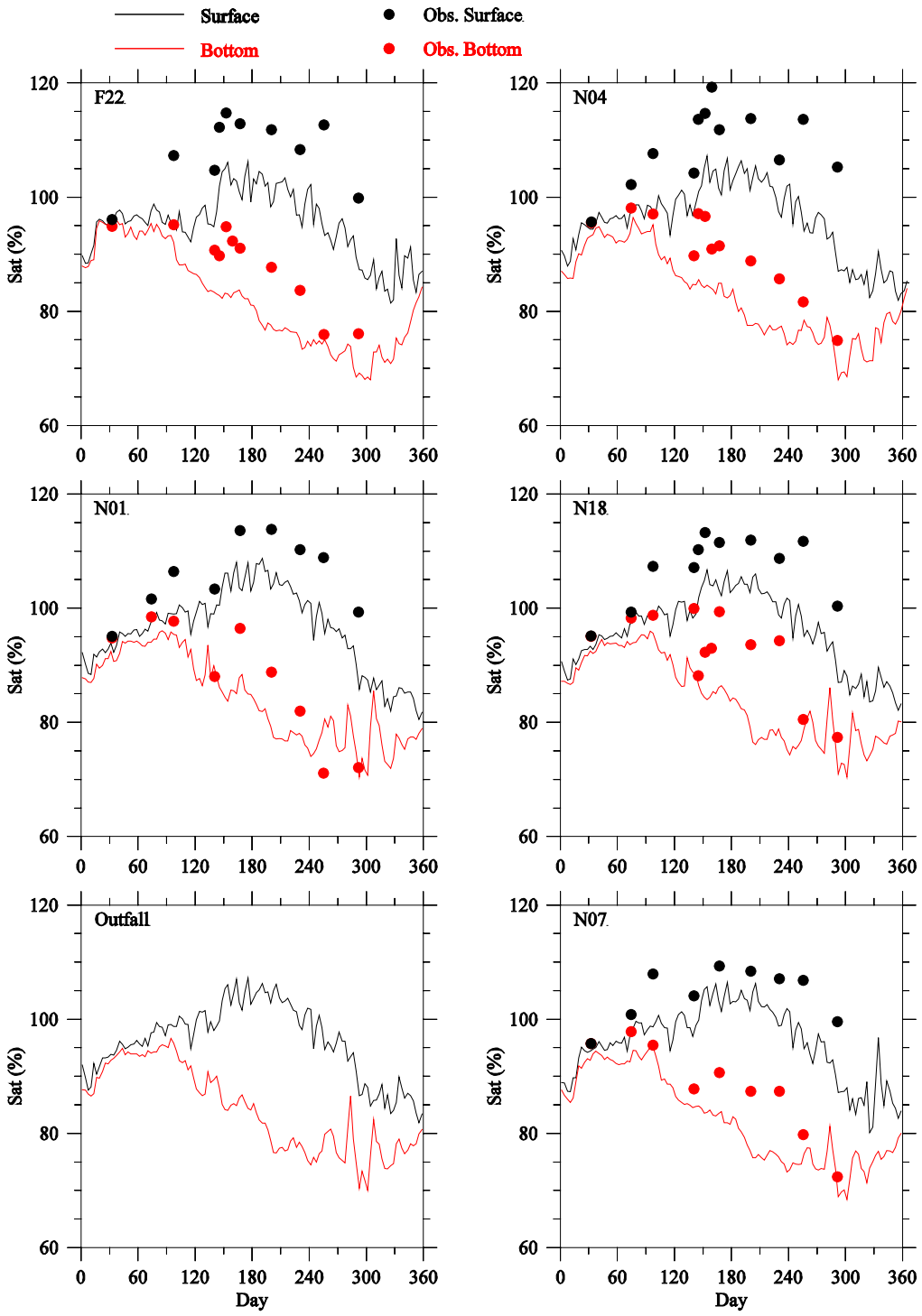

Figure 3. 49 DO saturation (%) time-series at the outfall site and selected Massachusetts Bay monitoring stations F22, N04, N01, N18, and N07 for 2011.

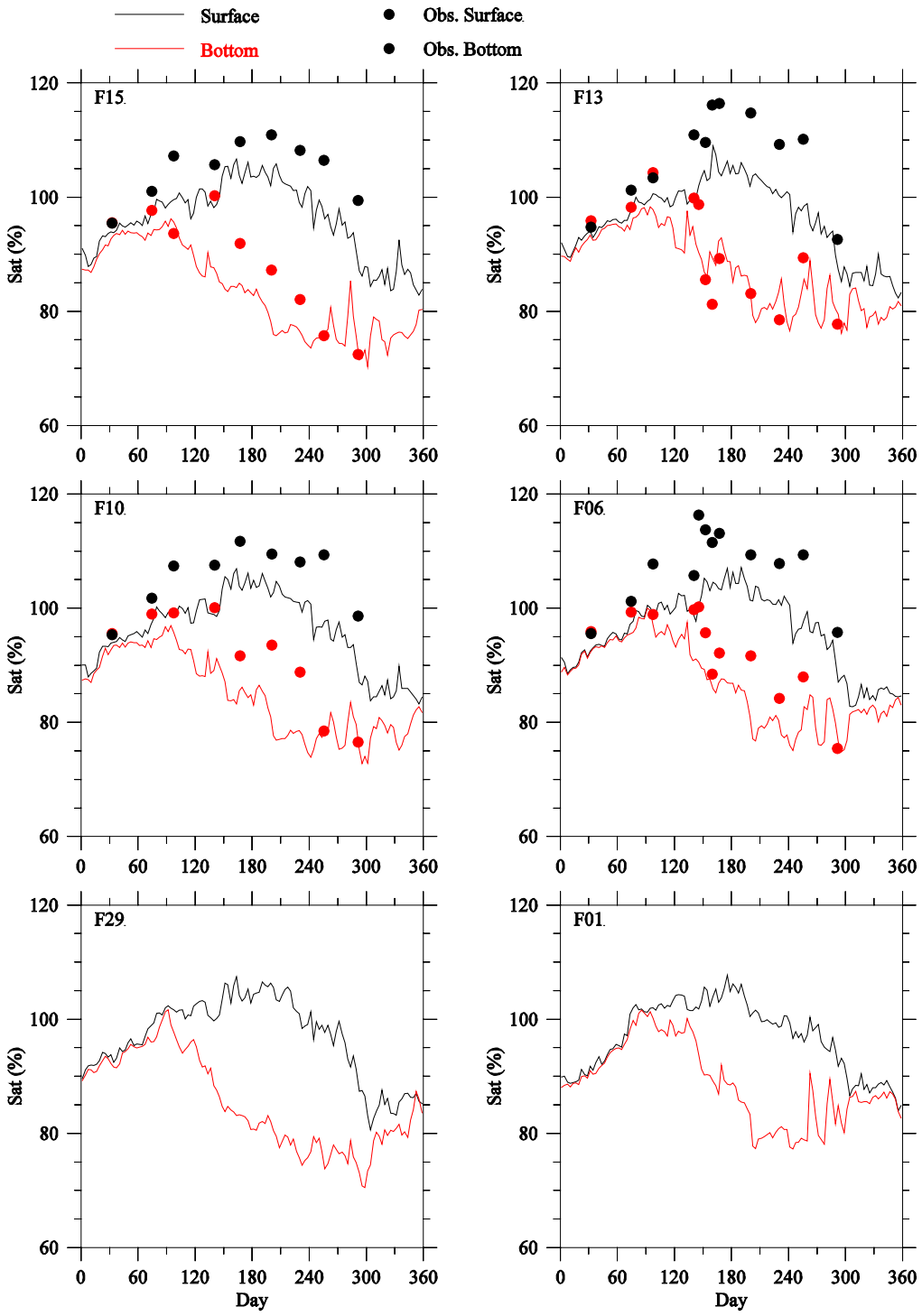

Figure 3. 50 DO saturation (%) time-series at the selected Massachusetts Bay monitoring stations F15, F13, F10, F06, F29 and F01 for 2011.

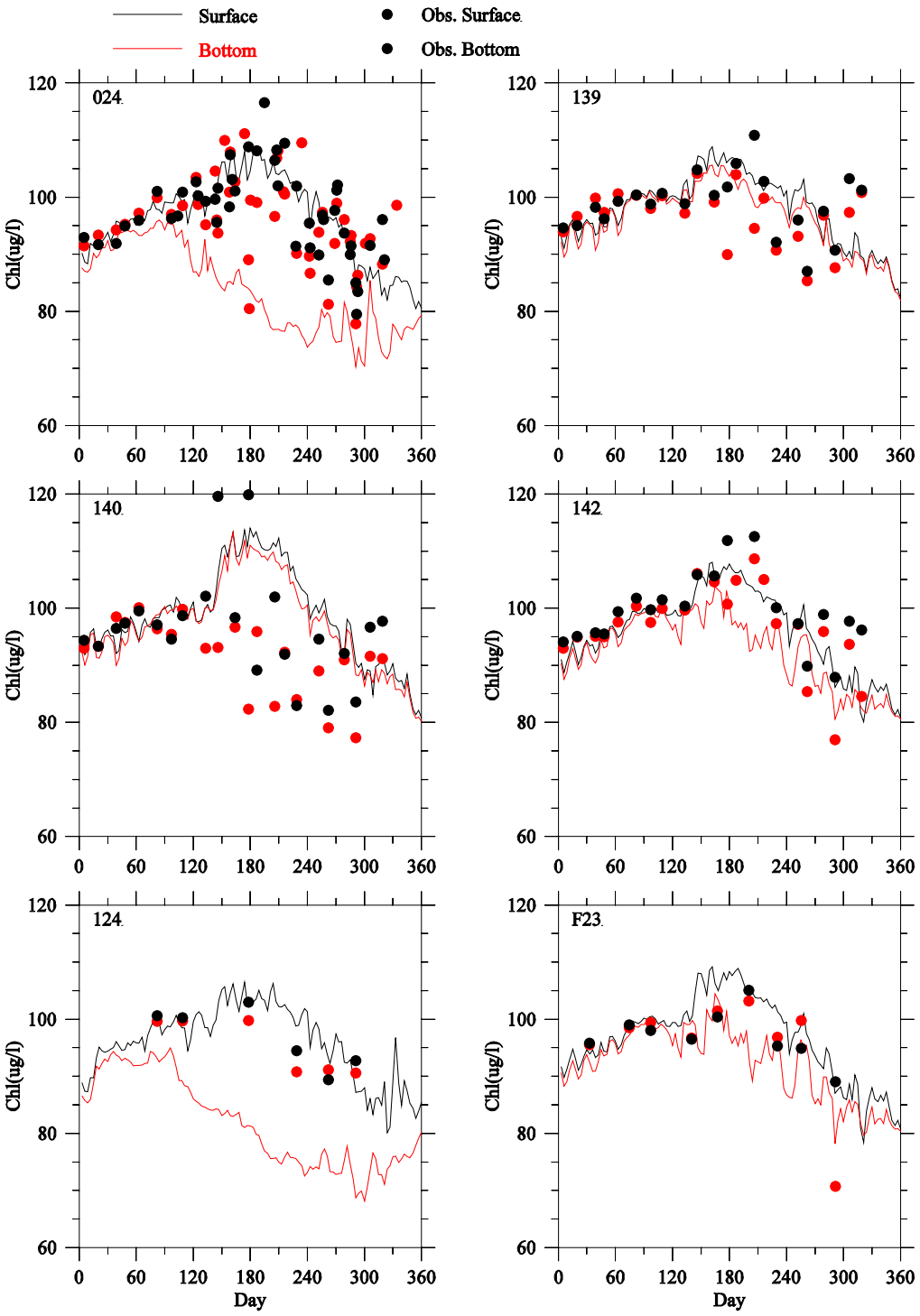

Figure 3. 51 DO saturation (%) time-series at the selected Boston Harbor monitoring stations 024, 139, 140, 142, 124 and F23 for 2011.

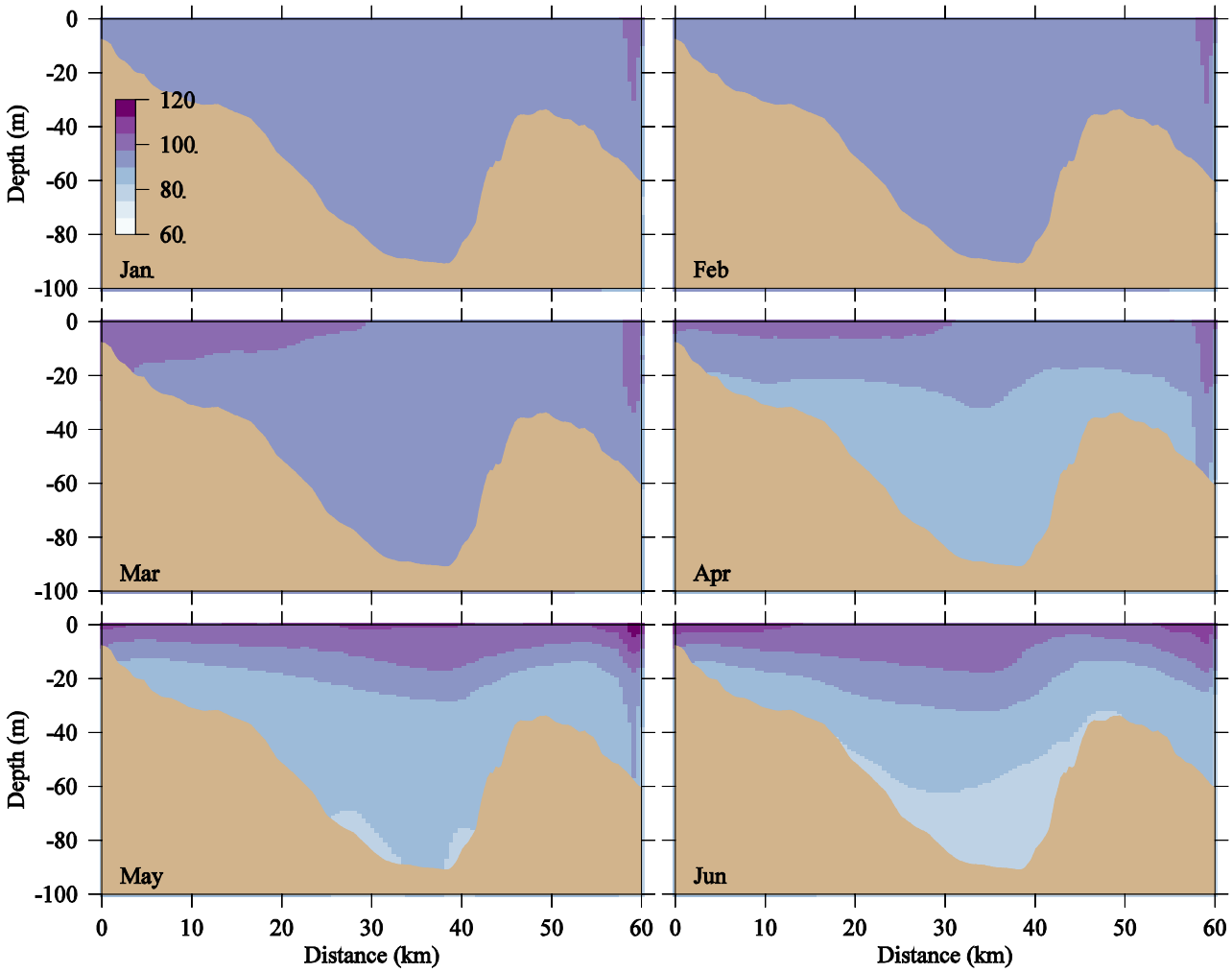

Figure 3. 52 DO saturation (%) on the east-west transect across the MWRA outfall at the end of each month from January through June in 2011.

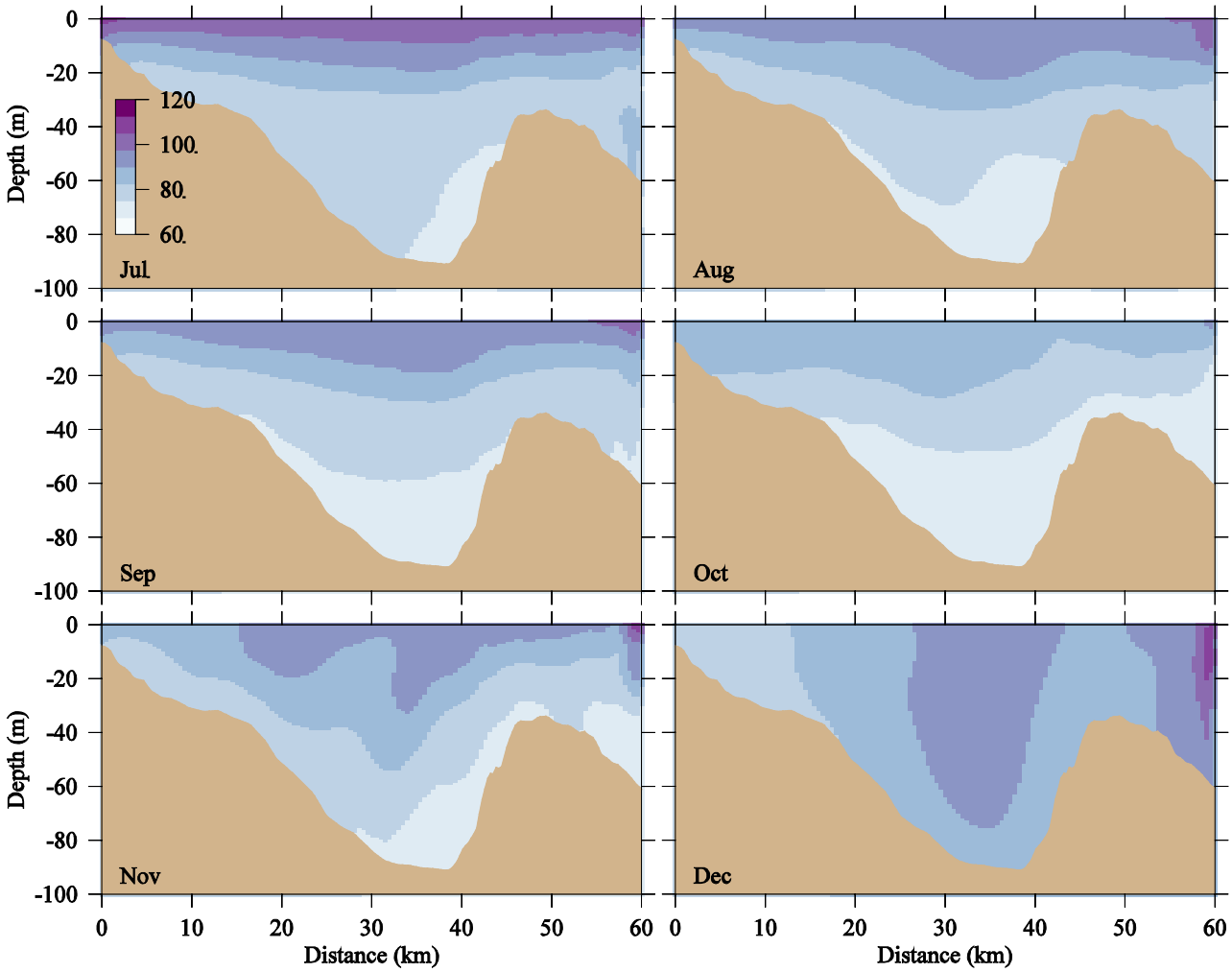

Figure 3. 53 DO saturation (%) on the east-west transect across the MWRA outfall at the end of each month from July through December in 2011.

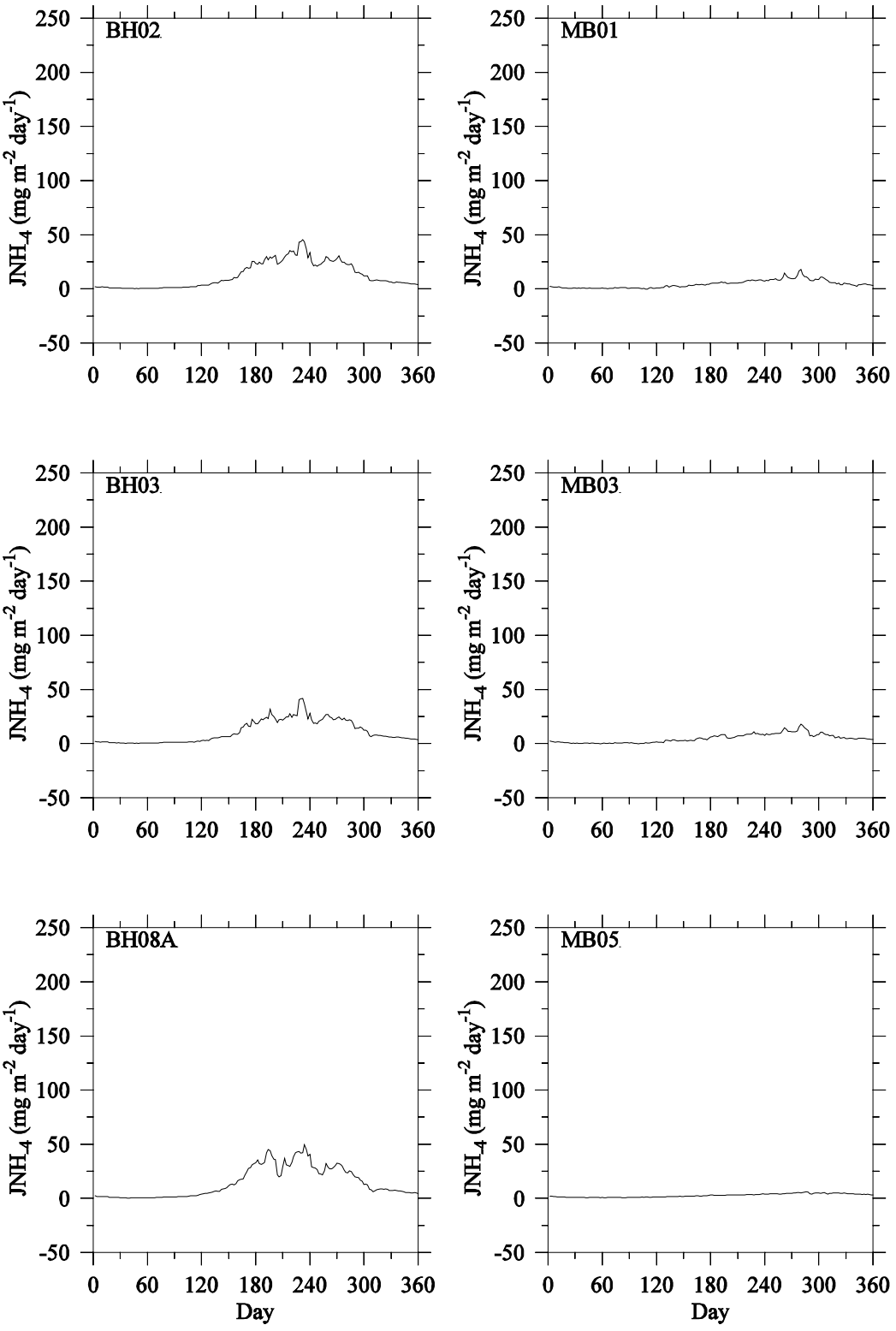

Figure 3. 54 Sediment NH_4^+ flux modeled time-series in 2011.

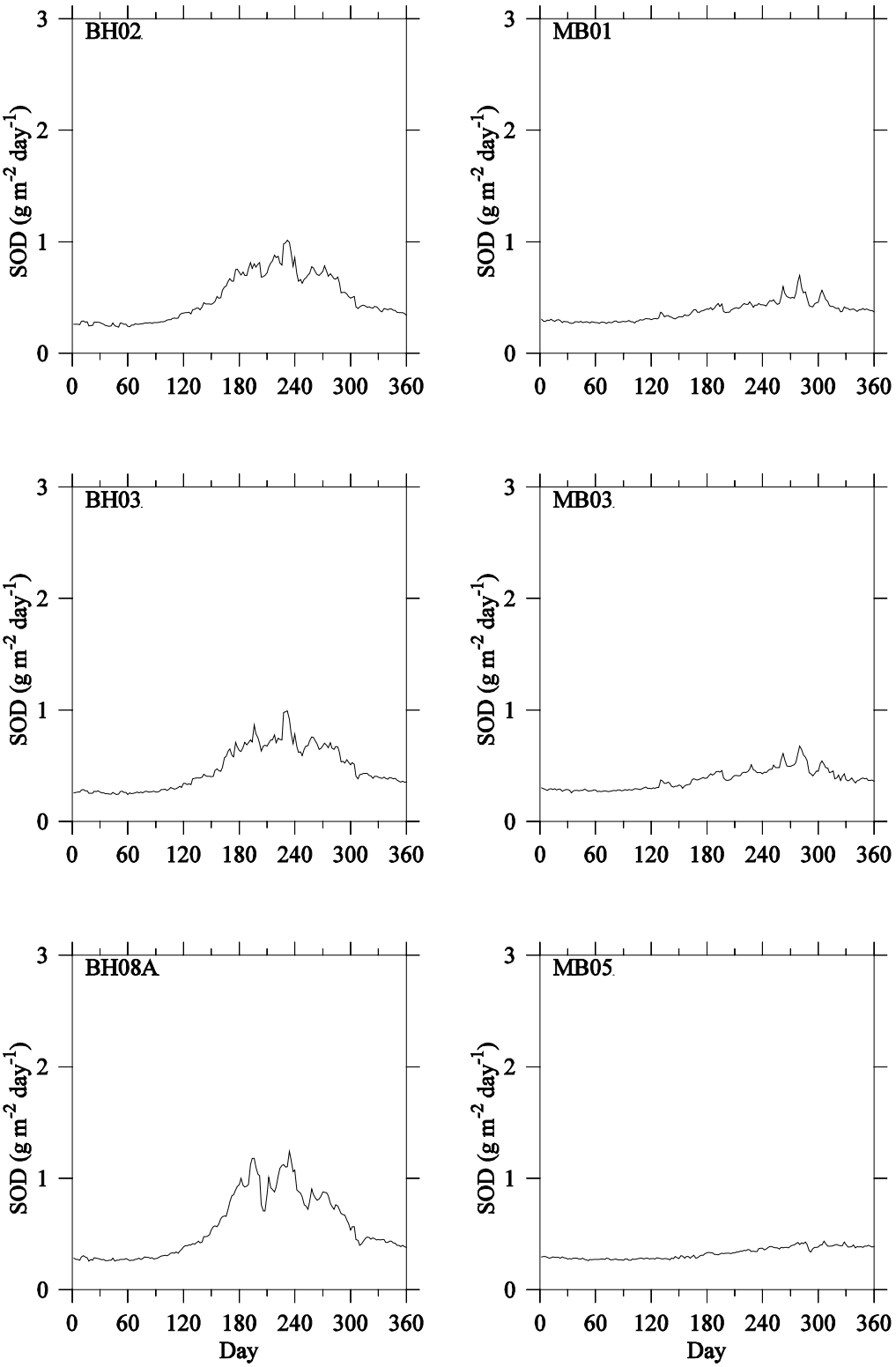

Figure 3. 55 Sediment oxygen demand modeled time-series in 2011.

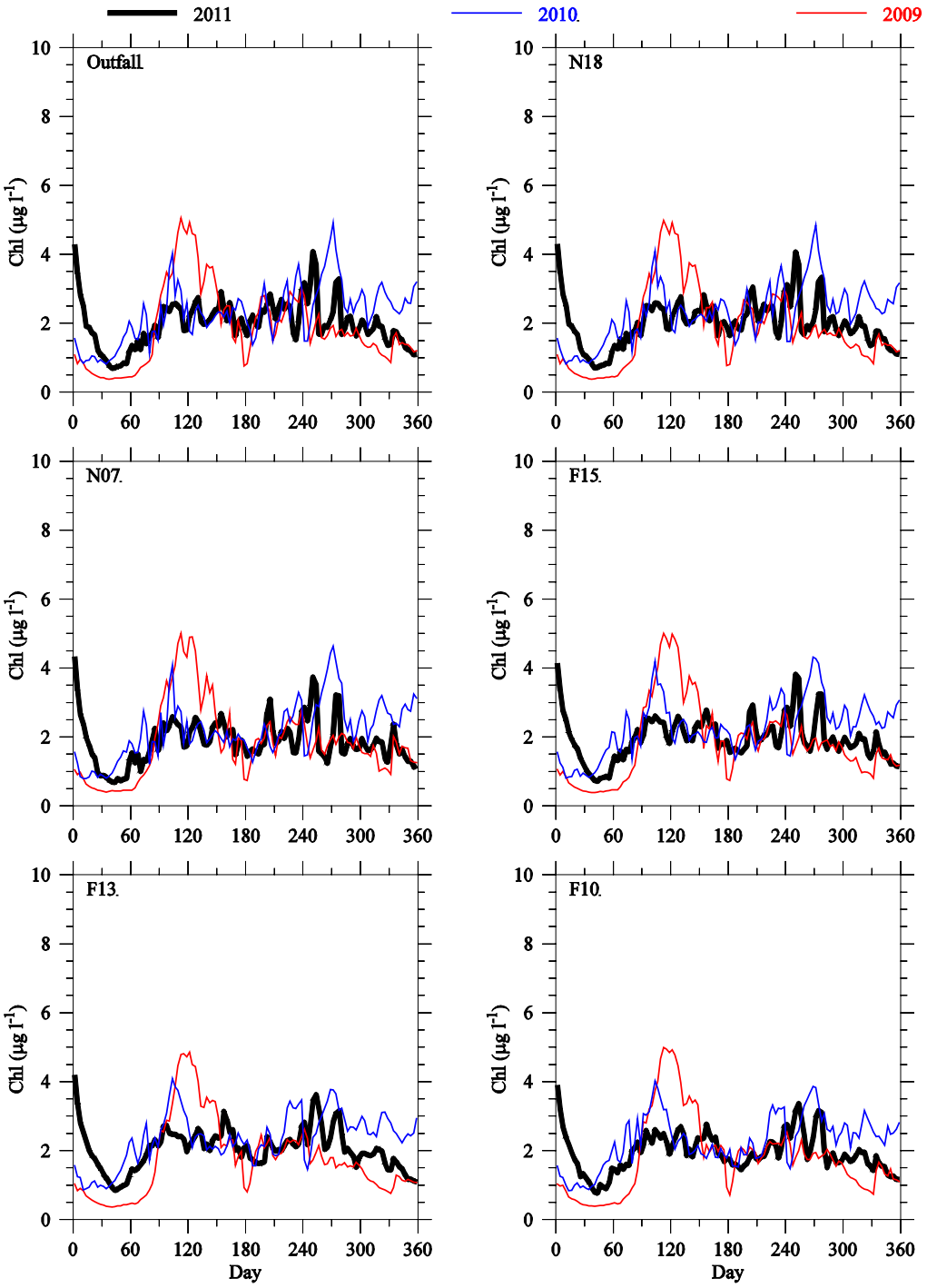

Figure 3. 56 Seasonal and interannual variations in surface chlorophyll concentration at the MWRA outfall site and Stations N18, N07, F15, F13 and F10 computed for 2009 (red lines), 2010 (blue lines) and 2011 (black lines).

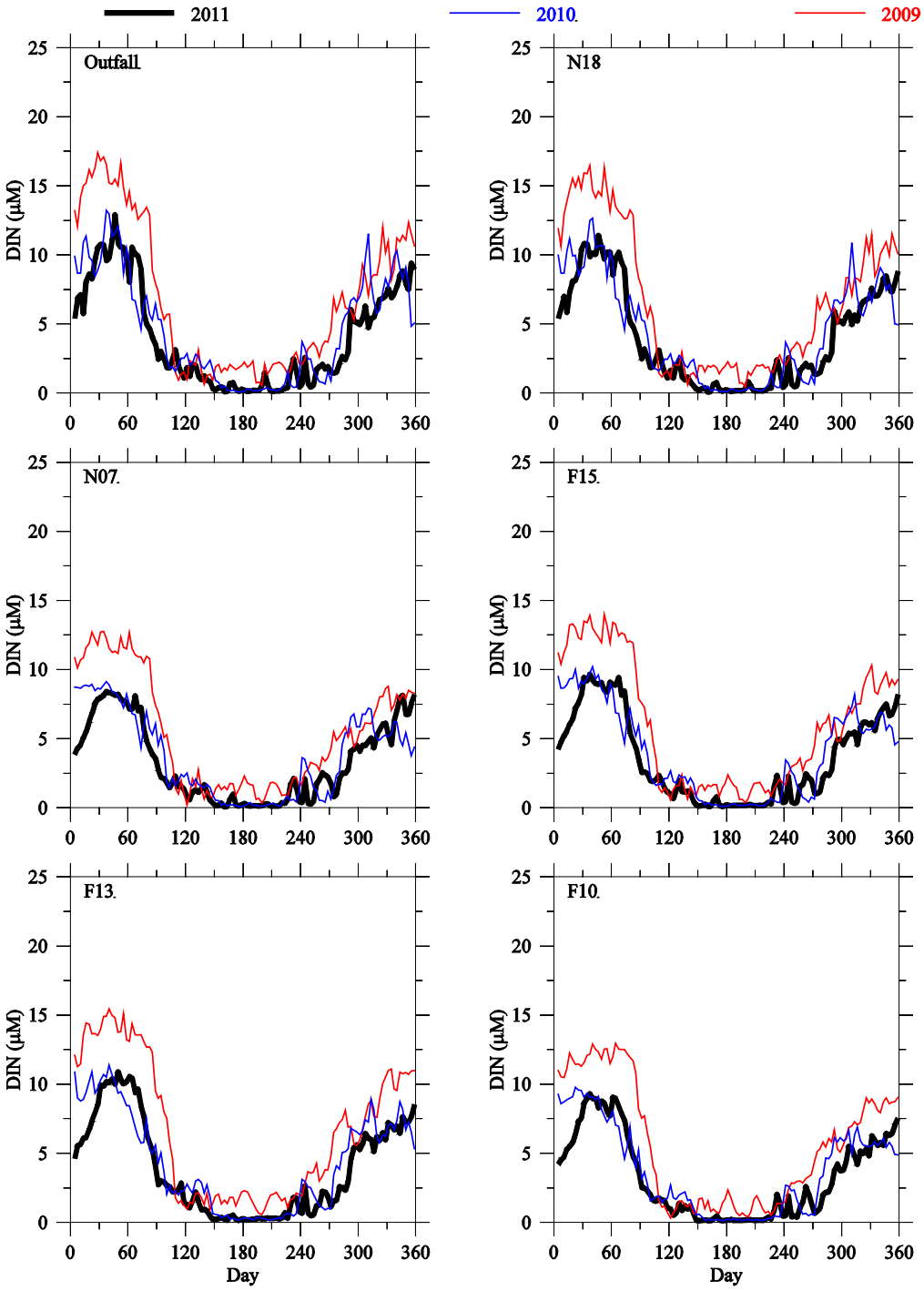

Figure 3. 57 Seasonal and interannual variations in surface DIN concentration at the MWRA outfall site and Stations N18, N07, F15, F13 and F10 computed for 2009 (red lines), 2010 (blue lines) and 2011 (black lines).

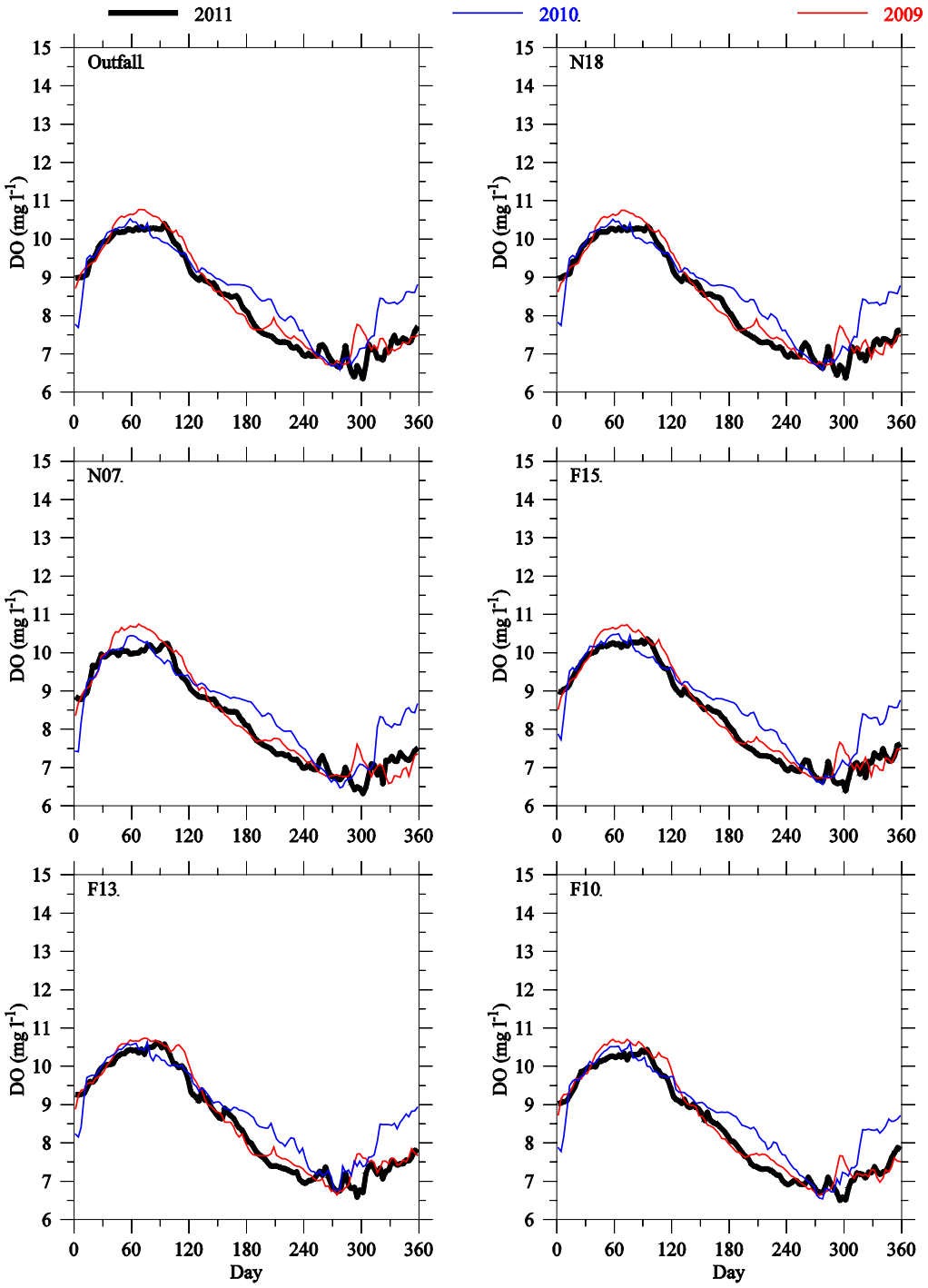

Figure 3. 58 Seasonal and interannual variations in bottom DO concentration at the MWRA outfall site and Stations N18, N07, F15, F13 and F10 computed for 2009 (red lines), 2010 (blue lines) and 2011 (black lines).

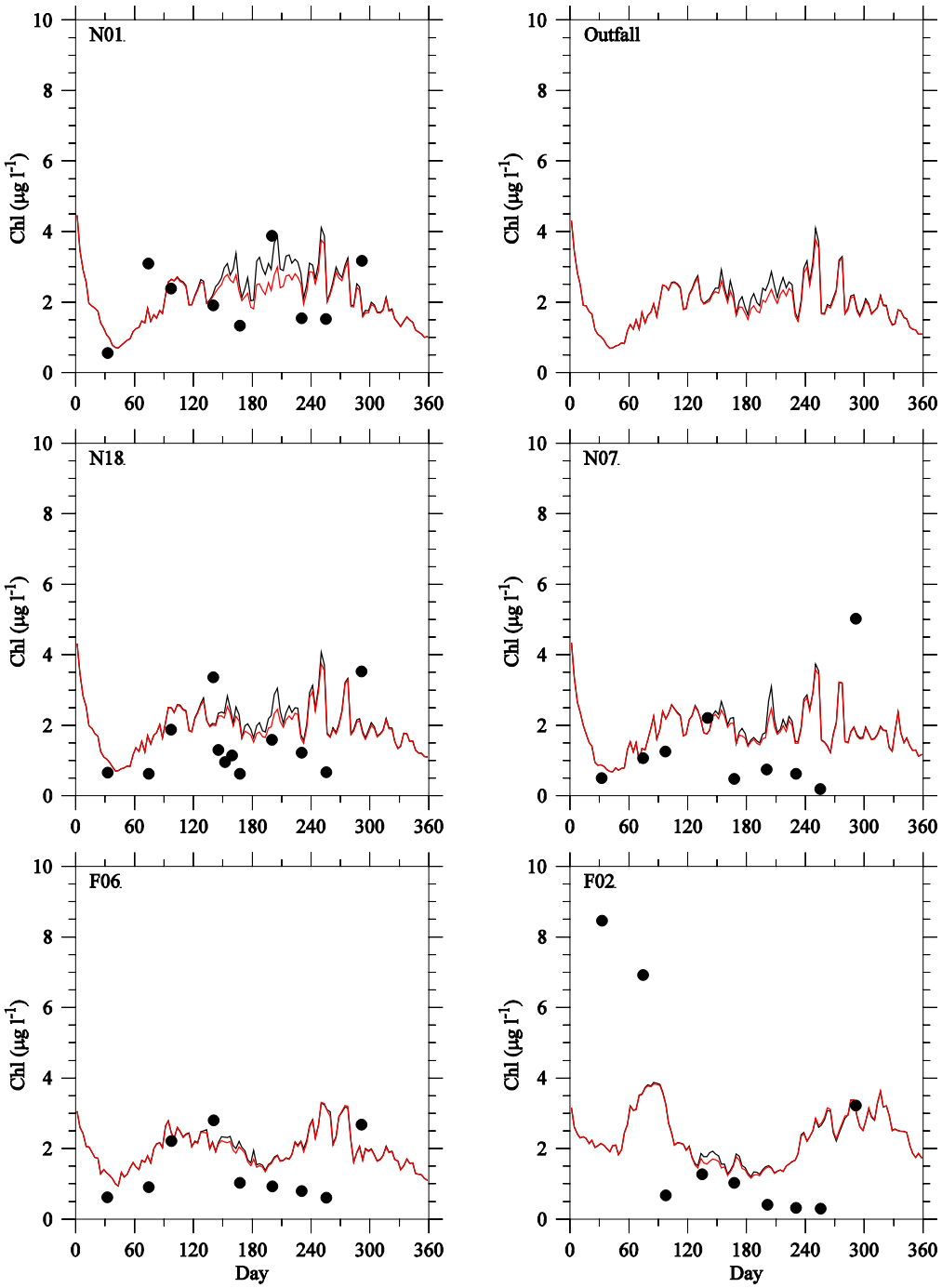

Figure 4. 1 Comparison of surface chlorophyll concentration between the Control (black) and Non-sewage (red) experiments at selected monitoring stations in 2011. Black dots show observed values.

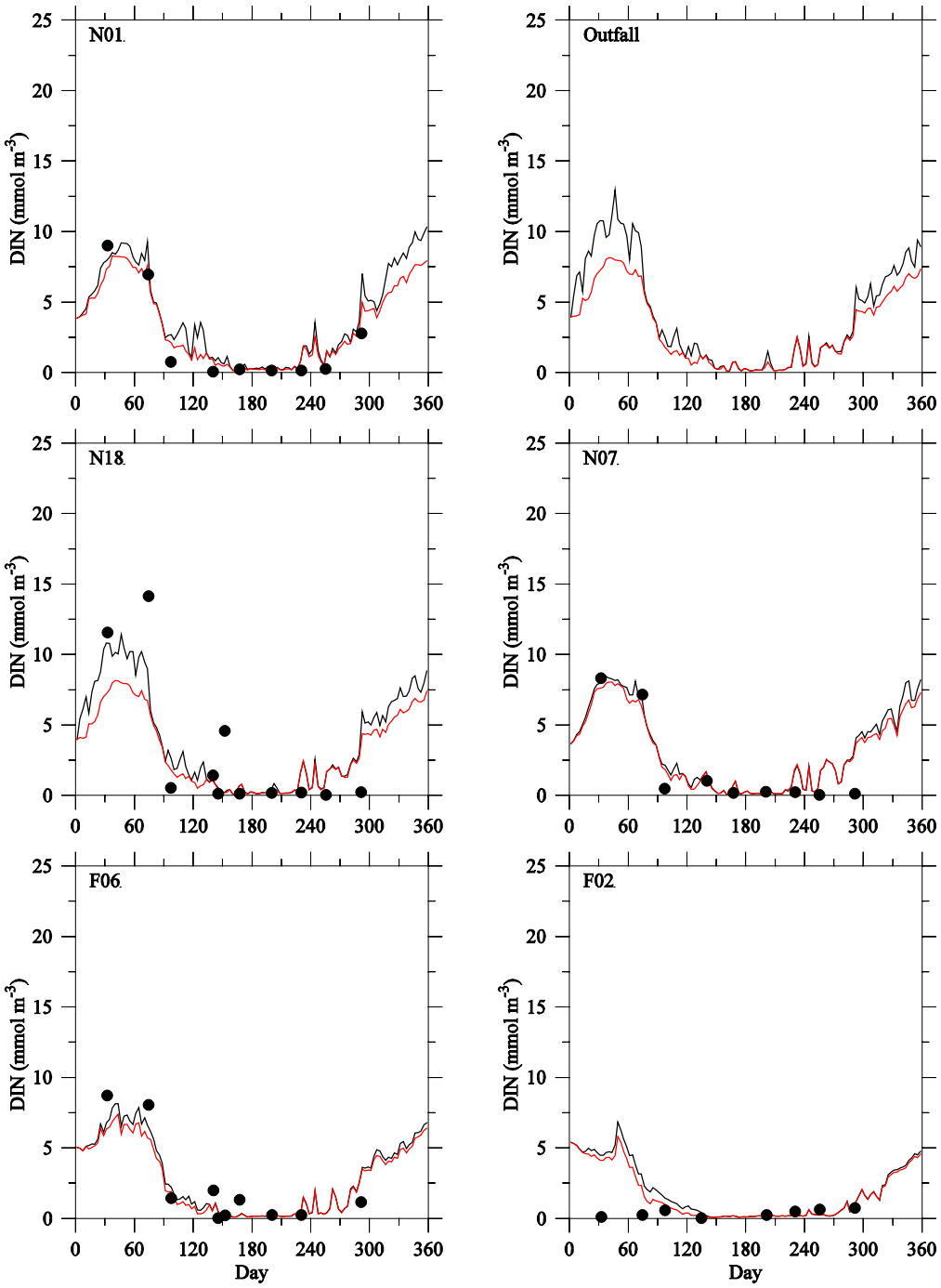

Figure 4. 2 Comparison of surface DIN concentration between the Control (black) and Non-sewage (red) experiments at selected monitoring stations in 2011.

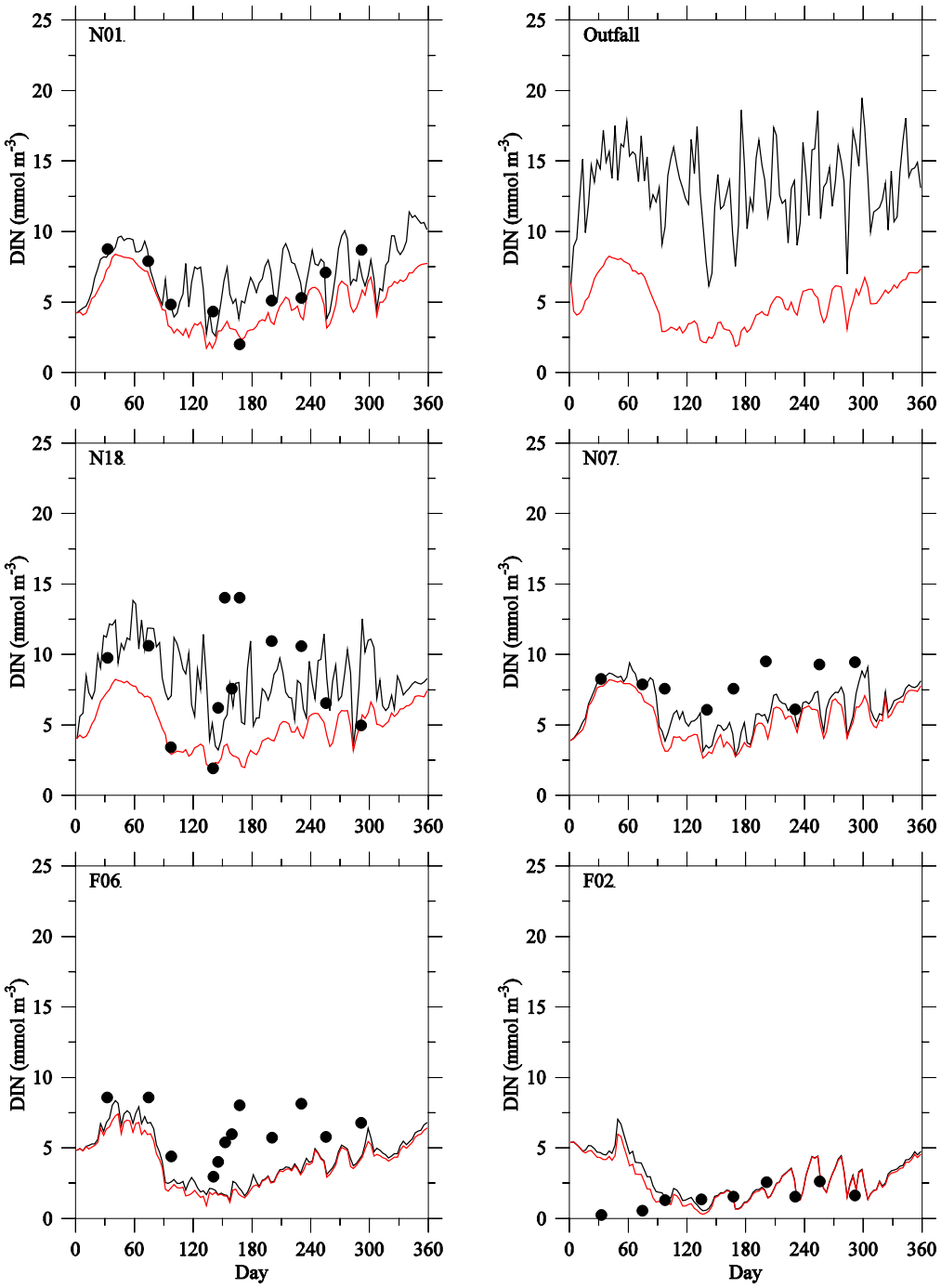

Figure 4. 3 Comparison of bottom DIN concentration between the Control (black) and Non-sewage (red) experiments at selected monitoring stations in 2011.

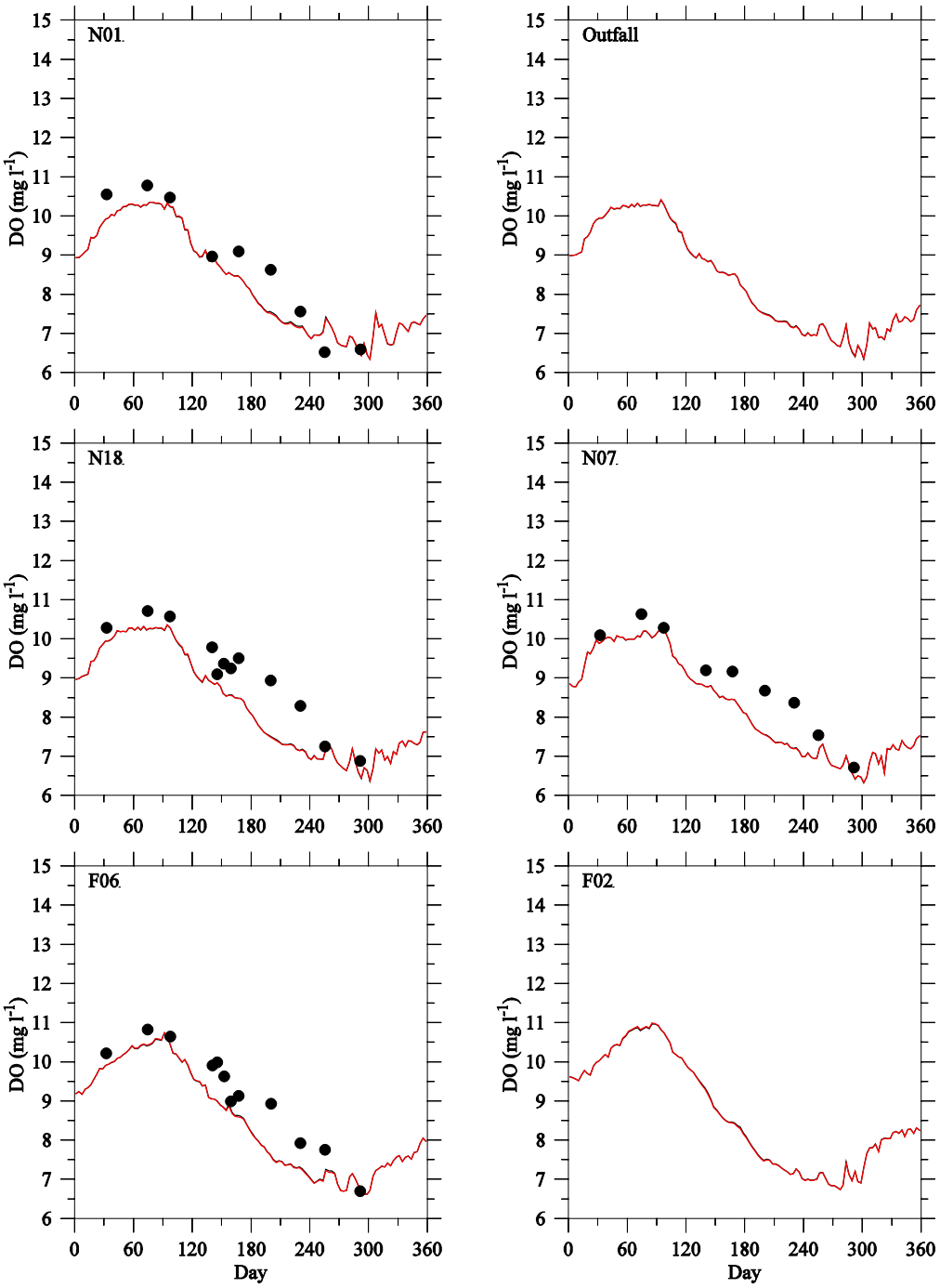

Figure 4. 4 Comparison of bottom dissolved oxygen concentration between the Control (black) and Non-sewage (red) experiments at selected monitoring stations in 2011.

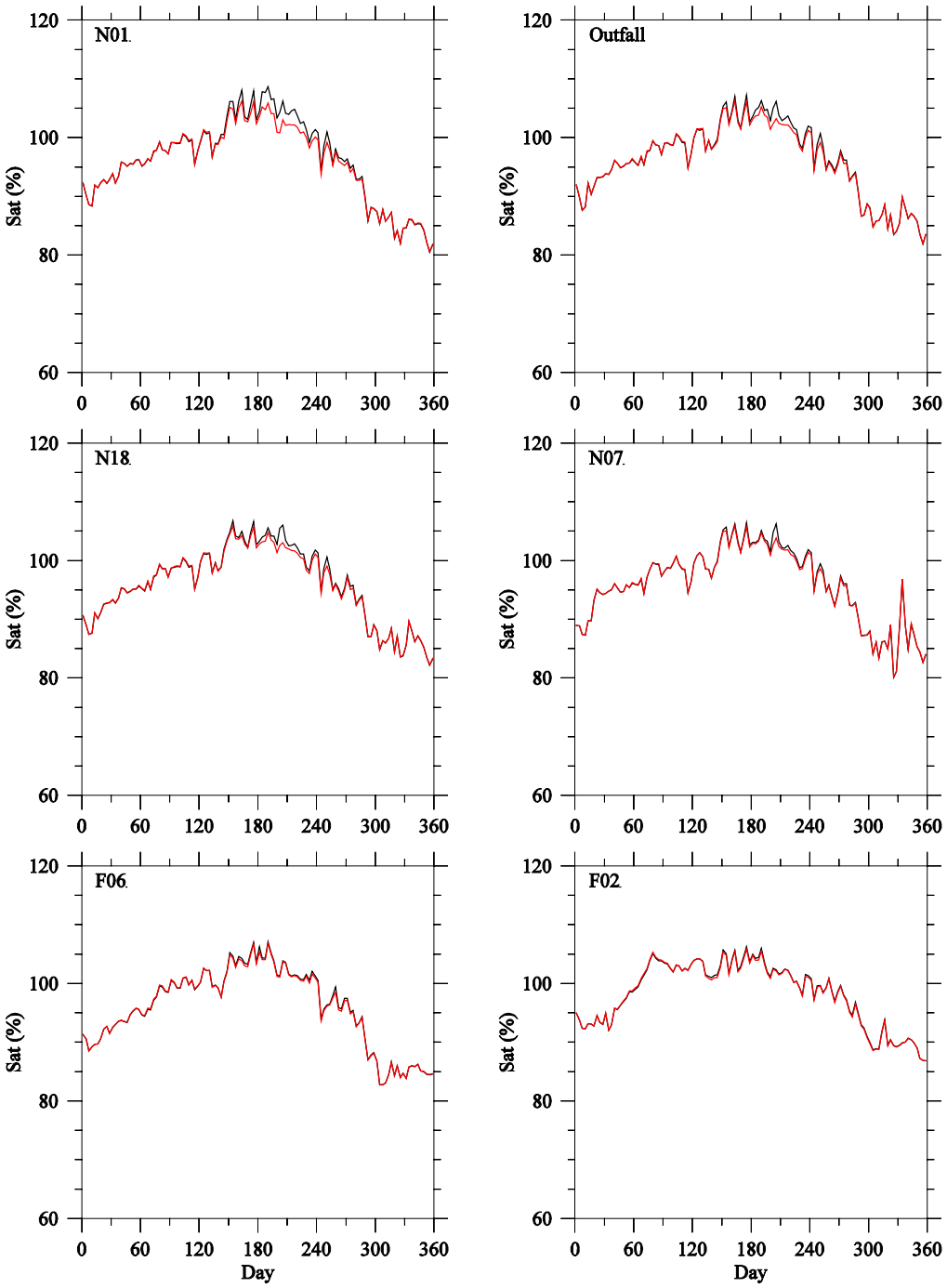

Figure 4. 5 Comparison of surface dissolved oxygen saturation between the Control (black) and Non-sewage (red) experiments at selected monitoring stations in 2011.

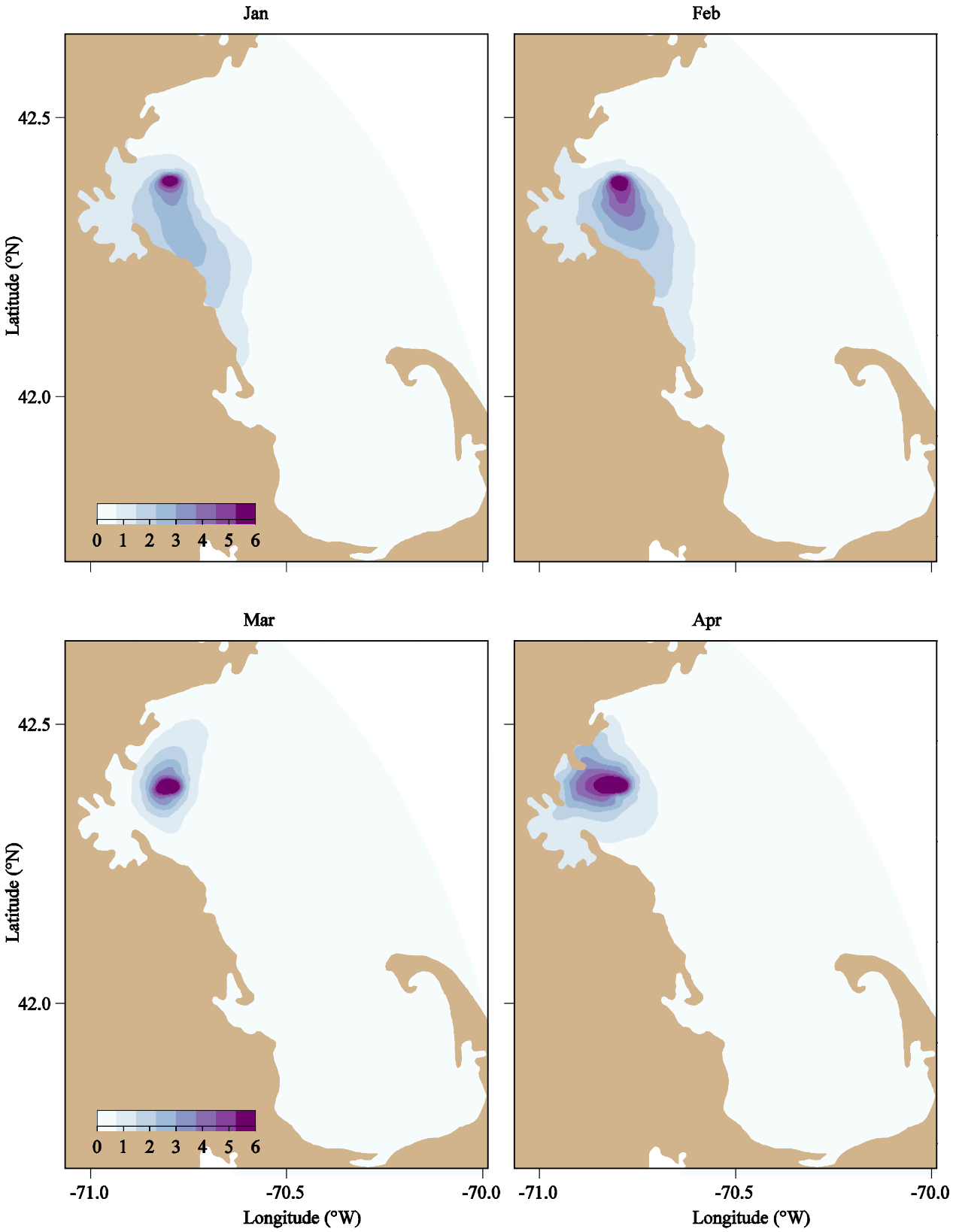

Figure 4. 6 Differences in bottom NH4+ concentrations (μM) at the end of January, February, March and April between the Control and Non-sewage experiments in 2011.

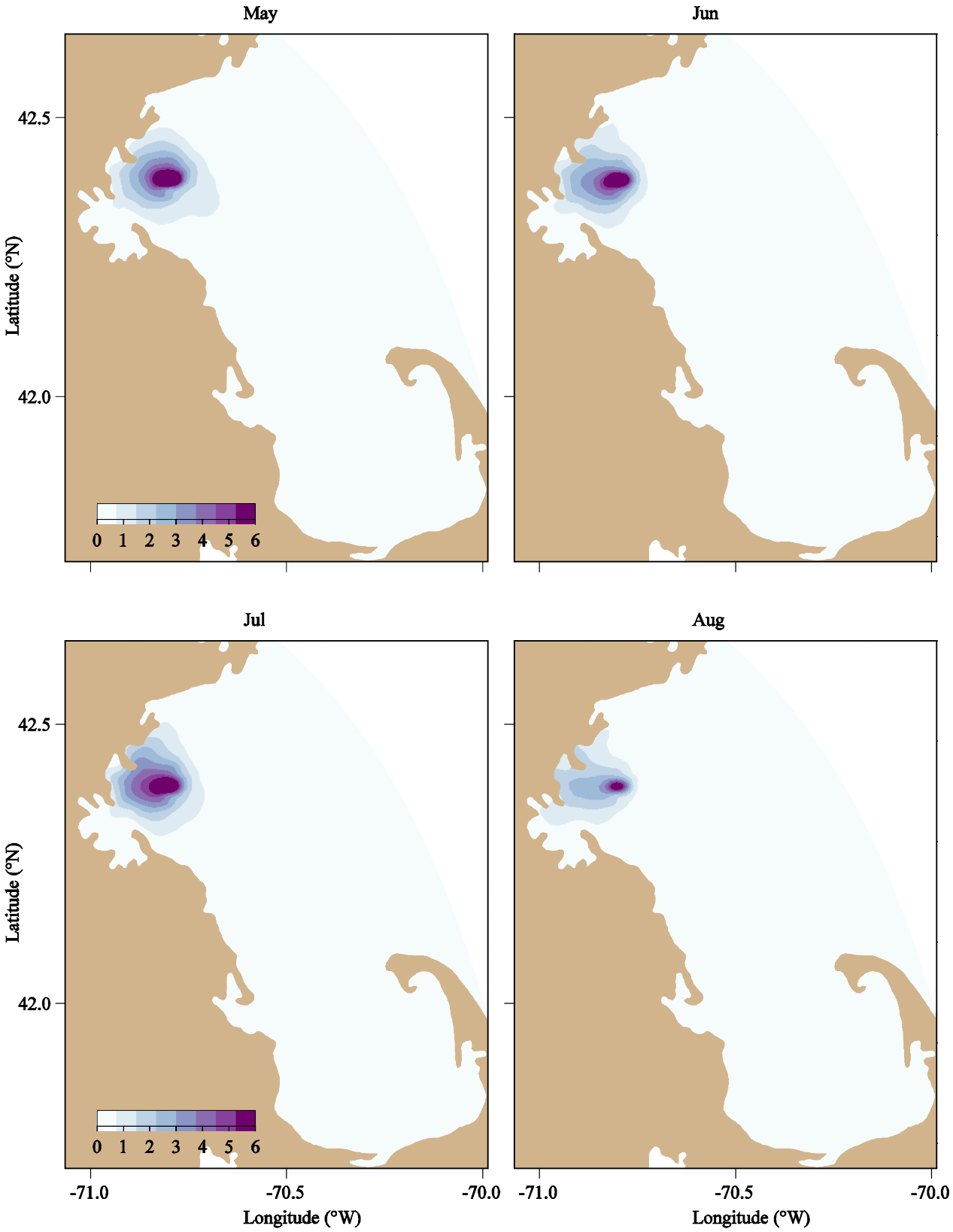

Figure 4. 7 Differences in bottom NH4+ concentrations (μM) at the end of May, June, July and August between the Control and Non-sewage experiments in 2011.

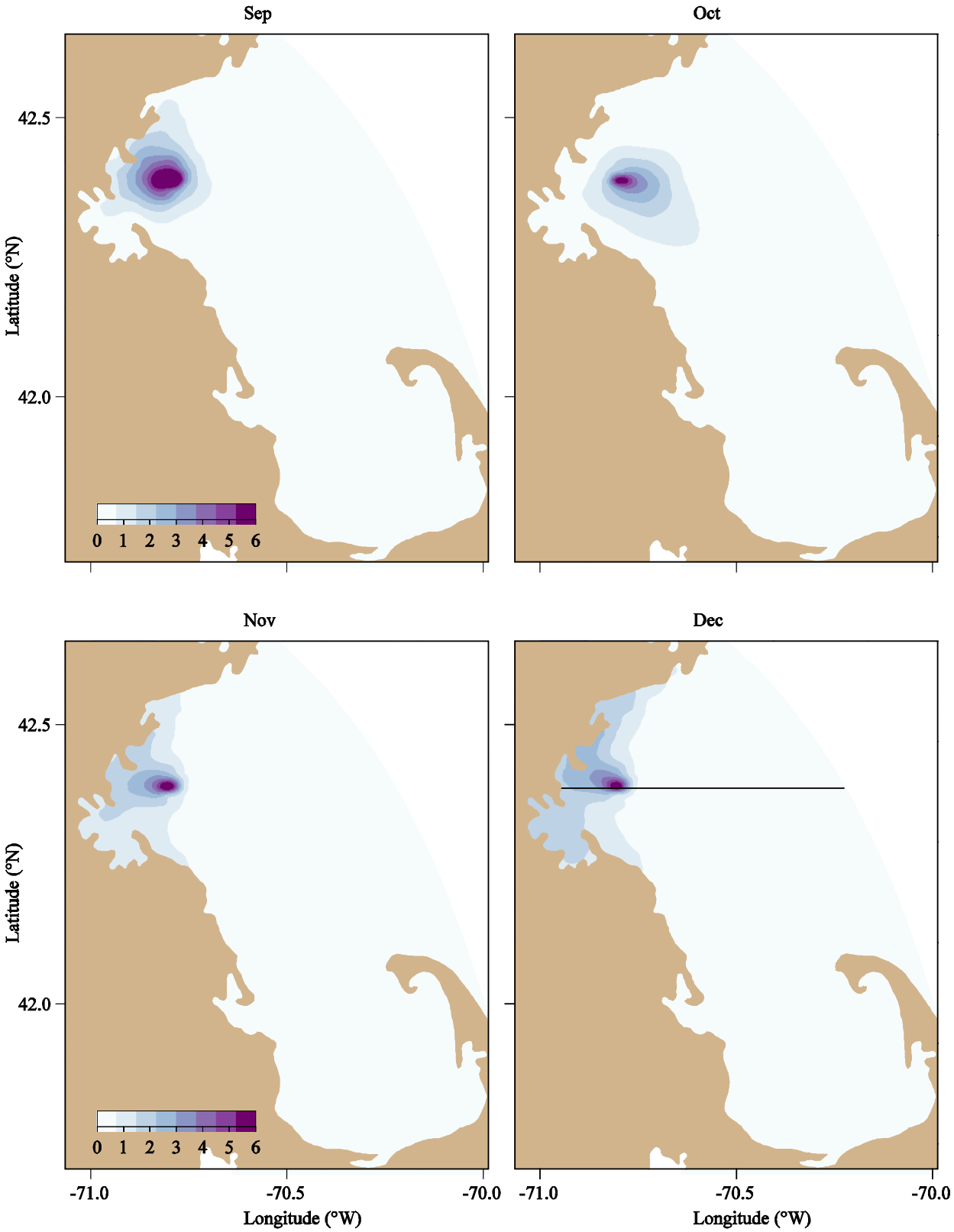

Figure 4. 8 Differences in bottom NH4+ concentrations (μM) at the end of September, October, November and December between the Control and Non-sewage experiments in 2011. Black line indicates the transect depicted in the following figures.

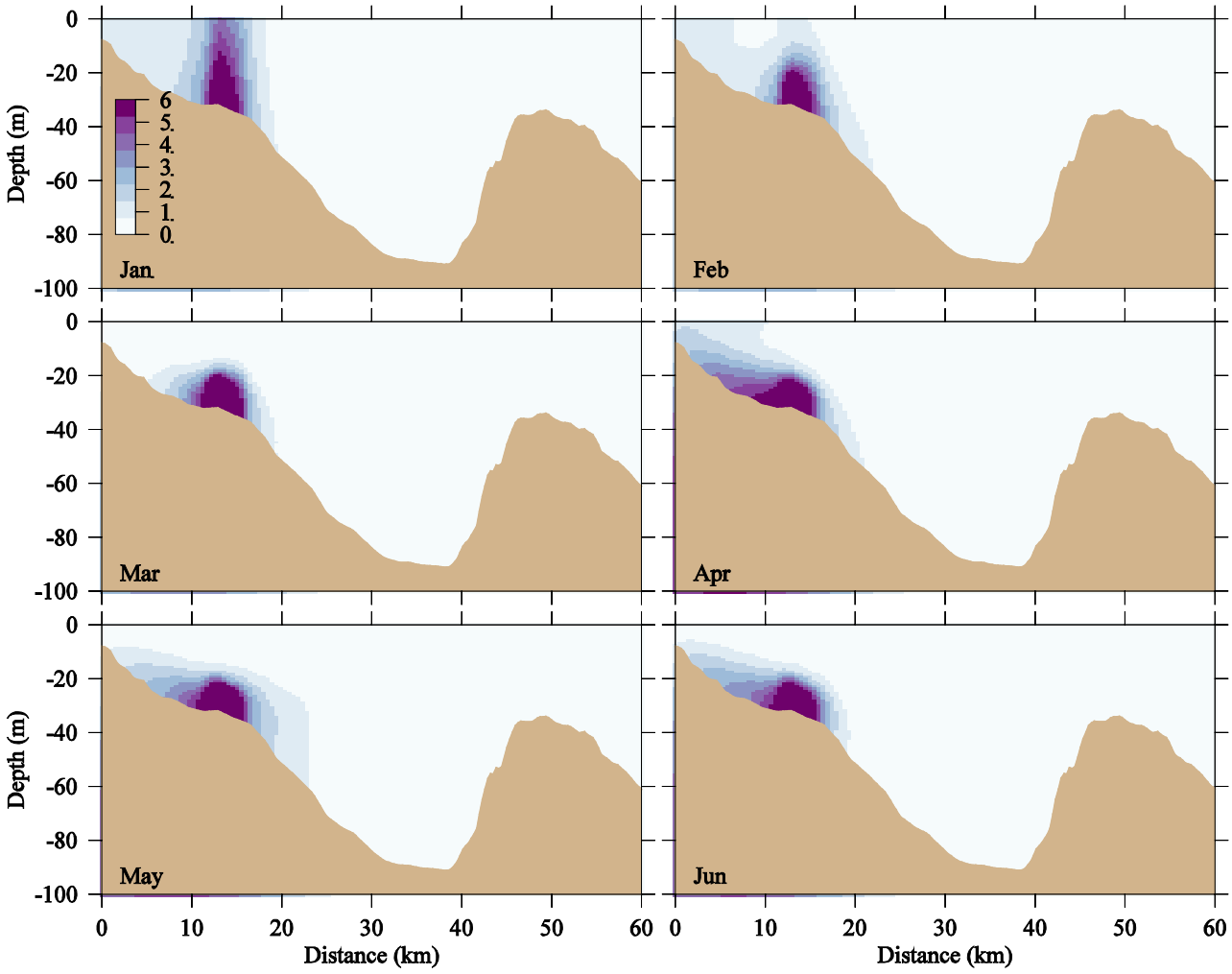

Figure 4. 9 Differences in NH_4^+ concentration (μM) on an east-west transect across the MWRA outfall at the end of each month from January through June between the Control and Non-sewage experiments in 2011.

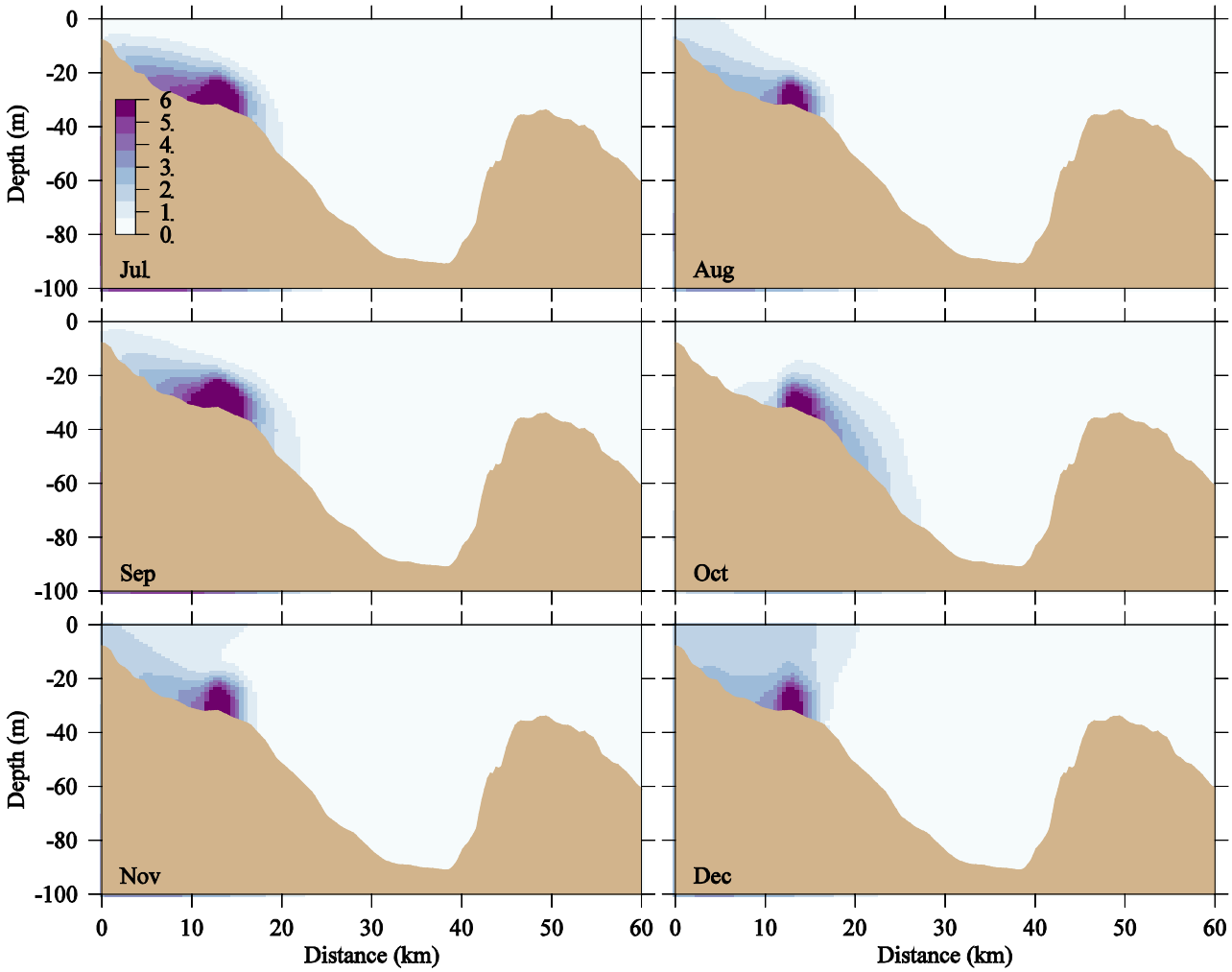

Figure 4. 10 Differences in NH4+ concentration (μM) on an east-west transect across the MWRA outfall at the end of each month from July through December between the Control and Non-sewage experiments in 2011.

Massachusetts Water Resources Authority
Charlestown Navy Yard
100 First Avenue
Boston, MA 02129
(617) 242-6000
http://www.mwra.state.ma.us